

SOLAR SUPERGRANULATION

by

Simon Peter Worden

A Dissertation Submitted to the Faculty of the

DEPARTMENT OF ASTRONOMY

In Partial Fulfillment of the Requirements
For the Degree of

DOCTOR OF PHILOSOPHY

In the Graduate College

THE UNIVERSITY OF ARIZONA

1 9 7 5

INFORMATION TO USERS

This material was produced from a microfilm copy of the original document. While the most advanced technological means to photograph and reproduce this document have been used, the quality is heavily dependent upon the quality of the original submitted.

The following explanation of techniques is provided to help you understand markings or patterns which may appear on this reproduction.

1. The sign or "target" for pages apparently lacking from the document photographed is "Missing Page(s)". If it was possible to obtain the missing page(s) or section, they are spliced into the film along with adjacent pages. This may have necessitated cutting thru an image and duplicating adjacent pages to insure you complete continuity.
2. When an image on the film is obliterated with a large round black mark, it is an indication that the photographer suspected that the copy may have moved during exposure and thus cause a blurred image. You will find a good image of the page in the adjacent frame.
3. When a map, drawing or chart, etc., was part of the material being photographed the photographer followed a definite method in "sectioning" the material. It is customary to begin photoing at the upper left hand corner of a large sheet and to continue photoing from left to right in equal sections with a small overlap. If necessary, sectioning is continued again — beginning below the first row and continuing on until complete.
4. The majority of users indicate that the textual content is of greatest value, however, a somewhat higher quality reproduction could be made from "photographs" if essential to the understanding of the dissertation. Silver prints of "photographs" may be ordered at additional charge by writing the Order Department, giving the catalog number, title, author and specific pages you wish reproduced.
5. PLEASE NOTE: Some pages may have indistinct print. Filmed as received.

Xerox University Microfilms

300 North Zeeb Road
Ann Arbor, Michigan 48106

75-19,576

WORDEN, Simon Peter, 1949-
SOLAR SUPERGRANULATION.

The University of Arizona, Ph.D., 1975
Astronomy

Xerox University Microfilms, Ann Arbor, Michigan 48106

SOLAR SUPERGRANULATION

by

Simon Peter Worden

A Dissertation Submitted to the Faculty of the

DEPARTMENT OF ASTRONOMY

In Partial Fulfillment of the Requirements
For the Degree of

DOCTOR OF PHILOSOPHY

In the Graduate College

THE UNIVERSITY OF ARIZONA

1 9 7 5

THE UNIVERSITY OF ARIZONA

GRADUATE COLLEGE

I hereby recommend that this dissertation prepared under my
direction by Simon Peter Worden
entitled Solar Supergranulation

be accepted as fulfilling the dissertation requirement of the
degree of Doctor of Philosophy

P. A. Strittmatter
Dissertation Director

March 3 1975
Date

After inspection of the final copy of the dissertation, the
following members of the Final Examination Committee concur in
its approval and recommend its acceptance:*

Ray J. Weyman
Keith J. Wood
George W. Kinn
John W. Harvey

March 3, 1975
March 3rd 1975
March 7, 1975
March 12, 1975

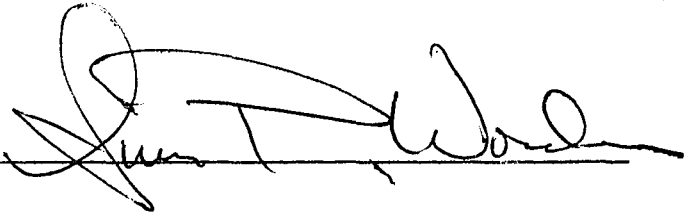
*This approval and acceptance is contingent on the candidate's
adequate performance and defense of this dissertation at the
final oral examination. The inclusion of this sheet bound into
the library copy of the dissertation is evidence of satisfactory
performance at the final examination.

STATEMENT BY AUTHOR

This dissertation has been submitted in partial fulfillment of requirements for an advanced degree at The University of Arizona and is deposited in the University Library to be made available to borrowers under rules of the Library.

Brief quotations from this dissertation are allowable without special permission, provided that accurate acknowledgment of source is made. Requests for permission for extended quotation from or reproduction of this manuscript in whole or in part may be granted by the head of the major department or the Dean of the Graduate College when in his judgment the proposed use of the material is in the interests of scholarship. In all other instances, however, permission must be obtained from the author.

SIGNED: _____

A handwritten signature in black ink, appearing to read "John T. Wood", is written over a horizontal line that serves as a signature line.

ACKNOWLEDGMENTS

The research presented in this dissertation was undertaken at three observatories: Steward Observatory (SO), Kitt Peak National Observatory (KPNO), and Sacramento Peak Observatory (SPO). I would like to thank the staffs of these three institutions for their generally cheerful, and sometimes less than cheerful but still invaluable, assistance in this work. I would especially like to thank J. W. Harvey (KPNO), P. A. Strittmatter (SO), and G. W. Simon (SPO), who with full knowledge and forethought, undertook the task of guiding this work. I would also like to thank R. G. Allen (KPNO), D. N. B. Hall (KPNO), G. L. Grasdalen (KPNO), E. B. Jensen (SO), and J. S. Scott (SO) for their assistance. Last, but certainly not the least, I would just like to say: "Hail to the Victors."

TABLE OF CONTENTS

	Page
LIST OF ILLUSTRATIONS	vi
LIST OF TABLES	viii
ABSTRACT	ix
CHAPTER	
1. INTRODUCTION	1
Convection: Theoretical Background	3
Convection: Observational Background	17
2. INFRARED OBSERVATIONS OF SUPERGRANULE TEMPERATURE STRUCTURE	30
The Infrared Spectrograph and Observations	33
Reduction of the Infrared Observations and Results	36
Discussion of the Infrared Results	51
3. VELOCITY AND MAGNETIC FIELD OBSERVATIONS OF SOLAR SUPERGRANULATION	57
The Sacramento Peak Observatory Diode Array System	60
Analysis and Results	67
The Lifetime of Supergranulation	68
Horizontal Transport of Magnetic Field Associated with Supergranulation	75
Vertical Velocity Flow Within the Supergranule	79
Discussion of Diode Array Results	87
4. STELLAR CONVECTION: THE dMe STARS	92
The Narrow Band Observational Scheme	95
Observations of Selected dMe Stars	100
Ross 614	102
FF And (BD+34°106)	107
YY Gem	107

TABLE OF CONTENTS--Continued

	Page
BD+5°1668	111
Ross 128	111
The Origin of dMe Star Magnetic Fields . . .	111
5. DISCUSSION OF RESULTS AND MODELS	125
Implications of the New Results for Models for Convection Zone and Magnetic Field Interactions	132
The Current State of Research on Convection and Further Work Which is Needed	143
REFERENCES	151

LIST OF ILLUSTRATIONS

Figure	Page
1. Summed autocorrelation functions for the one-dimensional infrared data	41
2. Summed cross-correlation functions for the one-dimensional infrared data	45
3. Contoured scatter diagrams for the one-dimensional infrared data	48
4. Two-dimensional pictures for the chromospheric and deep photospheric levels . .	50
5. All day filtered and unfiltered velocity observations for 5 March 1974	70
6. Cross-correlation in time for the velocity observations in Figure 5	74
7. Example of slow form of flux motion: splitting of existing flux	76
8. Example of fast form of flux motion: the appearance of new flux	78
9. Filtered and unfiltered velocities in different lines from 16 July 1974	81
10. Velocities and magnetic fields above a minimum threshold which correlate over forty minutes in center of the disk data . . .	83
11. Radial spatial autocorrelations for the center of the disk data	86
12. Line profile calculations for the non-magnetic lines with facular and non-facular atmospheres	91
13. TiO band strength as a function of spectral type in the dwarf M stars	99

LIST OF ILLUSTRATIONS--Continued

Figure		Page
14.	Magnitude-magnitude plots for the dMe star Ross 614	106
15.	Magnitude-magnitude plots for the dMe star FF And	108
16.	Magnitude-magnitude plots for the dMe star YY Gem	109
17.	Magnitude-magnitude plots for the dM star BD+5°1668	112
18.	Color-color plots for all dMe stars observed	113
19.	Magnitudes as a function of phase for the dMe star YY Gem	114
20.	Calculated toroidal magnetic field as a function of rotational period compared with stars of known periods	121

LIST OF TABLES

Table	Page
1. Data on Bands Used for Infrared Observations . . . ,	34
2. Derived Parameters of Magnetic Elements for the Infrared Levels	54
3. Effects of Magnetic Fields on Velocity Observations with the $\lambda 8468$ Line	64
4. Data for Non-Magnetic Lines Used in the Vertical Velocity Investigation	66
5. Mean Vertical Velocities in Magnetic Field Regions (Unfiltered Data-Downflows Positive)	84
6. Parameters of Bandpasses Used in the dMe Star Observations	96
7. Dwarf M Star Spectral Type Standards	98
8. dMe Stars Observed	101
9. Table of dMe Star Observations	103
10. Magnetic Fields Needed to Dominate Fluid Motions as a Function of Depth in a G2V Star and an M0V Star	134
11. Light Element Depletion Information	138

ABSTRACT

Supergranulation is a horizontally outflowing pattern of gas on the solar surface. It has subsequently been interpreted as a convective process originating some 10,000 km below the solar surface. As a convective phenomenon supergranulation is believed to play an important role in the generation, distribution, and dissipation of solar magnetic fields. This dissertation presents several observations designed to study these processes. An alternate approach in understanding stellar convection is the study of the dMe stars; a class of late spectral-type dwarf stars which exhibit characteristics qualitatively similar to solar magnetic activity. An observational test of this hypothesis is presented in this dissertation. Concluding this work a discussion of these observational results within the framework of solar and stellar convection zone-magnetic interactions is provided.

As convection cells, supergranules would be expected to show a temperature structure indicative of convective energy transport. Previous studies of this possible temperature structure have produced negative results. However, magnetically induced temperature effects could mask any convective temperature system which may be present. An attempt to disentangle these two processes was made

involving observations in the near-infrared, the deepest observable atmospheric level. Even though magnetic field temperature effects at this level are substantially altered from the higher levels, it was found that the only large-scale temperature structure was a temperature decrease of 50-500K confined to the magnetic field regions which are concentrated at supergranular boundaries. Since this result is entirely attributable to the effects of strong magnetic fields it is concluded that the levels at which supergranules are the primary means of energy transport lie much deeper than the observable levels of the solar atmosphere.

Simultaneous velocity, magnetic field, and chromospheric emission network data were used to study the lifetimes, the vertical velocity flow, and the transport of magnetic fields associated with supergranulation. From cross-correlations of the velocity observations over 10-hour periods, supergranules appear to have a mean lifetime close to 36 hours, rather than 24 hours as previously derived. Supergranules have a vertical velocity structure which consists of an upflow of ~ 50 m/sec in their centers and a downflow of ~ 200 m/sec confined to the magnetic field regions at their boundaries. Horizontal magnetic field motions take two forms: first, an apparent slow breakup of existing flux points; and secondly, a rapid motion of flux following the emergence of new magnetic field. The latter may be associated with the formation of a new supergranule.

A set of narrow band filters was used in the photometric study of the presumed active regions on the dMe star surfaces. These observations were somewhat limited, but they do tend to show that decreases in photospheric light intensity, presumably caused by the appearance of dark cool spots, were accompanied by increases in chromospheric light levels, perhaps due to chromospheric emission regions surrounding the spots. This behavior is qualitatively similar to solar effects induced by magnetic fields. By using a "Biermann Battery" mechanism to generate magnetic fields within a radiative stellar core, it is possible to predict field strengths up to 10^5 G on the dMe stars.

These results are consistent with a generalized stellar model in which strong magnetic fields are generated deep within the star. These fields subsequently interact with convective motions to produce the observed manifestations of solar and stellar magnetic surface activity. The main new conclusion of this dissertation is that the processes responsible for this behavior may occur at substantially deeper levels than previously thought.

CHAPTER 1

INTRODUCTION

An important achievement in astrophysics during the last three decades has been the development of a partial understanding of the process of energy generation and subsequent transport and radiation of that energy in stars. The success of theory in explaining many features of the traditional Hertzsprung-Russell diagram has been a truly remarkable result. Schwarzschild (1958) has presented what remains a good description of this work. However, detailed observations of many stars, including the sun, have shown inconsistencies which current theory is unable to satisfactorily explain. It is the purpose of this thesis to discuss observations which have a bearing on this problem.

The central difficulty in stellar interior models is often the treatment of convection which occurs somewhere in most stars. Spiegel (1971, 1972) has discussed the current treatment of convection in astrophysics. From these reviews and other literature on the subject it is clear that a serious problem is the lack of a satisfactory solution to the complex equations of convective energy transport. Thus, all work has entailed the making of suitable approximations to the complete equations. The uncertainty in observed stellar boundary conditions such as radii and luminosities

is sufficient to insure that many treatments of convection will produce satisfactory models. Direct comparison of theory with observations of convective phenomena to determine valid approximations and methods of solution is possible for only the sun and laboratory convection. Since astrophysical conditions are difficult to reproduce in the laboratory, convective studies in the laboratory are of limited use. Consequently one turns to the sun, upon which several processes believed to be convective in nature have been observed. White light photography reveals the solar surface to be covered with a small cellular pattern. These "granules" are bright cells surrounded by a dark boundary with diameters about 1000 km and lifetimes close to ten minutes (Bahng and Schwarzschild 1961). The pattern of rising hot gas in their centers and falling cooler gas at the granular boundaries has led to the granules' identification as convective cells (Beckers and Parnell 1969). Early attempts to measure the solar rotational velocity produced large scatter in the results (Evershed and Royds 1913, Plaskett 1915, Schlesinger 1916, Plasket 1916). This scatter has subsequently been shown to be due to a larger scale cellular velocity pattern (Hart 1954, 1956; Leighton, Noyes, and Simon 1962) or "supergranulation" consisting of horizontally outflowing cells with diameters averaging 30,000 km (Leighton et al. 1962). As the name suggests, these cells have been identified by Simon and Leighton

(1964) and Simon and Weiss (1968) as manifestations of a convective phenomenon similar to the granulation but deeper in origin. As such they have been used to check convective theory and hold central roles in magnetic field processes. The remainder of this introduction will cover this work and elaborate on observations which are needed to further understand stellar convection. While this dissertation is fundamentally observational, the theoretical background will be briefly covered.

Convection: Theoretical Background

Conceptually, convection is simple to understand; it is the process of hot gas rising and cool gas falling. The standard mathematical test for convection involves the displacement of a small test "bubble" from its original position and the determination whether it will return to that position, in which case convection does not occur (Schwarzschild 1958). The rising (or falling) bubble will undergo changes in its temperature and density obeying an adiabatic relationship, adjusting its pressure to equal that of its surroundings quickly relative to the time which the bubble takes to rise or fall. If the bubble has risen to a new level by a small perturbation and the ambient temperature gradient is such that the adiabatic temperature change results in a higher bubble temperature than that of the surrounding gas, the bubble will have a lower density than

its surroundings and will continue to rise because of the bouyancy force. The stability condition against convection is therefore the requirement that the adiabatic temperature gradient be less steep than the actual gradient, or from Schwarzschild (1958):

$$-(1 - \frac{1}{\gamma}) \frac{T}{P} \frac{dP}{dr} > - \frac{dT}{dr} \quad (1.1)$$

where T is temperature; P , pressure; and γ , the ratio of specific heats c_p/c_v , which is $5/3$ for a highly ionized gas. For example, in the computation of a stellar model the condition in Equation (1.1) is checked at each point in the star. At any point where it does not hold the equations for convective energy transport replace those for radiative energy flow.

Many investigators (see, for example, Mullan 1971) have demonstrated that stars with spectral types later than AO have convective outer envelopes attributable to ionization effects (Schwarzschild 1958). Later spectral type stars like the sun have outer envelopes which are cool enough for hydrogen and helium to be incompletely ionized. This affects the temperature stability in two ways. First, ionization contributes to the value of the adiabatic temperature gradient. The adiabatic temperature will rise more slowly in an ionization region since in the compression of a partially ionized gas much of the compression energy goes into an increased ionization, resulting in a smaller

adiabatic gradient. Secondly, the partially ionized gas produces an increase in opacity through bound-bound and bound-free interactions. The increased opacity produces a steeper ambient temperature gradient. The combined effect of these two processes is to decrease stability against convection, as can be seen from Equation (1.1).

Spiegel (1971) discussed in detail analytical methods to approach astrophysical convection. The complete equations for convective energy transport contain non-linear terms and have not yet been solved. However, assumptions and approximations have been made to make them more tractable. Laboratory convection represents a special case where the equations become linear and solutions have been made (Chandrasekhar 1961). In the laboratory the vertical extent of the incompressible convecting fluid is much less than one scale height and a steady state is quickly reached with hexagonal convective cells. This is termed Bénard convection and is unlike that which is expected in stellar interiors since stellar convection zones are not incompressible and usually extend over several scale heights. The Boussinesq approximation (Spiegel 1971) or a form of it is generally used for stellar convection. Although not strictly valid, it does enable a quantitative model to be calculated. The two approximations central to the Boussinesq approximation are the anelastic approximation, in which high frequency phenomena, like sound waves are

ignored, and the additional assumption that the vertical extent of the fluid is much less than a density or pressure scale height. However, the material is not necessarily incompressible, and often the additional constraint that viscosity and conductivity are insensitive to temperature is used.

For stellar interior calculations the so-called "mixing length theory" developed by Vitense (1953) is usually used. Treating turbulent convection as a process similar to molecular diffusion, it represents a special case in which a particular type of flow is assumed and is a form of the Boussinesq approximation (Spiegel 1971). A brief summary of the assumptions used is given here following Schwarzschild (1958). The total convective flux is derived by computing the amount of energy carried upward less that carried downward by a unit volume of convecting material.

The temperature excess in the rising bubble, $\nabla \Delta T dr$, is the difference between the adiabatic gradient, and the actual temperature gradient at the distance dr from the point of bubble origin:

$$\nabla \Delta T = \left(1 - \frac{1}{\gamma}\right) \frac{T}{P} \frac{dP}{dr} - \frac{dT}{dr} \quad (1.2)$$

where γ is the ratio of specific heats c_p/c_v . The amount of energy per unit volume carried upward is the temperature difference 1.2 multiplied by the specific heat, c_p , times the density ρ . To obtain the flux, this quantity is

multiplied by the velocity of the rising bubble v . The convective flux, F_c , is therefore:

$$F_c = \nabla \Delta T \, dr \, c_p \rho v \quad (1.3)$$

A value for v must be derived, and this is the point at which approximations enter. The temperature excess in the rising bubble produces a decrease in the bubble density. It is this density decrease which results in the buoyancy force that drives the convection. This force will cause an acceleration of the bubble generating kinetic energy. By equating the kinetic energy to $1/2 \, m \bar{v}^2$, a mean velocity is obtained. The density decrease $d\rho$ in the bubble is derived from the adiabatic gradient less the actual density gradient in a manner similar to the temperature difference.

$$\begin{aligned} d\rho &= 1 \, \frac{1}{\gamma} \, \frac{\rho}{P} \, \frac{dP}{dr} \, dr + \frac{d\rho}{dr} \, dr \\ &= \frac{\rho}{T} \, \nabla \Delta T \, dr \end{aligned} \quad (1.4)$$

The work done in raising the bubble is force times distance:

$$\begin{aligned} W &= 1/2 \, g \, d\rho \, dr \\ &= \frac{\rho}{T} \, \nabla \Delta T \, dr \, \frac{GM}{r^2} \, 1/2 \, dr \\ &= 1/2 \, \rho \bar{v}^2 \end{aligned} \quad (1.5)$$

The mean velocity, \bar{v} , is obtained by solving Equation (1.5). One additional approximation is made. It is assumed that the bubble loses its identity after some length of travel, L , which has been given the name "mixing length." Since

the quantities computed are mean quantities, it is assumed they represent the bubble at the midpoint in its travel. Thus $dr = 1/2 L$. Substitution of the above into Equation (1.3) results in the convective flux equation:

$$F_c = C_p \rho \left(\frac{GM_r}{Tr^3} \right)^{1/2} (\nabla \Delta T)^{3/2} \frac{L^2}{4} \quad (1.6)$$

In laboratory convection, cells maintain their identity through about one scale height, thus the mixing length is generally identified as one scale height. Since stellar convection zones extend over several scale heights, there is some question of the validity of this assumption.

A test of mixing length theory validity is its success in making solar models. Schwarzschild, Howard, and Härm (1957) constructed a reasonable model using mixing length in which the convective zone extended to a depth of about 150,000 km, at which level the temperature was $10^6 K$. The success of mixing length theory in describing the sun and other stars to a reasonable degree must be taken as a strong point in its favor. However, there is no facet of conventional mixing length theory which can explain the preference for cells of any particular size like the super-granular size. Additionally, mixing length fails at just the point where observation becomes possible; that is, at the surface where physical parameters are rapidly varying.

Since mixing length is valid over scales small in comparison with scales over which fundamental parameters, such as temperature, pressure, and density vary, and presumed convection processes such as granulation and supergranulation seem to occur over scales large with respect to these parameters, a generalization of mixing length is needed. Indeed, the presence of any preferred cell size at all is somewhat surprising, since the solar convection zone is highly unstable against convection. The resulting turbulent convection predicted by mixing length has no such preferred sizes as one of its properties.

As a result of the need for a theory with mixing lengths large with respect to fundamental parameters Spiegel (1963) generalized mixing length theory to account for large mixing lengths. This was accomplished by including radiative losses in the outer part of the convection zone and the transfer of flux by convective elements which "overshoot" into the radiative zone of the solar photosphere. With this approach he developed a set of equations resembling radiative transfer equations and was able to compare the computed distribution of convective cell sizes with the observed solar granulation. In subsequent work Spiegel (1964, 1965) included the effects of a compressible atmosphere and in his 1965 paper the basic equations for convection in a deep compressible atmosphere are developed.

The first successful calculation of a preferred convective cell size corresponding to supergranulation was reported by Simon and Weiss (1968). A model was derived with convective cells extending over several scale heights on the theory that a large cell extending over many scale heights is more efficient in transporting energy since it builds up its temperature difference over the entire length of travel rather than the single scale height of a small cell as mixing length would imply. The large cell will rise until the horizontal motions demanded by mass continuity (i.e., $\nabla \cdot \rho \vec{v} = 0$) near the top of the cell, which do not contribute to energy transport and result in parasitic energy loss, become significant enough so that the local superadiabatic gradient exceeds that built up over the entire length of the large cell. At the location where this occurs new convection cells with characteristic sizes near the scale height at that level form. The process then repeats until new smaller cells form. Simon and Weiss performed these calculations using a polytropic atmosphere from which three characteristic sizes were obtained. The first representing the bottom of the convection zone (depth ~ 150,000 km) produced cell sizes of about 300,000 km. These were identified with the giant cells of Bumba and Howard (1965) and Bumba (1967). The second characteristic cell size originates at a depth of 10,000 - 15,000 km and is identified with the supergranulation with horizontal extent

averaging 30,000 km. Near the top of the convection zone at depths of 500 to 1000 km the granulation forms. These derived convection cells have geometries in which the horizontal extent is 2 to 4 times the depth of the cells in agreement with laboratory results and convective theory. A similar analysis by Vickers (1971) including variable viscosity and conductivity found scales of convection matching the Simon and Weiss (1968) results with the difference that the derived scale which corresponded to supergranulation did not have as narrow a distribution of sizes as the observed supergranulation distribution of sizes.

Mullan (1971) used a theory based on slightly different approximations than mixing length and obtained interesting results. The theory of Öpik (1950) includes turbulent exchange of material and radiative losses between rising and falling bubbles following Bohm-Vitense (1958). Using this theory Mullan (1971) obtained the interesting result that the convection zone stops at a depth of 10,000 km, much less than the 100,000 km or so found in other work. The supergranules are identified with the bottom of the convection zone, and granules with cells formed at depths of about 300 km, having horizontal size to depth ratios of about 4 in line with Öpik's (1950) prediction. Alternately, the giant cells are explained as large scale cyclonic motions rather than convective cells. Iroshnikov (1969) obtained a similar shallow convection zone of only

"supergranular" (10,000 km) thickness by including the effect of solar rotation on viscosity in his analysis.

Mullan (1971) made additional calculations by generalizing his work to main sequence stars of spectral type different than the sun. A sudden decrease in the depth of the stellar convection zone by a factor of four is calculated to occur at spectral type G0 and earlier. This would imply a decrease in the size of the stellar supergranules. If magnetic surface fields are the result of a convective dynamo process as suggested by Parker (1970) and Mullan (1974) with the field strengths a function of the size of the convective cell dynamo (Weiss 1966), then as Mullan suggested, the magnetic fields on these earlier spectral type stars would be significantly less strong due to the small convective cells. He further stated that since magnetic fields seem to play a dominant role in the heating of stellar chromospheres (Osterbrock 1961), the reduced chromospheric heating observed in early G stars by Vaughn and Zirin (1968) can be explained as an effect of weaker surface magnetic fields. Other implications of this result and further observational studies with a bearing on this problem will be discussed in the following section of this introduction.

The detailed source of the instability causing the formation of supergranules at their preferred depth has been discussed by several authors (Simon and Leighton 1964, Simon

and Weiss 1968, Schwarzschild 1975). A decrease in the adiabatic gradient caused by the HeI-HeII ionization zone is calculated to occur at the depth of the supergranulation (10,000 km) formation. The resulting increase in super-adiabatic conditions within a rising convective cell is conducive to the formation of new cells with sizes representing the scale height in this region (i.e., supergranules). An interesting consequence of this theory is the prediction that there are very large convective cells on the surface of late type supergiants (Schwarzschild 1975). Each cell would be enormous, covering 10-20% of the stellar surface, due to the large scale height in the cool extended atmospheres of these stars. It is important to point out at this point that in all of the theoretical work described here the only observable manifestation of supergranules and giant cells will be a convective overshoot, since the primary supergranules and giant cell convective motions are calculated to terminate well below the visible surface.

Since the development of magnetographs (Babcock 1953) it has been clear that solar surface features are intimately involved with strong magnetic fields. A comparison of magnetic energy density with kinetic energy density for the photosphere using the relation:

$$\frac{B^2}{8\pi} \approx \frac{\rho v^2}{2} \quad (1.7)$$

with $\rho = 10^{-7} \text{ gm/cm}^3$; and with $v = 1 \text{ km/sec}$, a typical value

for convective velocities in the photosphere; shows that fields of about 100 G will interact strongly with convective motions on the surface. Since this is on the order of the size of surface fields, the effects of magnetic fields must be accounted for in any observation of convective phenomena in the photosphere.

An important aspect of solar magnetic field behavior is the twenty-two year cycle during which magnetic field activity twice reaches a maximum. During these cycles, the magnetic active regions occur in different latitudes at different times, and are observed to have a bipolar nature with polarities depending on which hemisphere and which half of the 22-year cycle they occur in. Babcock (1961) offered an explanation of this behavior in terms of an initially uniform magnetic dipolar field through the solar poles, which is "wound up" and amplified by differential rotation. When the amplification is strong enough, elements of field "burst" through the surface in small bipolar active regions. These are progressively formed and dispersed until the entire solar bipolar field is reversed and the process repeats. The complete cycle thus entails two magnetic field maxima during which the originally uniform bipolar field is returned to its original polarity. However, Babcock was unable to explain the mechanism for field dispersal within the small active regions.

Leighton (1964) suggested supergranulation as the cause of magnetic field dispersal. Weiss (1966), Parker (1963), and Clark and Johnson (1967) showed that uniform vertical magnetic fields would quickly be transported horizontally to the boundaries of a convective cell where they would be amplified. This process would result in especially strong magnetic fields at the vertices where several supergranules meet. Leighton showed that this process could account for the observed dispersal of magnetic fields from initially compact active regions, with magnetic fields "random walked" by the supergranulation and thus dispersed. The observation of Leighton et al. (1962) and Simon and Leighton (1964) which showed magnetic fields and corresponding chromospheric emission concentrated at supergranular boundaries enhanced the above argument. In his complete model of the solar cycle, Leighton (1969) used this process as the mechanism to disperse the magnetic field, and was able to reproduce all of the observed features of the solar cycle.

The origin of the solar magnetic field is another problem upon which supergranular flow may have a bearing. Parker (1970) has discussed this role in magnetic field generation. The fast changing nature of surface magnetic fields may indicate a local source for their generation. Parker proposed that the convective motions themselves provide the source of the magnetic fields. A dynamo process

arising out of an interaction between the convective motion and a weak field could provide for the strong surface fields as discussed by Weiss (1966). A small rotation of the convective cells through a coriolis mechanism would further produce the observed tilt to the bipolar active regions on the solar surface.

Active region magnetic fields reach strengths of over 4000 Gauss in sunspots (Livingston 1974) and 2000 Gauss in nearby facular regions (Harvey and Hall 1974). These strong fields can deform the material motions as far down as depths near the formation level of supergranules. Wilson (1972a) suggested a model in which these strong fields have subsurface components which deform the supergranule pattern resulting in radial outstreaming from sunspots encompassing several supergranules. This is similar to a Carnot cycle and Wilson proposed it as a mechanism for cooling the sunspots with the energy carried away from the spot to be dumped in the bright facular regions.

The proposal that the observed supergranular flow is actually due to counter cells driven by underlying convective cells was advanced by Spiegel (1966). Wilson (1972b) stated that this may be the case as there appears to be no observable temperature decrease at supergranule boundaries as would be expected of a convective cell itself (Beckers 1968, Frazier 1970). A counter cell, since it is not the primary means of energy transport, may be expected

to show a greatly reduced temperature structure. Since the observed supergranular flow may also be a convective overshoot, rather than the convective cell itself (Weiss 1966), which would similarly show reduced temperature structure, the observed lack of temperature structure does not in itself verify the counter cell hypothesis. However, extended studies of supergranular temperature structure are clearly important.

Convection: Observational Background

Early attempts to measure the solar rotational velocity (Evershed and Royds 1913; Plaskett 1915, Schlesinger 1916, Plaskett 1916) resulted in inconsistencies much larger than observational and measurement error. These early investigators correctly attributed this result to large scale motions within the solar atmosphere (Plaskett 1915). Frenkiel and Schwarzschild (1952) observed similar variations over a scale on the order of 15,000 km. Hart (1954, 1956) determined the reality of these variations near the limb and found they were spatially periodic with an amplitude of $\pm .17$ km/sec with an average surface extent of 26,000 km. The identification of these "supergranules" as horizontally outflowing cells of 30,000 km diameter was made by Leighton et al. (1962) and Simon and Leighton (1964). The existing data on this phenomenon are covered in this

section, at the conclusion of which additional observations made in this dissertation will be summarized.

In addition to supergranules, Leighton et al. (1962) discovered a 300 sec periodic vertical oscillation of .5 km/sec amplitude. The oscillations appear to be correlated over at least 4000 km. Deubner (1967, 1972a) and Evans and Michard (1962) found lifetimes of these oscillations of about 30 minutes and described their other observational properties. The origin of the oscillations is unclear, but they may represent a global solar oscillation (Wolff 1972). A fifty-minute oscillation has been reported by Deubner (1972b) as well. It is reasonable to assume these oscillations are not a primary convective phenomenon, as no theory of energy transport is consistent with such a short-lived highly periodic phenomenon. As a presumably non-convective motion they constitute velocity "noise" and most observations of supergranules are averaged over several oscillatory periods to remove its effect. It is interesting to note that Hart's (1956) work discovering supergranules by chance used data averaged over the 300 sec oscillation in such a manner as to reduce its effect.

The most extensive photographic observations of the supergranular flow patterns are those of Leighton et al. (1962) and Simon and Leighton (1964). Optical auto- and cross-correlation techniques were used in that work to

obtain sizes and lifetimes for the supergranules. Cells have an average horizontal size of 30,000 km distributed between 20,000 and 60,000 km, with horizontal velocities of about .5 km/sec. Photographic velocity data are rather noisy, so it was difficult to study the question of preferred orientation. However, there is some evidence for an elongation in the direction of solar rotation (Sykora 1970) and a possible difference in cell spacing dependent on latitude (Simon and Leighton 1964). Vertical velocities, while difficult to disentangle from 300 sec oscillations and granulation velocity fields, are of great interest. If the convective hypothesis for supergranule origins is correct, a vertical component of the velocities is expected, with upwelling velocities at cell center and downfalling at the cell boundary. At deeper levels the velocities should become more vertical in nature until at some deep level several thousand kilometers into the convection cell proper they become predominantly vertical. Simon and Leighton (1964) distinguished a small vertical flow in center of disk cells of .1 to .3 km/sec consisting of a downflow at supergranule cell boundaries. Subsequent work confirms this observation as Tannenbaum et al. (1969), Musman and Rust (1970), and Deubner (1972a) noted similar observations. Frazier (1970) in a detailed study using photoelectric two-dimensional data also reported the vertical velocities; additionally he observed especially strong "down-drafts" at

the vertices of several supergranular cells. Similar chromospheric downdrafts in $H\alpha$ and $H\beta$ are observed in the same locations. These observations are not surprising since it is an expected result that downdrafts are strongest at the vertices of several convective cells from studies of Bénard convection (Pellew and Southwell 1940).

The mean lifetime of supergranules is approximately one day making it a difficult quantity to determine exactly (Simon and Leighton 1964). A scheme to obtain this quantity was undertaken by Rogers (1970) who transported a telescope to Greenland and produced a 60 hour continuous $H\alpha$ movie. Since $H\alpha$ and other chromospheric emission features are observed to congregate at cell boundaries (Simon and Leighton 1964), Rogers used the $H\alpha$ emission to determine a lifetime for $H\alpha$ network cells of ~ 20 hours. Since this lifetime is for a network cell and not a supergranule, the lifetime for the velocity cells remains an unanswered question.

It is apparent from the appearance of calcium K line spectroheliograms that the sun is covered with a network of bright emission mottles. This pattern of "faculae" appears in virtually every level of the atmosphere above the photosphere, and is co-spatial with magnetic fields. Simon and Leighton (1964) demonstrated that a strong correlation existed between this network and the downflows at supergranular boundaries. However, it is important to distinguish between the supergranulation, which is a velocity

phenomenon, and the network, which is a pattern of emission or absorption. The magnetic network elements may have been swept from the center of the supergranule by velocity fields and perhaps are Leighton's (1964) random walk process in action since the magnetic fields are observed to be concentrated most strongly at the vertices of several cells. As these are the points of highest downflow (Frazier 1970) it can be shown (Musman 1971) that the magnetic field would be swept to these points and strongly concentrated.

Musman points out that the magnetic field at the vertex points would quickly be concentrated to enormous strengths. The fact that the field is apparently not overly strong at the vertices can be explained by a computer model constructed by Milkey (1972). The rapid concentration of very strong fields is avoided in Milkey's model by superimposing a small random walk, perhaps caused by granular motions, on top of the supergranular process. However, the magnetic field may be substantially stronger than previously thought (Harvey and Hall 1974) in which case this problem vanishes. Smithson (1973) observed magnetic field elements over a five day span and calculated observed random walk rates. He found two motions of the magnetic elements. The first was a random walk process whose characteristic time step was much shorter than 24 hours. This was too short to be caused by supergranulation. The r.m.s. displacement of this process was 7600 km over 24 hours. Furthermore, this

is too small by a factor of three to explain the previously observed dispersal rates of Sheeley (Leighton 1964) or that which is required by theory. In the second form of flux motion the magnetic elements seemed to have a lifetime of 3-4 days and were occasionally observed to move rapidly over distances of 5,000 to 20,000 km in times of from one to three hours with velocities of about 1 km/sec. Smithson (1973) suggested that the small r.m.s. scatter may be due to granulation but that the supergranular random walk was not directly responsible for this flux diffusion. To determine if the supergranular motions are indeed responsible for flux motions and whether the Smithson result indicates a longer lifetime for supergranules as it suggests, long time sequences of simultaneous velocity and magnetic field observations are needed. In addition the role of granulation in the small scale random walk process remains undetermined. The high resolution granulation photographs of Dunn and Zirker (1973) show that the photospheric magnetic fields may be excluded from granular cells, however the result is somewhat unclear and needs to be verified.

The name supergranulation suggests a process similar to granulation. This has prompted a search for intensity patterns similar in form to the granulation, the upwelling center of the cell hotter and brighter than the downfalling boundary of cooler gas. Clearly, if supergranules are convective cells, this must be true at some level in the solar

convective envelope. A number of investigators have searched for this intensity difference (Simon 1966, Beckers 1968, Frazier 1970). Intensity structures on the scale of the supergranulation have been observed in the white light photosphere (Stuart and Rush 1954, Vassiljeva 1967). The first attempt to correlate this structure with supergranular flow patterns was undertaken by Simon (1966). He correlated continuum data with $H\alpha$ photographs, in which the network shows up as dark mottles, and with calcium K line data, in which the network is in emission. A positive correlation was found between the continuum and $H\alpha$ data, and a negative correlation was observed between the continuum and K line data. These data can be interpreted to mean the boundaries of the supergranules are dark, as expected. However the correlation distance was small and could have been caused by the granulation pattern. In the two subsequent investigations, by Beckers (1968) and Frazier (1970), no indication of a darkening of the supergranular boundary was found. However, there was evidence the supergranular boundary was brighter than the cell center, perhaps by as much as 10K hotter than the cell center (Frazier 1970). Beckers interpreted this observation to mean the facular emission elements which are concentrated at the cell boundaries are masking any intensity decrease which may be present. This hypothesis is consistent with the model of a facular element calculated by Chapman (1970). Frazier

(1970) and Wilson (1972b) favored the interpretation that there is no observable temperature decrease at cellular boundaries. As explained previously, Wilson felt the observed supergranules are counter cells, not primary convection cells, and as such they transport little energy. Frazier (1970) derived an unobservable temperature difference between the center and boundary of .003 K considering mixing length arguments. However, as mentioned previously, mixing length calculations are probably inaccurate near the surface, the region under question. Using Equation (1.3) for the total convective flux, the average temperature structure within a convective cell is given by:

$$\Delta T = F_c / c_p \rho v$$

If the assumption is made that the supergranules carry the entire solar flux, and average densities and velocities for the supergranules are used along with stellar parameter data from Allen (1973) a temperature difference between a rising bubble and surrounding material of several hundred degrees Kelvin is derived as suggested by Weiss (1968). Thus, somewhere within the supergranular flows a large temperature difference may be present. Where this temperature difference goes when the material reaches the observed surface is an open question, and one which is important to the entire supergranular interpretation.

Observations of stellar convective processes are very limited, however their importance is great since many theories explaining solar convection can be generalized to predict similar phenomena, modified by changes in physical conditions, in stellar convection zones. As mentioned previously, supergiant stars like α Orionis (Betelgeuse) would be expected to have very large convection cells, large enough so that only 3 to 5 would appear on the surface at a particular time (Schwarzschild 1975). Observations of variations in radial velocity, polarization, and intensity discussed by Weymann (1963) and Schwarzschild (1975) are consistent with the convective cell hypothesis. Direct observations of these cells should now be possible with newly developed diffraction limited large telescope techniques.

The extensive chromospheres observed in late type stars are good evidence for surface magnetic field activity, since the magnetic fields are presumably responsible for chromospheric heating (Osterbrock 1961). If the mechanism of Parker (1970) is correct, rotating convecting stars may be expected to have magnetic fields. Surface inhomogeneities, or "starspots," have been observed on a number of late type stars (Torres and Mello 1973, Bopp and Evans 1973). Recent observations of these stars by Bopp (1974) showed behavior qualitatively similar to solar active regions. Consequently, these stars present possibilities to

study the interaction of convective processes with magnetic fields. For example, the time evolution and structure of stellar active regions presents an opportunity to check the theory of Leighton (1964) by observing the stellar cycle process and checking its behavior with that expected from Leighton's theory. The observations of Olin Wilson at Hale Observatories on stellar cycles analogous to the 22 year solar cycle is a program of this type and when complete may provide this information.

Several key observations discussed in this introduction are now possible. These observations have been carried out and the results will be described in the remainder of this dissertation. A summary of these observational programs is given below.

1. Central to the problem concerning the convective nature of supergranulation is the question of whether a temperature difference between rising and falling gas due to convective energy transport is present. Previous observations in the visible tend to indicate no such temperature difference exists. The presence of a temperature difference and the size of this difference would help to differentiate between the counter cell hypothesis and the convective overshoot hypothesis. However, as suggested by Beckers (1968), any temperature structure in the sense of increases in cell centers and decreases at

cell boundaries, as theoretically expected, may be masked by a temperature increase within the magnetic field elements concentrated at the cell boundaries. The model of Chapman (1970) for the magnetic field elements indicates that observations in the infrared at $\lambda = 1.6\mu$, which is the solar opacity minimum, will represent levels below the magnetic field emission levels. Not only do observations of this nature offer the opportunity to disentangle the magnetic field effects from convective processes, it also presents a chance to study the field regions themselves. For if the strong magnetic fields reported by Harvey and Hall (1974) are real, a temperature decrease is expected in the levels immediately underlying the photosphere (Parker 1974). The data relevant to these questions were obtained from one and two dimensional intensity observations taken at the opacity minimum and higher level comparison wavelengths using the Kitt Peak National Observatory infrared spectrograph. The results of this study are reported in Chapter 2.

2. The direct observation of the dispersal of magnetic field by the supergranules from simultaneous magnetic and velocity data over the lifetime of a supergranule cell is of great importance as it would provide a test of Leighton's random walk dispersal

of magnetic fields by the supergranules. Long sequences of magnetic field and velocity observations would enable a determination of the lifetime and evolution of supergranules to be made directly from the velocities which more closely represent the convective phenomena being studied than do the emission network which has been used for this purpose. Additionally, a careful study of whether vertical velocities in supergranules only occur in magnetic field regions can be made. If this is the case, magnetic fields may play a far more important role in supergranule processes than just being moved around by supergranular motions. On several days in March, 1974, approximately 10 hour-continuous observations from which velocity, magnetic field, and chromospheric emission data were available were obtained on the Sacramento Peak Observatory Diode Array Magnetograph. This material and the results of this study are discussed in Chapter 3.

3. A verification of whether the variability behavior of late type emission line stars (dMe stars) is due to solar type magnetic activity can be of great interest. If the activity is solar, calculations concerning magnetic field generation and evolution can be made from the observed parameters and magnetohydrodynamic theory. Coupled with solar

observations and theory, a generalized lower main sequence convection zone and magnetic field model may be made. Observations to test the solar activity theory were obtained using a set of narrow band filters in a photometric study of several dMe stars at the Steward Observatory. The narrow band filters were chosen to represent levels high and deep within the stellar atmosphere. As stellar activity rotated into and out of view, the variations in light enabled a qualitative model of the stellar active regions to be made. This model was compared to the solar active region behavior and magnetic field strength calculations for lower main sequence stars were made. This study is discussed in Chapter 4.

CHAPTER 2

INFRARED OBSERVATIONS OF SUPERGRANULE TEMPERATURE STRUCTURE

Referring to the horizontal velocity flow first observed by Leighton et al. (1962) as "supergranulation" may well be misleading since the analogy between supergranulation and granulation suggested by the name is not complete. One of the most notable features of the granulation is the marked temperature difference between the hot rising center of the granule and the cooler falling boundary (Beckers and Parnell 1969). The temperature change of several hundred degrees reported by Bahng and Schwarzschild (1961) is consistent with the hypothesis that granulation is a convective flow pattern arising in the hydrogen convection zone and is responsible for carrying a sizeable fraction of the solar flux in the layers immediately beneath the visible photosphere. If the observed supergranulation is a direct counterpart of granulation, being a convective process arising in the helium convection zone (Simon and Weiss 1968), a temperature difference of several hundred degrees is also required for it to carry any fraction of the solar flux (Weiss 1968). Consequently, several studies have been conducted to observe this certainly detectable temperature change between center and boundary of supergranules (Simon

1966, Beckers 1968, Frazier 1970). Simon (1966) reported an intensity decrease which appeared to be present at supergranular boundaries. Beckers (1968) and Frazier (1970) were unable to find this but did report an apparent temperature increase of the order of 10K at supergranular vertices, the locations where material downflow had been observed by Frazier.

The lack of a significant temperature decrease, and indeed the possibility of a temperature increase in the downflowing portion of the supergranule is confusing. However, several explanations exist. Beckers (1968) attributed the observed temperature increase to the effects of magnetic field elements which coincide with the downflowing portions of the supergranule. The model of Chapman (1974) for magnetic field regions is consistent with this hypothesis, since a significant temperature increase in these regions exists from the photosphere up. Additionally, Liu (1974) has observed in white light a bright pattern which corresponds to the chromospheric emission network. An alternative possibility is related to the assumption that supergranulation is a directly observable convective process. It is possible that the observed velocity flow is only an overshoot of a much deeper convective process, or perhaps a counter-rotating reflex motion due to the deep convection (Spiegel 1966). In these cases, the observed velocity field may be carrying only a small fraction of the

solar flux, producing unobservably small temperature changes. Clearly, the magnetic field effects must be separated from possible convective temperature structure to study these questions.

One method of attacking this problem is to compare temperature information from different layers of the solar atmosphere. The deepest observable layer is roughly 30 km ($2/3$ of a density scale height) deeper than the visible photosphere, access to which is provided by infrared observations. At $\lambda = 1.63\mu$ a minimum in the opacity exists caused by the rapid decrease of H^- as an opacity source at this wavelength. Model atmosphere calculations of Gingerich et al. (1971) for the HSRA atmosphere reveal that this layer is close to 7000° in effective temperature. At the higher temperatures and densities present in this layer, the effects of magnetic fields differ from those in the overlying levels and the Chapman (1974) model shows a temperature decrease would occur at this level in the magnetic field regions relative to undisturbed regions. Additionally, this atmospheric level is at the boundary of the convection zone where radiative effects are minimized, so that observations at 1.63μ may be expected to represent conditions close to those within the outer convection zone.

This chapter describes a series of observations taken in the infrared with the Kitt Peak National Observatory infrared spectrograph, from which data horizontal

temperature variations in the deep photosphere are investigated.

The Infrared Spectrograph and Observations

The infrared spectrograph system consists of a conventional grating spectrograph used in conjunction with the f/60 west auxiliary image of the McMath Solar Telescope with an image scale of 6"/mm at the spectrograph entrance slit. The system was used in a single pass mode with a liquid nitrogen cooled InSb cell as the detector at the spectrograph exit slit. The data are recorded on magnetic tape interfaced via a XDS Sigma 2 computer. The maximum data acquisition rate of this system is one sample per millisecond.

For this program a 500μ by 500μ square entrance aperture was used in place of the entrance slit, providing a spatial resolution of the sun of 3". An exit aperture was added so that the spectral window was 1\AA at 1.6μ . Three wavelength regions were chosen for study. For the deep level continuum at 1.6359μ was isolated. Reference to the HSRA model atmosphere (Gingerich et al, 1971) revealed that the continuum near 1.17μ was formed at a level similar to $\tau = 1$ at 5000\AA , so it was chosen to represent the visible photosphere. In order to define the chromospheric emission network which coincides with the magnetic field elements at supergranular boundaries, a strong MgI line at 1.7108μ was

chosen. The core of this line has a residual intensity of .6 of the continuum and is formed near the temperature minimum. A summary including depth of formation, band-passes and other spectrograph information for these three levels is given in Table 1.

Table 1, Data on Bands Used for Infrared Observations

Wavelength (Å)	$\Delta\lambda$	Grating Order	Brightness Temperature	Depth of Formation (km)	Optical Depth
17108	.8Å	7	~4200K	~550	~.006
11730	1.2Å	10	6200K	0	1.0
16359	1.0Å	7	6800K	~25	1.9

Two types of observations were obtained for this program. The initial set of observations consisted of a series of drift scans in which the telescope drive was turned off and the sun allowed to drift across the entrance aperture. Each series of observations consisted of twelve such drift scans, four at each wavelength. Each scan contained 8192 17-millisecond integrations. To obtain the 3" resolution corresponding to the aperture resolution eight individual integrations were averaged, so that the final scan was 1024 data points in length. The series of

twelve scans took a total of 20 minutes. Repositioning of the solar image after each scan was accomplished using a pair of limb guiders at the north and west limbs. The accuracy of this repositioning was $\sim 3''$ depending on seeing conditions. The instrumental noise level was measured from a scan in which the image was held fixed yielding mean noise per data point of $\pm .3\%$ for each of the three bandpasses used. Ten complete series including all three wavelengths were obtained in July and August of 1973.

This system can also be used to obtain two-dimensional information. Turon and Lena (1973) used the McMath telescope system to obtain 1.6μ pictures. In their data structures appeared which had a size scale similar to that of supergranulation (30,000 km). However, there was no way to compare those results with the position of the supergranular network or supergranule boundaries. Consequently an attempt was made to obtain two-dimensional pictures in the three wavelengths used for the one-dimensional data. This was accomplished using the equipment already described in conjunction with a rotating prism device designed by R. G. Allen of the Kitt Peak National Observatory. The prism rotated so as to scan a small portion of the solar image across the entrance aperture of the spectrograph. Orienting this device so that it moved the sun across the entrance aperture in a direction 90° to the drifting direction effectively produced a raster scan of a region on

the sun. Two-dimensional scans 3' by 20' with 3" resolution could thus be produced for each wavelength in a time span of 20 minutes. As with the previous data limb guiders were used to reposition the image after each scan. This system was in a preliminary state of development at the time of these observations which is reflected in the rather crude nature of the data.

Reduction of the Infrared Observations and Results

Visual inspection of the drift scan data revealed that small scale intensity variations on the sun of 3-5% were present in all three wavelength regions. However, these variations were not strictly repeatable from scan to scan and many of the features were difficult to follow in consecutive scans. Since the granulation pattern has a lifetime of about ten minutes, it is reasonable to assume that much of this variation was due to the changing granulation pattern. A four scan average in each wavelength removed some of this variation. The resulting average scans had variations of ~3% with apparent spatial size near the supergranular size (30,000 km). Since supergranulation has a well-defined spatial size and shows up very strongly in cross-correlation and autocorrelation studies (Simon and Leighton 1964), this form of mathematical analysis was chosen to investigate the question of whether the infrared data showed evidence of supergranular size scale.

The non-normalized autocorrelation function or autocovariance function is given by:

$$\text{A.C.}(\Delta X) = \int_{-\infty}^{\infty} f(X)f(X-\Delta X) \, dX \quad (2.1)$$

where $f(X)$ is the data field being analyzed. The autocorrelation function can be thought of as a "self-convolution" of the data where the resulting value, $\text{AC}(\Delta X)$, is the value of the data multiplied by itself under various relative shifts ΔX . If the data are periodic at a shift $\Delta X'$ corresponding to the periodicity, a local maximum in the autocorrelation function will exist at $\Delta X'$. The function is normalized so that its value at zero shift ($\Delta X = 0$) is one. The full width at half maximum (FWHM) of the central peak near $\Delta X = 0$ is a measure of the mean size scale of variations within the data. The autocorrelation function can be calculated using Fourier transforms following Bracewell (1965):

$$\text{A.C.}(\Delta X) = \int_{-\infty}^{\infty} |F(s)|^2 e^{i2\pi s\Delta X} ds \quad (2.2)$$

where $|F(s)|^2$ is the power spectrum or the amplitude squared of the Fourier transform of the data for which the autocorrelation is desired. The autocorrelation can therefore be used to determine the mean size scale and the existence of periodic structures like supergranules in the solar infrared intensity data.

The cross correlation (XC) function is similar in nature to the autocorrelation, and it is useful for comparing two different scans. The cross correlation function is given by:

$$\text{X.C.}(\Delta X) = \int_{-\infty}^{\infty} g(X)h(X + \Delta X)dX \quad (2.3)$$

As with the autocorrelation this can be written in terms of Fourier transforms:

$$\text{X.C.}(\Delta X) = \int_{-\infty}^{\infty} G(s)H^*(s)e^{i2\pi\Delta Xs}ds \quad (2.4)$$

where g and h are the data functions being correlated and G and H are their Fourier transforms; the $*$ denoting the complex conjugate. As with the autocorrelation ΔX is the shift between the two data sets. For perfectly correlated data this becomes the autocorrelation function. For completely uncorrelated data the cross correlation is zero or near zero for all shifts ΔX . If the cross-correlation is negative at some $\Delta X'$, it indicates an anti-correlation, in other words bright structures are correlated with dark structures at that $\Delta X'$ shift. Consequently, this function can be used on the infrared data to determine if bright structures in the higher levels correlate with bright structures in the lower levels or whether the bright structures in the higher level correlate with dark features in the lower levels.

Fourier processing of the data was accomplished using the CDC 6400 computer at Kitt Peak. The Fast Fourier transform (FFT) algorithms in the REDUCER data reduction package developed by J. Brault and C. Slaughter proved useful for this purpose. The uses and limitations of the FFT are explained in Brault and White (1971). The processing of the one-dimensional data is described below:

1. The original 8192 word data records were averaged over eight point means to produce a 1024 point record with 3" spatial resolution. For the cross correlations, four such scans were averaged to reduce the effects of short-lived granulation and seeing.
2. To eliminate solar foreshortening near the limb the data were registered, expanded, and interpolated to represent equal distances on the sun. This was accomplished by identifying the solar limb position as the point on the limb where the intensity first reaches one-half its maximum value. The expansion was made around the central point so that each point represented 710 km. The resulting 1024 data points covered the sun over a position angle $\pm 30^\circ$ from the center of the disk.
3. The averaged and de-foreshortened data were prepared for Fourier processing by removing mean limb darkening and apodizing the data so it went smoothly

to zero at the edges. The limb darkening was removed by fitting each data array with a second order least squares function and subtracting this function from the data. The purpose of these procedures was to eliminate high frequency effects in the Fourier transform such as ringing due to discontinuities in the data, and very low frequency structures resulting from systematic trends like limb darkening.

4. The autocorrelation functions were calculated with the REDUCER program in two steps. First, each scan was Fourier transformed to produce 513 complex values for each 1024 point data record. The amplitude of each complex element was computed by adding the squares of the real and imaginary parts of each number. To obtain the autocorrelation this power spectrum was inverse Fourier transformed. The resulting 100 autocorrelation functions were added together and normalized so that the autocorrelation peak at zero shift was equal to one.

Figure 1 shows the summed autocorrelations for the three wavelengths. The scale is in ΔX in the sun, where 1 unit is 712 km. The prominent central peak in the autocorrelations for the two deeper levels falls to zero with a FWHM of 3600 km. This is significantly larger than the

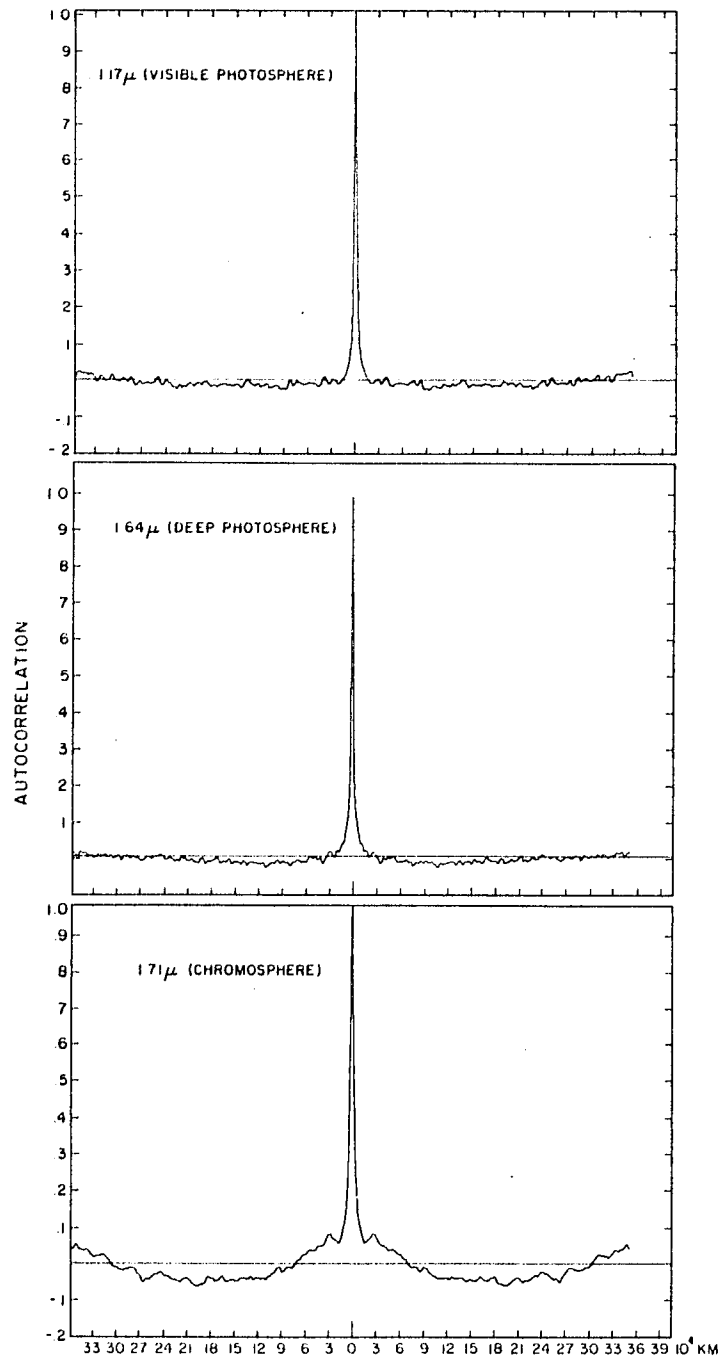


Figure 1. Summed autocorrelation functions for the one-dimensional infrared data,

granulation size but substantially smaller than the super-granular scale size (30,000 km). In the chromospheric level data the central peak has a FWHM of 4500 km, thus the predominant size structures in the chromospheric region are slightly larger than those in the deep photosphere. Since these FWHM sizes are somewhat larger than the telescope resolution ($3'' = 2200$ km) they probably represent real solar features.

Significant secondary maxima show up in the autocorrelation of the chromospheric data. The shift on the sun which these peaks represent is 28500 km with an autocorrelation coefficient of .09 the maximum value. These peaks are quite broad and are probably due to the chromospheric emission network since similar peaks were often seen in chromospheric intensity data by Simon and Leighton (1964). Evidence for corresponding secondary autocorrelation maxima also appears in the photospheric and deep levels. A small peak about twice as large as the mean noise in the autocorrelation with a coefficient of .02 the autocorrelation maximum is visible at a shift of 28500 km in the deep data. A similar but weaker peak is visible in the intermediate level data at the same shift. However, since the strength of this peak is not above the mean autocorrelation noise little significance can be attached to its existence. Several interpretations of these results are possible. The presence of the autocorrelation maximum at 28500 km in the

deepest level is evidence for noticeable supergranular effects at that level since it corresponds exactly in position to the secondary maxima in the chromospheric autocorrelation. As it is well known that the chromospheric emission structure defines the supergranular boundaries (Simon and Leighton 1964), structure of exactly the same size scales in the deep layers may also be associated with supergranulation. However, it is unclear whether this behavior is due to a generalized temperature change across the supergranule, or whether it is caused by the detailed behavior of the magnetic field elements themselves. Both possibilities are consistent with the strengthening of the effect in the deeper layer, as compared with the intermediate level. If a generalized temperature structure is present it could be expected to manifest itself more strongly in regions closer to the convection. Conversely, the magnetic field element model of Chapman (1970, 1974) predicts a very small temperature differential between the field region and non-field region in the visible photosphere, and a large ($\sim 50-400^\circ\text{K}$) temperature decrease for levels a scale height deeper.

To determine the detailed temperature behavior the cross-correlation method was tried. In order to reduce correlations due to short-lived granular effects the four scan data sets for each wavelength were averaged to produce a single scan in each bandpass. It was found that the cross

correlation functions between the different wavelength arrays in each data set were far too noisy to interpret, so the data for the 28 observations in which all three wavelengths were available were averaged to produce single cross-correlation functions. The results for the three wavelengths are displayed in Figure 2, with the axes representing the same parameters as the autocorrelation functions. As before, the curves were normalized so that the central cross-correlation maxima were unity. The necessity of averaging the cross-correlations to reduce the noise makes it difficult to determine mean sizes of correlated structures, since there is undoubtedly imperfect registration between the scans in a given set. Differences in registration would shift the cross-correlation maximum in the X direction resulting in smearing the maximum over a larger width than the structures represent. However, several features are notable in the cross-correlations. It is clear that the two deeper levels correlate much better at zero shift than the high level correlates with either of the deeper levels. This can readily be seen in Figure 2 where the central peak in the deep vs. intermediate cross correlation is roughly thirty times the mean noise, while in the high vs. intermediate and deep levels the peak is only a factor of ten larger than the mean cross-correlation noise. The most interesting feature in these functions is the anticorrelation of the high level vs. both the deeper

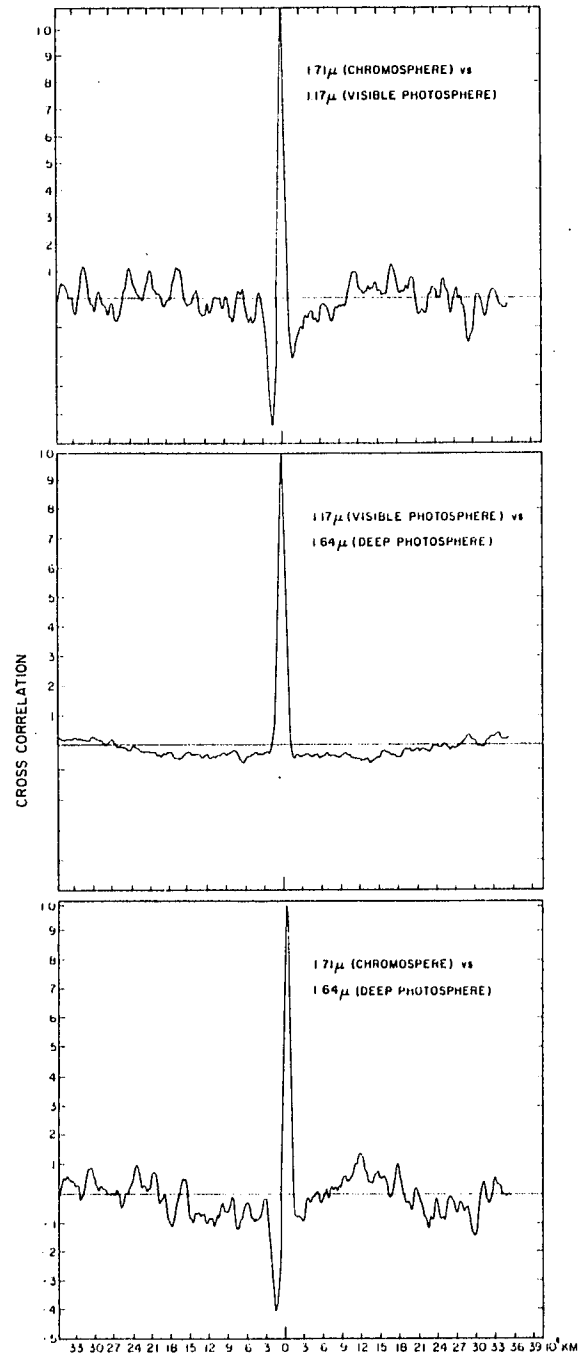


Figure 2. Summed cross-correlation functions for the one-dimensional infrared data.

levels at around 18,000 km. A negative correlation such as this would be expected at around half the supergranule size if there was a general temperature structure (i.e., cell center bright, cell boundary dark, or vice versa) of supergranular scale. However, the lack of any secondary maximum at 30,000 km in any of the cross-correlations and the absence of an anticorrelation at a similar shift in the deep vs. intermediate cross-correlation suggests that these secondary minima may be spurious since any structure against which the high level data were correlated in both the lower levels would be expected to show up in the cross-correlation of the two deep levels. A possible explanation of the observed behavior is that the strong correlation of the two lower levels is due to groups of persistent granules which correlate over time spans of 20 minutes. Long-lived granular patterns have been observed by Labonte and Simon (1975) so this is a possibility. Since granular contrast is much lower in the chromosphere, only weak correlations would be expected with the deeper level, as observed. Additionally, small temperature differences may be present in the chromosphere above long-lived granule fields which may explain the negative correlation in the cross-correlation. The inconclusiveness of the cross-correlation analysis makes it necessary to investigate other means of analysis.

If a large scale temperature structure exists in the supergranule, it would be expected to show in a plot of

intensities in one wavelength against the intensities for the same points in other wavelengths. For a generalized supergranule temperature structure bright, hot rising gas in supergranule centers would be expected to correlate in both the deeper levels as would the dark cool falling boundaries. In a plot of intensity in one wavelength vs. intensity in another, this would result in a straight line correlation. Consequently intensity "scatter" plots were constructed for the data in each wavelength vs. the data in the other wavelengths. To more clearly exhibit the large amount of data present, the resulting scatter plots are displayed with contour levels in Figure 3. The plots show a lack of any obvious systematic behavior; however, this may be expected from the low degree of correlation in the cross-correlation function. There is a slight tendency for a systematic "bright correlating with bright" and "dark correlating with dark" between the two lower levels; however, this may well be the occasional correlation of long-lived granulation patterns. Almost no correlation of any type is seen between the high level and the two lower levels. However, the brightest features in the chromospheric data, presumably representing magnetic field emission elements, appear to be associated with slightly brighter than average points in the intermediate level, and with slightly darker than average points in the deep layer. This observation was borne out by a detailed study of

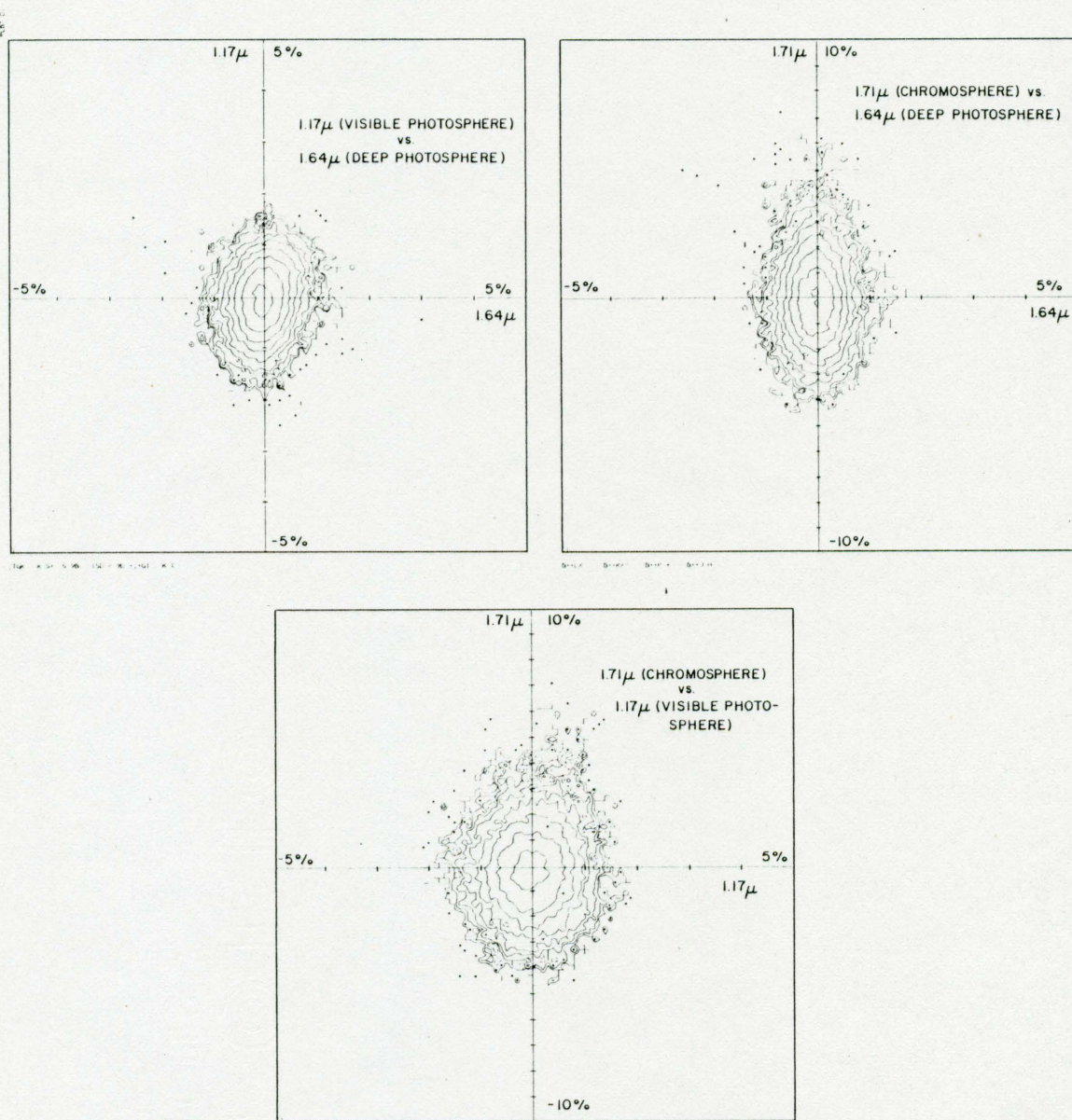


Figure 3. Contoured scatter diagrams for the one-dimensional infrared data.

individual sets of scans. Such behavior is to be expected if the predominant temperature effect of supergranular size scale in all levels of the observable solar atmosphere is the magnetic field element temperature structure. The brightest chromospheric points appear to be 5% brighter than the average with an apparent scatter of about 1%. These points seem to be associated with points about .4% brighter than the average in the intermediate level and .7% darker than the average in the deep level. These points appear to be scattered over about .7% in both of the deeper levels.

An alternative check on this result is provided in the two-dimensional data which are displayed in Figure 4. Due to the crude nature of the equipment, no extensive mathematical processing of the data was undertaken, other than a direct display of recorded intensities. The bright supergranular network can clearly be seen in Figure 4a, in which the chromospheric data, with a range of $\pm 5\%$ are displayed. These images crossed the edge of an active region which appears in the corner of the pictures. However, the deep level pictures with a range of $\pm 3\%$ in Figure 4b shows a dark network corresponding to the chromospheric emission network location. The strength of this chromospheric emission and corresponding deep cool areas matches that expected from the one-dimensional data. Since the pictures show no evidence of a general temperature structure it is concluded that most, if not all, temperature structure

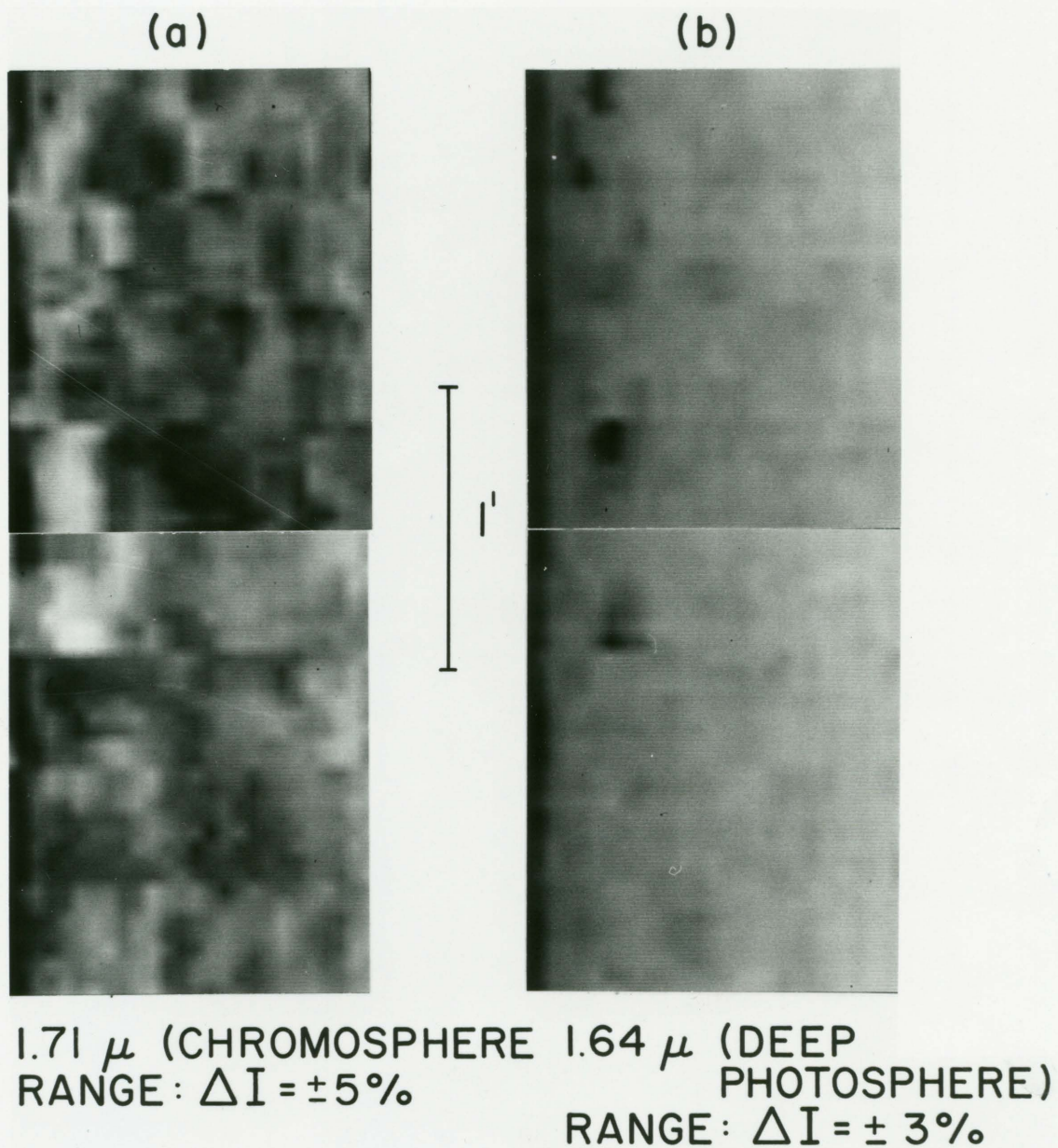


Figure 4. Two-dimensional pictures for the chromospheric and deep photospheric levels.

with a supergranular size scale arises from magnetic field induced temperature structure in all observable levels of the solar atmosphere.

Discussion of the Infrared Results

The results of this study are summarized below:

1. The autocorrelation studies of chromospheric level data verify the results of Simon and Leighton (1964) for a similar study. At this level in the infrared spectral region substantial intensity structure with a distribution similar to supergranular size scales is present. The mean size of this structure is 4500 km with an intensity increase of 5% over the surrounding regions. These conclusions are consistent with the hypothesis that the chromospheric emission network has caused the correlation.
2. The same study of photospheric and subphotospheric infrared data reveals that intensity inhomogeneities of an identical spatial scale are present in the deepest observable photosphere. A similar intensity distribution may be present in the overlying visible photospheric level. However, the photospheric intensity distribution is probably dominated by granular effects.
3. The cause of the photospheric structure of supergranule size appears to be small intensity

inhomogeneities exactly corresponding to the chromospheric emission elements. These photospheric "network" elements change their behavior from an apparent .4% intensity increase over non-network regions in the visible photospheric level, to a .7% intensity decrease over surrounding regions in the deeper level.

The mean size of the chromospheric emission elements of 4500 km with a spatial resolution of 2200 km is consistent with that obtained by Simon and Leighton (1964). In their work they obtained sizes of 5000 km for the network as seen in $H\alpha$ and $H\beta$ and somewhat larger sizes for the higher CaII K line network. It is probable therefore that the 1.72μ MgI line is formed between 200-500 km above the visible photosphere rather than around the higher $H\alpha$ and $H\beta$ levels, since the mean size of network elements is known to become smaller in lower regions. It is more difficult to derive sizes for the corresponding photospheric and sub-photospheric network elements since the majority of the photospheric intensity variations are caused by granular effects. However, from the pictures in Figure 4 they appear to be larger than a single resolution element (2100 km). As they arise in deeper layers it is also probable that they do not exceed the chromospheric network size (4500 km). A good

estimate which is consistent with the width of the auto-correlation secondary maximum in the deep layer is 3500 km.

An important parameter for the network elements is the temperature structure relative to non-magnetic regions. A measure of this temperature difference can be obtained directly from the observed intensity difference. Since the emission elements appear to be larger than the scanning aperture the temperature derived in this way represents a mean temperature difference inside the magnetic field element. The infrared observations are on the far red end of the Planck function for temperatures at all levels in the sun, thus the Rayleigh-Jeans approximation for the intensity I_λ is valid.

$$I_\lambda = 2\pi ckT\lambda^{-4} \quad (2.5)$$

The difference with respect to T at a given wavelength λ is:

$$\frac{dI_\lambda}{I_\lambda} = \frac{dT}{T} \quad (2.6)$$

Using this approximation, the observed values of dI_λ/I_λ , and temperatures from Gingerich et al. (1971), it is found that the temperature difference becomes approximately 200K for the chromospheric level, 25K for the intermediate level, and -50K for the deep level. These values are listed in Table 2. The values of magnetic field element temperature predicted by Chapman's (1974) model for a range of depths around the level of observation are also listed in Table 2.

Table 2. Derived Parameters of Magnetic Elements for the Infrared Levels

Wave-length	Height (km)	$\Delta I/I$	$\Delta T(^{\circ}K)$	ΔT (Chapman 1974)	ΔT (Corrected for Resolution)
1.72 μ	200-500	.055	230	300 $^{\circ}$ -1000 $^{\circ}K$	230-2300 $^{\circ}K$
1.18 μ	+10	.004	25	0-30 $^{\circ}K$	250 $^{\circ}K$
1.63 μ	-20	-.007	-50	-10- -60 $^{\circ}K$	-500 $^{\circ}K$

While these values are in good agreement, a correction may be necessary to include the possibility that the temperature change does not cover the entire resolution element. The observations of Dunn and Zirker (1973) indicate that while magnetic fields may apparently permeate large regions, the area where the magnetic field actually exists may be confined to small chains of points or "filigree." If it is assumed that the temperature effect is confined to the magnetic regions it is necessary to turn to the question of values for the magnetic field. By measuring the complete Zeeman splitting of lines in the infrared, Harvey and Hall (1974) inferred a true magnetic field strength of close to 1500-2000 G within magnetic field elements. In most magnetographs, for example the Kitt Peak instrument, the observed field strength will be directly proportional to the area over which the observations are smeared.

$$H_{\text{obs}} = H_{\text{true}} \frac{A_{\text{true}}}{A_{\text{obs}}} \quad (2.7)$$

Typically, field strengths of 100-200 Gauss are observed for 2" resolution in the photosphere. Consequently, the true area covered by magnetic fields is probably only 10% of the infrared system aperture in the photosphere. Using this number the temperatures in Table 2 have been corrected giving larger values for the temperature change in the photosphere. Chromospheric field areas are undoubtedly larger due to the increase in field size with height, thus chromospheric temperatures may be less sensitive to this effect.

The results of this study indicate that the only temperature structure in the photosphere of supergranular size is directly associated with magnetic field regions. This temperature structure is far too small to represent a direct convective process, since it is insufficient to carry any but a tiny fraction of the solar flux. If supergranulation is indeed a convective phenomenon, it must be a much deeper process than it is possible to observe. The observation that the only supergranular surface temperature effect is apparently connected with magnetic fields suggests that magnetic fields may play a significant role in any underlying convective process associated with the supergranulation. Thus, while these observations preclude

supergranulation as the primary form of energy transport in the visible photosphere, they are of themselves insufficient to determine the exact role supergranulation plays in the solar convective process.

CHAPTER 3

VELOCITY AND MAGNETIC FIELD OBSERVATIONS OF SOLAR SUPERGRANULATION

Following Leighton et al. (1962) the term "supergranulation" refers only to a horizontal velocity phenomenon within the solar photosphere. Any study involving descriptive parameters, such as lifetimes and sizes, must consequently deal with the velocities directly. The development of fast photoelectric magnetographs makes it possible to study the supergranular velocity flow, rather than secondary effects such as the location of chromospheric emission regions, to parameterize supergranulation. Several questions concerning supergranulation can therefore be investigated,

Supergranulation has been interpreted as a convective flow pattern (Simon and Leighton 1964; Leighton 1964, 1969; Simon and Weiss 1968) and consequently used in discussion of convective theory. An important parameter in these discussions is the lifetime of the convective "supergranular cell," since convective theory can provide estimates of the velocity and temperature structure within a convection cell if the lifetime is known. Several studies of supergranular lifetimes have been undertaken. In the studies of Simon and Leighton (1964) and Rogers (1970) the

chromospheric emission network as observed in strong absorption lines was used to define supergranular boundaries. Lifetimes close to 24 hours were obtained in this indirect manner. However, detailed studies of magnetic field elements by Smithson (1973) revealed that these elements do not change significantly in their positions over periods of approximately 36 hours. If magnetic field elements delineate supergranular boundaries as presumed (Simon and Leighton 1964) this observation would lead to supergranular lifetime estimates somewhat longer than 24 hours. Additional evidence for this hypothesis is provided from Livingston and Orrall's (1974) observation of long-lived magnetic features with supergranular appearance. These "cells" had lifetimes of 3-5 days and occurred within active regions.

Smithson (1973) suggested that the shorter lifetime derived from emission network studies was misleading due to the manner in which it was derived. Lifetimes in the previous studies were derived from mathematical cross-correlations. However, since the emission network is a "thin" system defining only cell boundaries, and not the cell itself, small changes in the shape of a cell will cause a large decrease in cross-correlation coefficients. This may produce a spuriously short lifetime compared to the real lifetime of the velocity cell. For this reason supergranule lifetimes are more appropriately derived from measurements

of the horizontal velocity flow which extend over virtually the entire cell.

Supergranule cell lifetimes are important for another reason. Leighton (1964, 1969) in his theory of the solar activity cycle used supergranular flows to disperse magnetic fields over the solar surface in a random-walk process. However, if the supergranule lifetimes are significantly longer than 24 hours as discussed by Smithson (1973), the motions due to supergranular flow are too small to provide for the observed magnetic field dispersal. Moreover, field motions have never been correlated with any material motions, supergranular or any other. Smithson (1973) observed an occasional rapid movement of magnetic flux elements, however, the frequency of these occurrences is insufficient to explain observed changes in the magnetic field pattern. His data appear more consistent with the total disappearance of magnetic field elements. Clearly it is important to determine whether the rapid movement and disappearance of magnetic elements is associated with changes in the velocity flow.

In order to determine mass flow rates within the supergranule, knowledge of the vertical velocity field is needed. Simon and Leighton (1964), Frazier (1970), Deubner (1972a), and Musman and Rust (1970) have reported vertical flows associated with supergranulation. However, only the vertical downdrafts associated with magnetic field elements

appear well confirmed. A corresponding vertical upflow in cell centers has not yet been shown convincingly. Accurate photoelectric velocity observations are needed to investigate these questions.

This chapter reports a time series of observations including simultaneous magnetic, velocity, and emission network information obtained with the Sacramento Peak Observatory Diode Array Magnetograph (Dunn, Rust, and Spence 1974). The results of this study will be discussed in light of the problems mentioned above.

The Sacramento Peak Observatory Diode Array System

The Sacramento Peak Diode Array system uses the solar image from the vacuum solar telescope. The Array itself consists of 512 diode detectors arranged in linear groups of 32 detectors. Each group can be physically placed in the spectrum at the exit focal plane of the Sacramento Peak Echelle Spectrograph. The spectrum has been magnified so that each diode detector sees a spatial element of 1" (optics are available for 2" and 1/2" as well). Corresponding spectral resolution ranges from $1/4\text{\AA}$ to $1/20\text{\AA}$ depending on the degree to which the diode detectors are physically masked. Light-intensity signals from the diode detectors are read and recorded on magnetic tape using the Xerox Data Systems Sigma 3 computer with two-dimensional scanning accomplished by moving the sun

across the spectrograph entrance slit. Each 32 detector group is placed in the core or wings of suitable spectral lines. Those groups in line cores are used to obtain spectroheliogram-type intensity data. Magnetic and velocity measurements are obtained from diode groups situated in opposite wings of absorption lines. Line shifts due to Doppler velocity shifts can be derived from changes in intensity ratios between the detectors in opposite wings of the absorption lines. In a similar manner line shifts caused by the Zeeman effect in magnetic regions can be observed. The wavelength shift with a longitudinal magnetic field between the right and left hand circularly polarized components in a simple Zeeman triplet absorption line and the non-shifted line is given by:

$$\Delta\lambda(\text{\AA}) = 4.7 \times 10^{-13} g_{\text{eff}} \lambda^2(\text{\AA}) H \quad (3.1)$$

where g_{eff} is the effective Lande g factor for a simple Zeeman triplet, H the line of sight magnetic field strength in Gauss(G), and λ the wavelength of the line in \AA .

Circular polarization modulation is obtained by passing the light from a magnetically sensitive line through a Potassium di-Deuterium Phosphate (KDP) electro-optical crystal. This device becomes a variable $\lambda/4$ plate under suitable applied voltage. In conjunction with a linear polaroid it will pass only right handed or left handed circularly polarized light depending on the sign of an

applied a.c. voltage. Thus, the Zeeman shift between the oppositely polarized components can be obtained by recording changes of intensity ratios between the detectors in opposite wings of the magnetically sensitive line as the KDP crystal is modulated. Since the circular polarization states and intensities in both wings of the line have been recorded, the same data can be used to obtain magnetic field and velocity information.

For this study, each observation covered a region 128" by 128" on the sun, scanned in two 64" by 128" swaths with a spatial resolution of 1". Each 1" square data point consisted of two readings of the 512 diode detectors, one reading for each polarization state of the KDP modulator. The resulting velocity, magnetic field, and spectroheliogram data are processed on the XDS Sigma 5 computer with programs for calibration and reduction written by D. Ruff and G. Simon. Each 128" by 128" observation consisting of 16,384 data points required 48 seconds to record.

The diode array configuration for a large portion of the data consisted of sixteen 32-diode groups, two groups placed in each wing of the FeI 8468Å line, two groups respectively in the core of H α 6563Å, the core of CaII 8542Å, the continuum at 6521Å, and the core and both wings of the HeI 10830Å line. A single data recording with the solar image held fixed thus covered a line of 64" on the sun. The FeI 8468Å line with a magnetic sensitivity of

$g_{\text{eff}} = 2.5$ was used for the magnetic and velocity observations. The remaining diode groups produced spectroheliogram-type intensity data, from which the location of chromospheric emission network was obtained. The CaII 8542 \AA line proved to be most useful for this purpose.

The use of the strongly magnetically sensitive line FeI 8468 \AA proved to present problems in observing velocities in magnetic regions as recently discussed by Frazier (1974). Recent observations of magnetic field strengths by Harvey and Hall (1974) in the infrared indicate solar magnetic fields may be as strong as 2000 Gauss. At such high field strengths the strongly magnetically sensitive $\lambda 8468$ line becomes Zeeman split to such a degree that the components are completely separated. The magnitude of this splitting and the effect on velocity observations can be calculated. Assuming a Gaussian line profile, simple Zeeman triplet splitting, and with the total magnetic field vector in the line of sight, Equation (3.1) can be used to show under which conditions velocity observations are valid. Table 3 lists the field strengths, true velocity magnitude, and the velocity which would be observed using the Zeeman split line. At field strengths larger than 1000 G it can be seen that meaningful velocity observations become impossible. Since most solar magnetic fields may be of this strength, this effect must be kept in mind. Examination of velocity data obtained with the $\lambda 8468$ line in a strong

Table 3. Effects of Magnetic Fields on Velocity Observations with the $\lambda 8468$ Line

True Velocity (m/sec)	Magnetic Field (G)	Observed Velocity (m/sec)
100	0	100
100	200	95
100	400	85
100	600	60
100	800	30
100	1000	5
100	1200	-10
100	1400	-40
100	1600	-45
100	1800	-50
400	0	400
400	200	390
400	400	340
400	600	300
400	800	220
400	1000	60
400	1200	-180
400	1400	-220
400	1600	-260
400	1800	-270
800	0	800
800	200	790
800	400	700
800	600	600
800	800	450
800	1000	200
800	1200	-330
800	1400	-470
800	1600	-520
800	1800	-530

magnetic field active region clearly demonstrated the problem. In the active region virtually no velocities were visible. While it is true that magnetic fields may inhibit velocities to some extent it is unlikely they would totally eliminate any material flow. Since important velocity flows exist within magnetic regions, particularly the vertical downflows at supergranular vertices (Frazier 1970) a velocity measurement free from magnetic field effects is highly desirable. Such velocities can be obtained from Doppler shifts of non-magnetically sensitive lines ($g_{\text{eff}} = 0$). A list of suitable lines has been published by Sistla and Harvey (1970). The diode setup was altered to include three of these lines in addition to the magnetic line $\lambda 8468$. Further, these lines were chosen to represent a range of heights of formation within the solar atmosphere. Height of formation estimates are available for these lines in a paper by November et al. (1975). The lines chosen were as follows: FeI 4065\AA for the deep line, FeI 5123\AA for the intermediate line, and FeI 5434\AA for the high line. Table 4 lists relevant data for these lines.

The calibration of the diode system is done using a series of rotating optical cubes located immediately preceding the diode detectors. The cubes are rotated under computer control to artificially produce a wavelength shift as seen by the diodes. The solar image is placed out of focus for these calibrations to produce a solar spectrum

Table 4. Data for Non-Magnetic Lines Used in the Vertical Velocity Investigation

Line	Spectrograph Dispersion (Å/mm)	Order	Range of Formation Heights for Wings of the Line
FeI 5123.730 ⁰ Å	10.507	45	-51 → 286 km
FeI 5434.418 ⁰ Å	9.368	42	-47 → 316 km
FeI 4065.388 ⁰ Å	12.314	56	-57 → 122 km

free from wavelength shifts due to solar surface structure. The intensities for the diode pairs in the left and right wings of the lines used in this investigation, I_L and I_R , are recorded for precisely known wavelength shifts $\Delta\lambda$. The resulting I_L/I_R ratio versus $\Delta\lambda$ is fit with a least squares curve for each diode pair. This curve can then be used to convert observed I_L/I_R values for solar features to wavelength shifts $\Delta\lambda$. A $\Delta\lambda$ value can be directly converted to a velocity, or in the case of magnetic observations for which $\Delta\lambda$'s in both circular polarizations are available, to a magnetic field using Equation (3.1) with the difference between the right hand and left handed circularly polarized $\Delta\lambda$'s. The accuracy of this method is limited in part by the accuracy of the I_L/I_R vs. $\Delta\lambda$ fit, which was generally such that a single observation is accurate to ± 70 m/sec.

The rotating cubes were additionally used to correct for spectrograph drift during the course of the observations. The cubes were moved so that the net $\Delta\lambda$ for all of the diodes, averaged over the entire 128 arc-second square, remained at zero.

Analysis and Results

Leighton et al. (1962) reported a vertical oscillatory velocity in the photosphere with a period of roughly 300 sec (5 minutes) and with an amplitude of approximately .5 km/sec. This phenomenon is of similar amplitude and size to the supergranular field. As it constitutes an interference to direct observation of the non-oscillatory flow pattern of supergranules it is necessary to remove the 300 second oscillations from these observations. This was accomplished by averaging together the signals from a sequence of individual scans (each taking 48 seconds of time) over one or more 300 second periods,

The digital nature of the two-dimensional data made it possible to use two-dimensional Fourier analysis. A two-dimensional Fast Fourier Transform (FFT) computer algorithm was written for this purpose. Since Fourier transforms have the property of separating in frequency space information on differing size scales they are ideal for supergranular studies. The various velocity phenomena,

granulation, supergranulation, and 300 sec oscillations have well-defined size scales so the information on each of these velocity fields is well separated within the frequency space of the Fourier transform. Thus to isolate supergranular effects the data are transformed and all frequencies representing size scales significantly smaller than supergranular flow (30,000 km) are removed, then the transform is inverted producing a filtered picture. However, these filtered pictures suffer from the disadvantage that small scale effects which may be associated with supergranulation, such as the downflows at cell boundaries, may also be removed. In conjunction with conventional means of analysis, such as cinematography of the time sequences obtained, the lifetime of the supergranular velocity flow, the transport of magnetic field, and the vertical velocity structure of the supergranule were studied,

The Lifetime of Supergranulation

Several sequences of observations covered roughly 10 hours each on a single region. While this time was less than the presumed lifetimes (20-40 hours) changes in some supergranules within the observed area may be expected. The data from 5 March 1974 covered 9-1/2 hours at radius vector $\rho = \frac{r}{R_0} = .6$. During that run the seeing remained consistently good, so the 5 March data were chosen for detailed analysis.

A movie was made from the original data. The only processing in addition to magnetic and velocity reductions consisting of time averages to remove the 300 sec oscillation effects. Each frame in the movie consisted of one 288 second average of six 48 second observations. The movie gives the impression that few changes occurred in the supergranular flow pattern during the 9-hour observation period. However, granular velocities were strong and interfered with the definition of supergranular cells. Additionally, when the seeing became slightly variable, as in the late afternoon, leakage of the 300 second oscillation was present due to the inconsistent seeing during the 288 second average. These problems were reduced using the two-dimensional Fourier filtering scheme described earlier to remove granulation and 300 second leakage. Figure 5 shows the unfiltered data and corresponding filtered data. Each frame consists of an average over four 300 second oscillations (20 minutes) or 24 observations. These observations cover nine hours on 5 March 1974. Averages over periods longer than 20 minutes were impractical due to imperfect guiding in the telescope.

It is apparent that a small scale velocity field exists in the unfiltered data. The noise in an individual observation derived from the accuracy of the calibration is ± 70 m/sec. The accuracy in the 24 frame averages shown should correspondingly be about ± 20 m/sec. The small scale

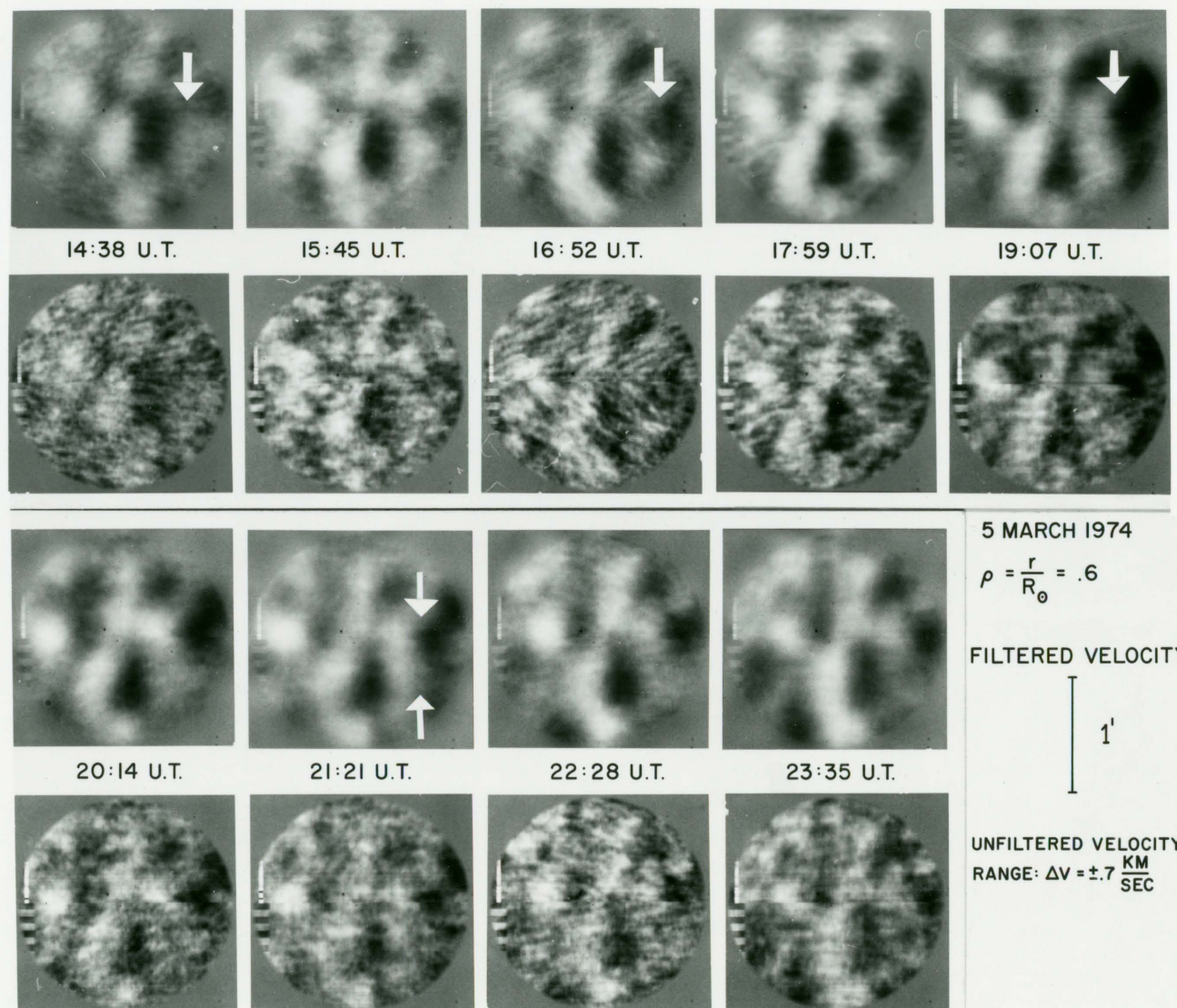


Figure 5, All day filtered and unfiltered velocity observations for 5 March 1974.

signals of 200-500 m/sec are therefore real and attributable to granulation. Since the granules have a mean lifetime of roughly 10 minutes, with some granules persisting for up to 30-40 minutes (Labonte and Simon 1975), it is impossible to remove the granular effects by time averages of reasonable duration. The alternative Fourier filtering which was used is superior for this purpose. This filtering was accomplished by setting to zero the frequency components in the Fourier transform that represented periodic spatial structures smaller than 8 arc-seconds. To avoid edge effects and ringing in the filtered frame the original data were multiplied by a circular function which went smoothly to zero at its edges. This accounts for the round pictures in Figure 5. It was discovered that the resulting pictures have a better appearance if a small fraction ($< .1$) of each high frequency component was left in the data. This artificial "grain" probably includes the high frequency components needed to correctly represent the more sharply defined supergranular edges.

From the time sequence in Figure 5 the impression of minimal change in the supergranular pattern derived from the movies is strengthened. Over the 9 hours covered by the data a significant change can be observed in only one of the approximately 9 supergranules present. In the early frames the supergranular flow in the right central part of the picture appears weak; however, later in the day the flow has

strengthened. Similar behavior was observed in the data of 11 March 1974 and 16 March 1974; however, only 1-2 supergranules in the region under observation appeared to change significantly in the course of the day's observations. The relatively infrequent changes observed are inconsistent with a mean lifetime of approximately 24 hours. If the lifetimes were that short, roughly 1/2 or 3-4 supergranules per day would be expected to change dramatically in an area covering 9-10 supergranules.

The lifetime of the supergranular flow can be derived from the two-dimensional cross-correlation function. This function is given by:

$$\begin{aligned}
 XC(\Delta x, \Delta y) &= \int_{-\infty}^{\infty} \int_{-\infty}^{\infty} f(x, y) g(x+\Delta x, y+\Delta y) dx dy \\
 &= \int_{-\infty}^{\infty} \int_{-\infty}^{\infty} F(u, v) G^*(u, v) e^{i2\pi(u\Delta x + v\Delta y)} du dv
 \end{aligned} \tag{3.2}$$

The latter function is the inverse Fourier transform of the cross product of the Fourier transforms of the data fields f and g under study. Where Δx and Δy are the shifts in x and y of the two data arrays, f and g , relative to one another. The cross-correlation coefficient at zero shift ($\Delta x = 0$; $\Delta y = 0$) is a measure of differences between two sets of data when they are perfectly matched, as such it can be used to derive lifetimes of structures present in time series of data. The mean lifetime is defined as the

time needed for the cross-correlation function to fall to $1/e$ of its original value at zero Δx and Δy shifts (Simon and Leighton 1964). The two-dimensional FFT program was used to calculate these functions for the velocity data of 5 March 1974 shown in Figure 5. The results are plotted in Figure 6 in which the normalized cross-correlation coefficients for zero spatial lag ($\Delta x = 0$, $\Delta y = 0$) are plotted against time. This result is independent of signals due to granular velocity structure, since the first data for which cross-correlations were computed are separated by 1 hour in time, during which the granular pattern should have completely changed. Figure 6 shows that the correlation fell to .7 of its maximum after 9 hours. A least squares fit to these points yielded a mean lifetime of 36^{+70}_{-12} hours.

In an attempt to follow supergranules through their entire lifetimes, a four day set of observations following a single solar region was obtained from 12-16 May 1974. Examination of the raw data gives the impression that certain elements of the chromospheric network and magnetic field network persist for the entire 4 day period as suggested by Smithson (1973). An attempt to follow the velocity cells by removing solar foreshortening was made. However, substantial variations in the horizontal velocity field caused by differing solar aspect are present and no conclusions regarding the velocity evolution in the data will be made in this investigation.

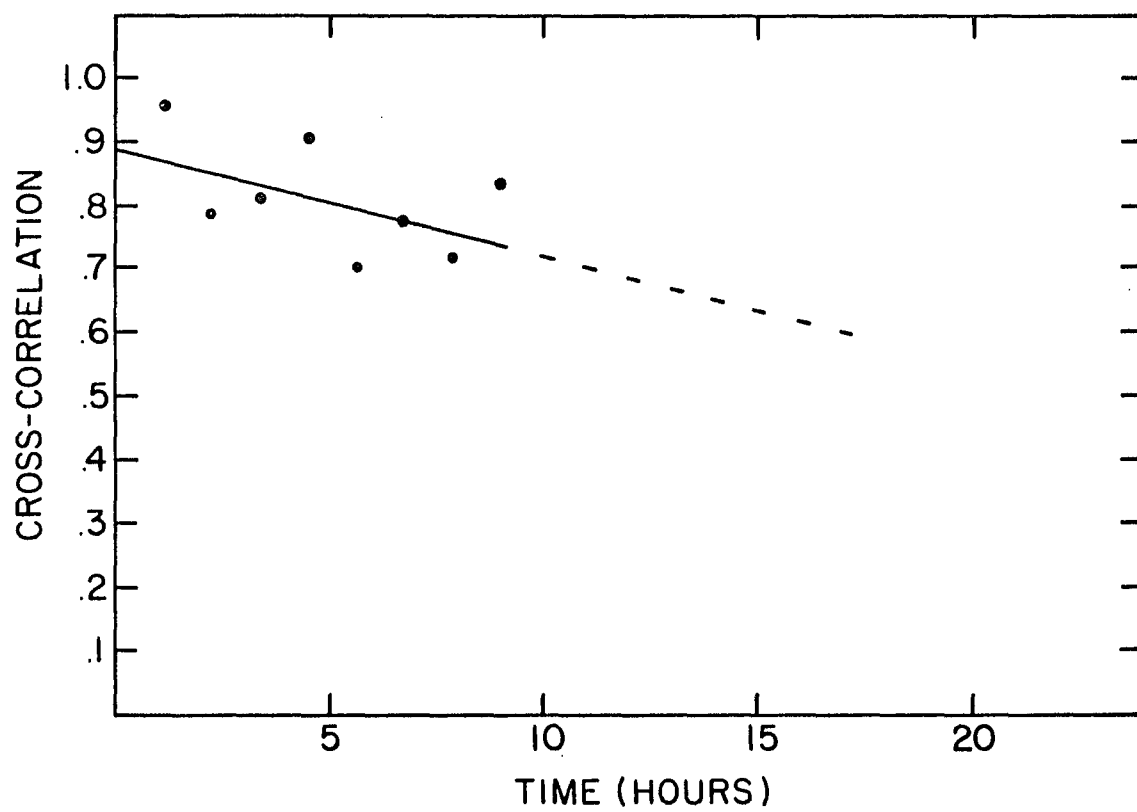


Figure 6. Cross-correlation in time for the velocity observations in Figure 5.

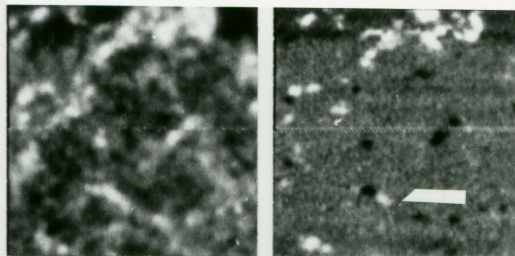
Horizontal Transport of Magnetic Field Associated with Supergranulation

Several of the longer data runs showed evidence of magnetic field motions. Just as for the velocity data, casual inspection of the movies leaves the impression of relative inactivity; however, an occasional horizontal motion of magnetic flux points occurred. As with Smithson's (1973) observations these motions were of several forms. The most frequent form of motion appeared to be a slow (< 1 km/sec) motion of existing flux points in which part of the relatively stationary flux point splits off from the magnetic element and moves away. Figure 7 shows an example of this phenomenon. In most cases the moving flux-element moved less than 5000 km and then dissipated. In a few cases of larger velocity ($.5$ km/sec $< v < 1$ km/sec) the daughter flux point moved 5000-10,000 km and remained visible for the remainder of the day.

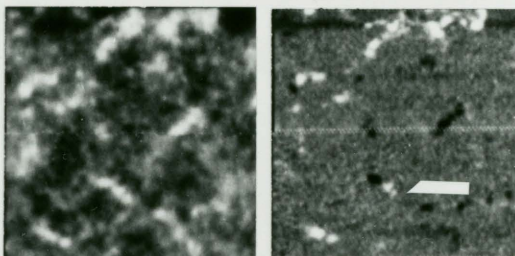
A more dramatic form of magnetic field motion was associated with the emergence of new flux. In the few cases of this behavior, new flux emerged and moved rapidly (1-2 km/sec) for a distance of 5-10,000 km. In the three single day's observations available no more than one, or in one case, two of these events occurred. Additionally, they always appeared in regions where changes in the velocity flow were underway. One such example is present in the data of 5 March 1974. As mentioned previously a velocity cell

20 APRIL 1974
CENTER OF DISK

1438 U.T.

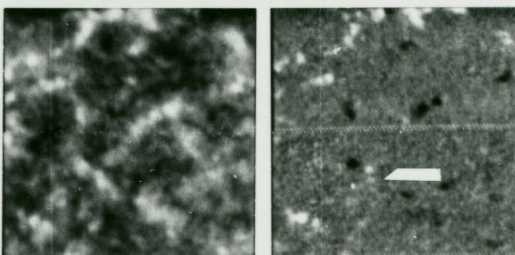


1511 U.T.

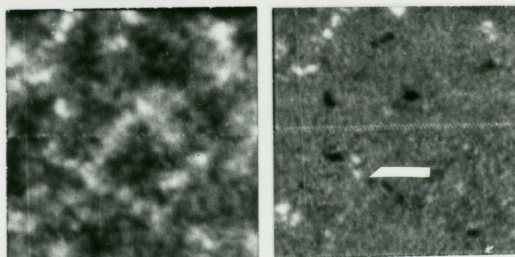


1"
|

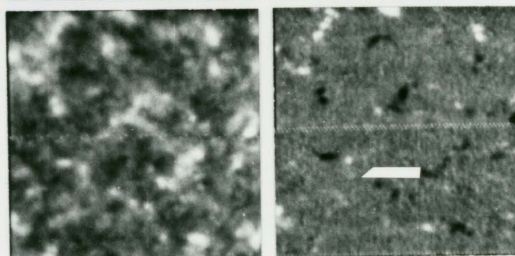
1643 U.T.



1745 U.T.



1902 U.T.



$\lambda 8542$

MAGNETIC

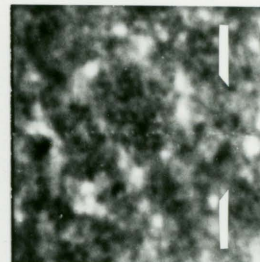
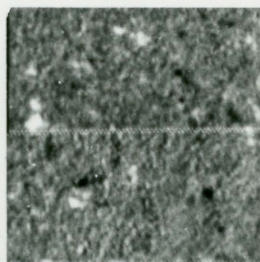
Figure 7. Example of slow form of flux motion: splitting of existing flux.

was observed to change during the day in the right central portion of Figure 5. During this period a small flux point appeared and rapidly moved to the boundary of the developing supergranule. Figure 8 shows this motion. Associated with this phenomenon changes in the chromospheric emission network occurred. In Figure 8 the $\lambda 8542$ intensity data for 5 March 1974 are also displayed to show these changes. In the data from early in that day the emission network in the region where the velocity cell changes appears chaotic. Later, when the velocity flow has strengthened, the emission network has arranged itself into a well-defined network "cell." During this period the emission network showed rapid and frequent disappearances, motions, and reappearances. Similar behavior was observed in other cases of cell development from the data on different days. In all three of these cases the cell strengthening may well represent the formation of a new supergranule cell.

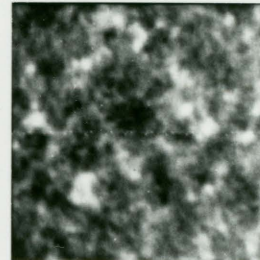
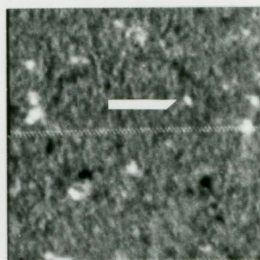
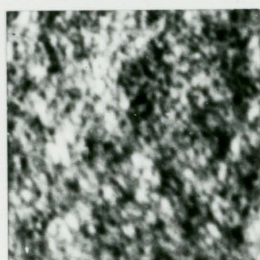
A more detailed study of the slower "splitting" type motions was possible using data taken at disk center. The observations of 8 April 1974 were chosen for this study. From a digital printout of the magnetic field strengths several of these motions were analyzed. The size of individual flux points seemed to be 3-6", somewhat larger than that expected from the hypothesis of very small flux elements smeared by seeing. However, the actual fields may be confined to the small photospheric "filigree" observed by Dunn

5 MARCH '74

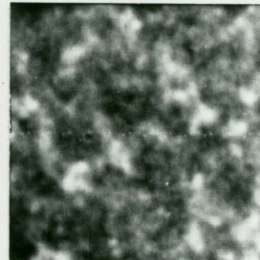
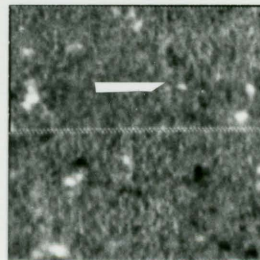
1628 U.T.



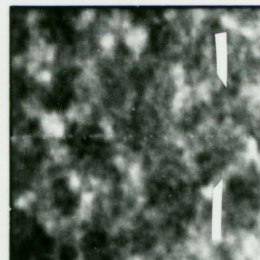
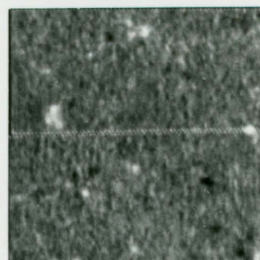
1716 U.T.



1804 U.T.



2311 U.T.



VELOCITY

MAGNETIC

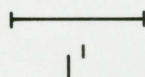
λ 8542
INTENSITY

Figure 8. Example of fast form of flux motion: the appearance of new flux.

and Zirker (1973). One of the more interesting motions was observed where two opposite polarity flux elements were separated by 7 arc seconds in the earliest frames. During the following six hours the larger flux element exhibited at least five splittings, as did the smaller opposite polarity region, with velocities ranging from .1-.3 km/sec. At the end of this period the smaller flux element had completely disappeared, apparently totally engulfed by the larger region. While it would be desirable to obtain values for flux changes during this period, there were substantial seeing changes and variations in instrumental magnetic sensitivity so it was impossible to assign quantitative values to these observations.

Vertical Velocity Flow Within the Supergranule

Vertical velocities within supergranules have been reported by several investigators. Simon and Leighton (1964), Tannenbaum et al. (1969), Deubner (1972a), Musman and Rust (1970), and Frazier (1970) have detected what appeared to be downdrafts at supergranular vertices. However, since Frazier (1970) was only able to observe these downdrafts in certain lines there exists the possibility that the downdrafts may not be real, but may represent an artifact of the differing line formation, or the magnetic sensitivity of the lines used in the magnetic field regions (Frazier 1974). Since the observed downflows occur only

within the flux elements concentrated at supergranular boundaries this latter suggestion is a distinct possibility. The group of non-magnetically sensitive lines is ideal for a study of this problem, since they present a range of heights of formation, from levels where magnetic regions differ little in temperature structure from non-magnetic regions to levels where a large temperature differential exists.

The disk center observations of 16 July 1974 were used for this portion of the study. During several hours of the morning during which these data were obtained, the seeing remained excellent (1 to 1.5"). As with the previous data 24 frame averages over 20 minutes were computed. A resulting 20 minute average velocity map for the wavelengths $\lambda 4065$, $\lambda 5123$, $\lambda 5434$, and $\lambda 8468$ is shown in Figure 9. Also shown in this figure are the filtered images with the granular velocities removed, as well as the simultaneous magnetogram. In the velocity data a large scale pattern, which shows especially well in the filtered images, is apparent. While this pattern appears to have a supergranular size scale, the mean velocity signal is only slightly higher than the noise level. Several methods were used to sort out the true nature of this pattern.

Observations obtained twenty minutes later during the same run were compared with the earlier data to see if the same velocity structures remained. While a similar

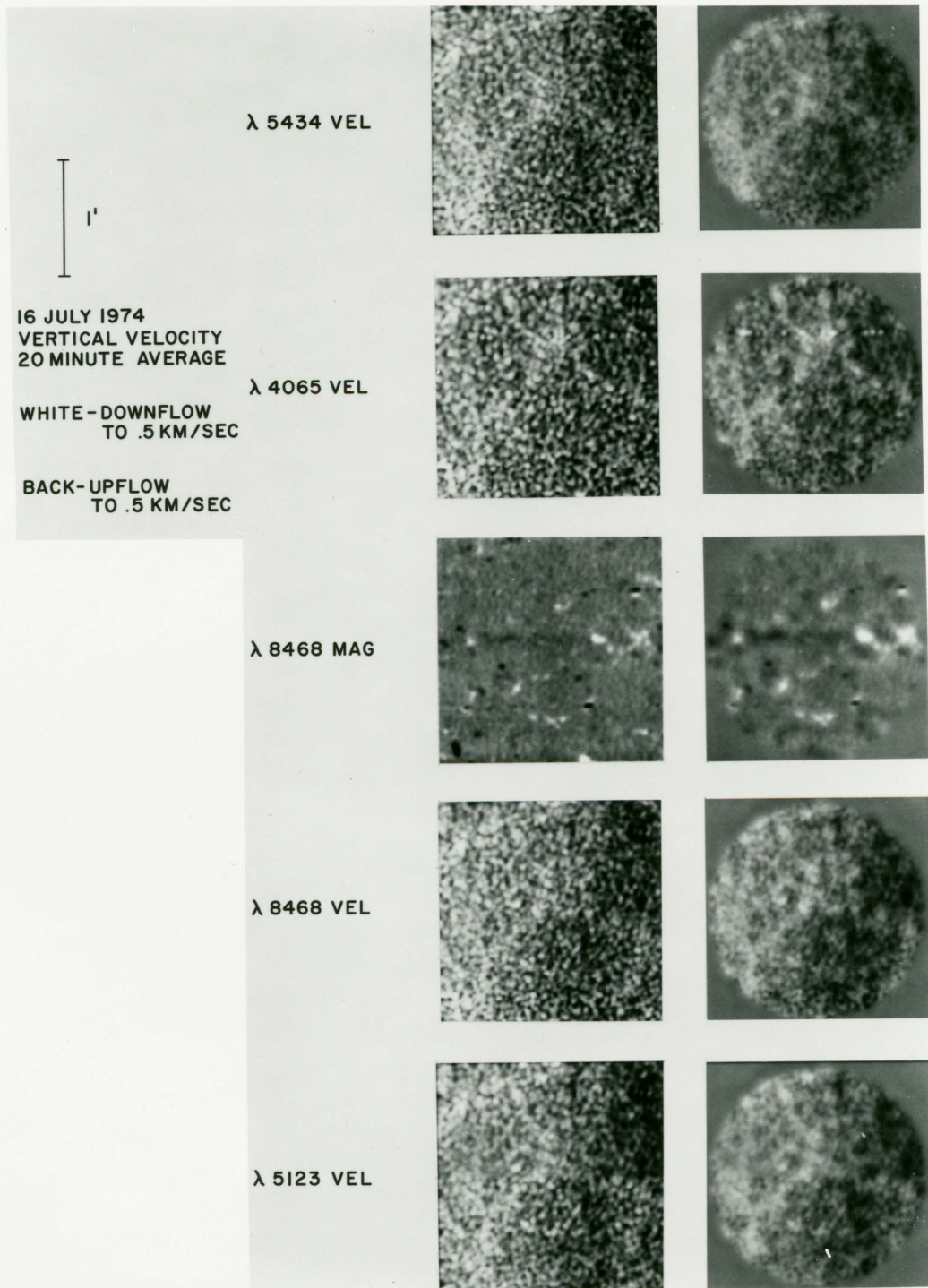


Figure 9. Filtered and unfiltered velocities in different lines from 16 July 1974.

large scale velocity pattern was evident, detailed agreement was only partial. Consequently other methods were attempted to study the results,

As mentioned previously, magnetic field elements have been observed to define the vertices of the horizontal supergranule pattern (Simon and Leighton 1964). A comparison was therefore made between the magnetic field and velocity observations. Only those velocity features which appeared on both consecutive 20 minute time averages were used, since supergranular motions should persist over substantially longer periods. Figure 10 shows the result of this procedure, with all velocities less than a threshold of 40 m/sec on both sets of data removed. For comparison the magnetic field structure is also displayed in Figure 10; as expected, the emission network is clearly outlined by the magnetic field. In each of the velocity frames an upflow of roughly 50 m/sec relative to the average velocity over the entire frame appears in the center of the emission network cells. However, downflows in magnetic field regions are apparent only in the $\lambda 4065$ data. Table 5 lists the velocities observed for each of the lines as a function of observed magnetic field strength. For small field strength $\lambda 8468$ seems to show downdrafts; however, as the field becomes progressively stronger this downflow diminishes in strength, until it disappears entirely. This behavior may

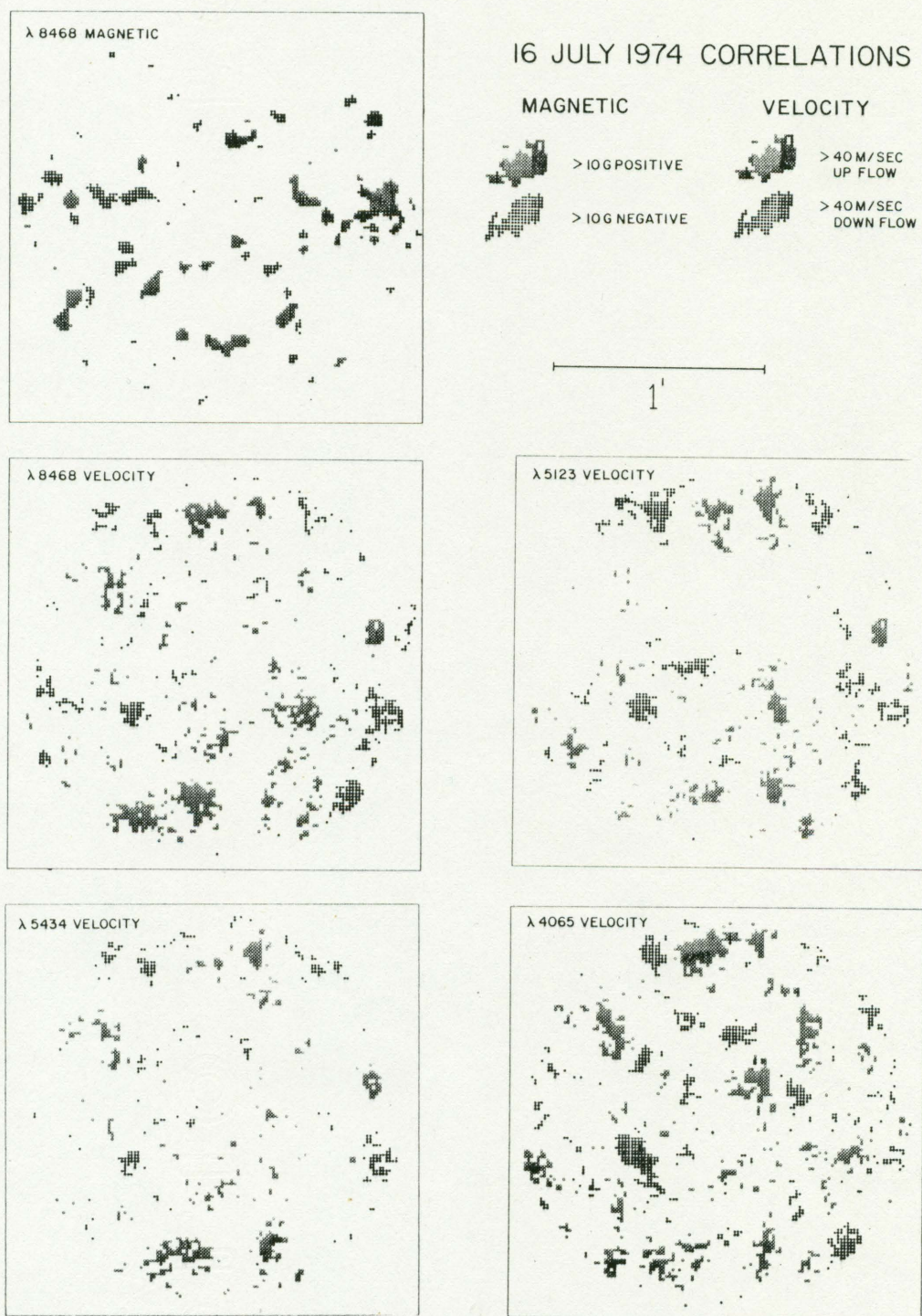


Figure 10. Velocities and magnetic fields above a minimum threshold which correlate over forty minutes in center of the disk data,

Table 5. Mean Vertical Velocities in Magnetic Field Regions
(Unfiltered Data-Downflows Positive)

Magnetic Field Threshold	Number of 1" Points Used	Velocity (m/sec)			
		$\lambda 8468$	$\lambda 4065$	$\lambda 5123$	$\lambda 5434$
5G	3140	3 ± 2	14 ± 2	2 ± 1	0 ± 1
10G	594	13 ± 4	49 ± 4	-3 ± 3	-4 ± 3
15G	217	15 ± 5	85 ± 7	-16 ± 5	-7 ± 5
20G	114	13 ± 8.2	105 ± 10	-33 ± 7	-6 ± 6
25G	67	3 ± 10	116 ± 14	-45 ± 10	-15 ± 8
30G	39	10 ± 14	153 ± 18	-70 ± 12	-23 ± 8
35G	28	0 ± 14	174 ± 22	-84 ± 14	-29 ± 10
40G	19	-9 ± 19	193 ± 26	-92 ± 18	-38 ± 13

be attributable to the magnetic splitting and distortion of this line profile as discussed previously,

Two-dimensional autocorrelation functions were used to verify these ideas. The two-dimensional autocorrelation of a data field $f(x,y)$ is given by:

$$\begin{aligned}
 A.C.(\Delta x, \Delta y) &= \int_{-\infty}^{\infty} \int_{-\infty}^{\infty} f(x,y) f(x-\Delta x, y-\Delta y) dx dy \\
 &= \int_{-\infty}^{\infty} \int_{-\infty}^{\infty} |F(u,v)|^2 e^{i2\pi(u\Delta x + v\Delta y)} du dv
 \end{aligned} \tag{3.3}$$

which is identical to Equation (3.2) if $g(x)$ is replaced by $f(x)$. As with the cross-correlation function, this may be calculated by inverse Fourier transforming the amplitude (power spectrum) of the Fourier transform of the data under investigation. This two-dimensional function can be converted to a one-dimensional function by summing the two-dimensional function over radial annuli. The resulting one-dimensional function is a measure of the correlation of the data field with itself for radial displacements. The mean size scale in the data is given by the half width of the central autocorrelation peak. Highly periodic data will show secondary maxima at displacements representing the mean size of the periodic structures. The radial autocorrelation function summed over 20 minutes for each of the wavelengths is shown in Figure 11. The sharp fall-offs of the central maxima with full widths at half maximum (FWHM) of 1500 km are probably attributable to granular signal. However, the more gradual fall-off out to 20,000 km and the weak secondary maximum at 30,000 km are strong indications of velocity structure on a supergranular size scale. The magnetic field autocorrelation function shown in Figure 11 is interesting since its FWHM fall-off of 3500 km is indicative of a mean size of magnetic elements of 4-7", significantly larger than the seeing size and in line with the visual appearance of the data.

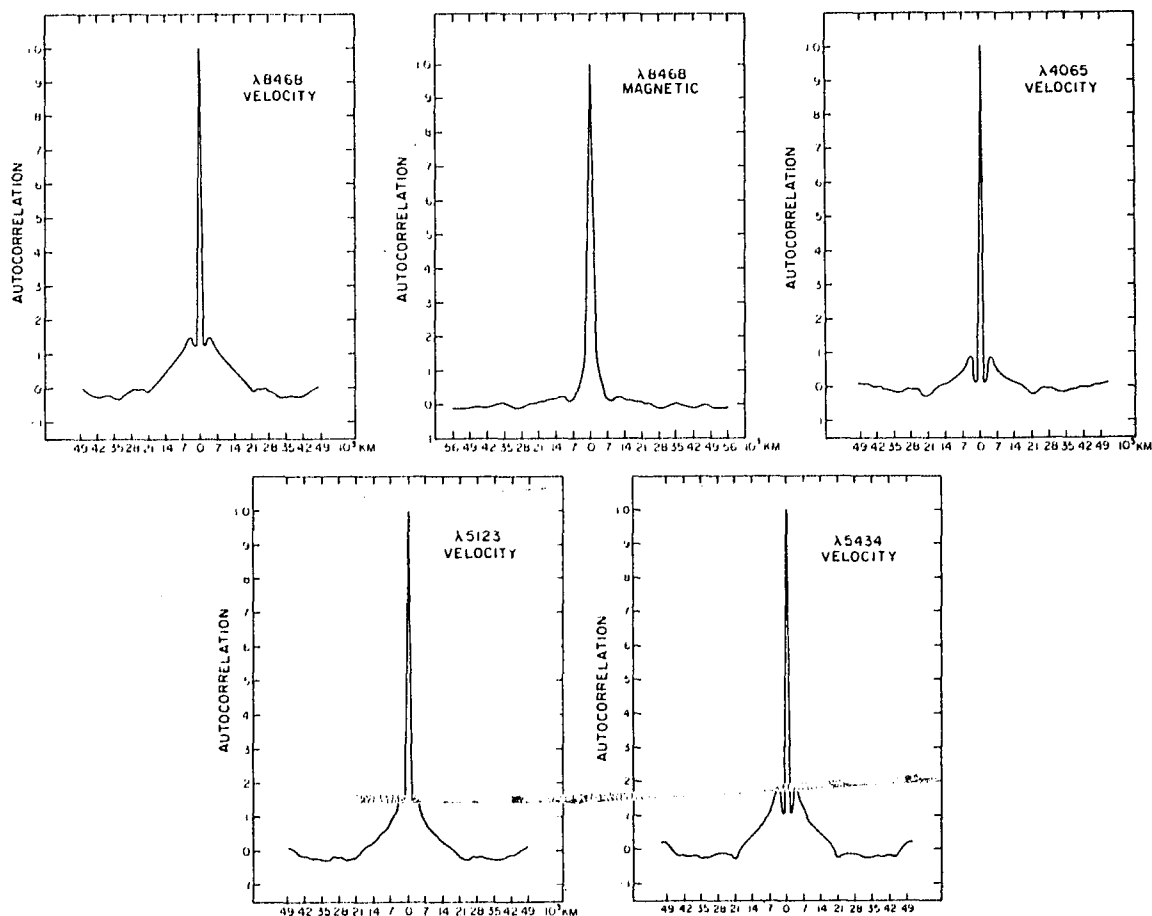


Figure 11. Radial spatial autocorrelations for the center of the disk data.

Discussion of Diode Array Results

The observational results of this study are summarized below:

1. Supergranule velocity cells have mean lifetimes considerably longer than the previously accepted value of 24 hours, with probable values near 36 hours. However, detailed several day observations are still needed to verify this lifetime.
2. No realignments of magnetic field elements already present at supergranular boundaries in a manner expected from Leighton's "random walk" mechanism were observed in any of the 10 hour runs which were studied. Since 10 hours is only a small fraction of a supergranule lifetime this negative result does not preclude the operation of supergranule random walk processes. However, two forms of magnetic flux motion were observed. Often an existing field element will split and a portion of the flux move away and dissipate. A second form of flux motion occurred when new flux appeared and moved rapidly in regions of changing supergranular flow. The motions are large ($\sim 10,000$ km) and rapid ($v \sim 2$ km/sec) in the latter process.
3. Magnetic field elements have an apparent size of 5" (~ 3500 km) in data with 1 arc second resolution,

This is larger than the seeing size and is presumably real.

4. Supergranules may exhibit an upflow of ~ 50 m/sec in the center of each cell; however, this observation needs to be verified with higher accuracy data. A corresponding downflow of ~ 200 m/sec is observed in magnetic field regions at the boundaries of supergranules. However, this downflow is only observed in the most deeply formed line. The disappearance of this downflow when observed in strongly magnetically sensitive lines is consistent with the hypothesis that strong fields ($B \sim 1000\text{G}$) are present within these regions.

The longer lifetimes of velocity supergranules indicated from this work match Smithson's (1973) values for lifetimes obtained from magnetic field elements. As shown by Smithson this value is too small by a factor of two to explain the observed diffusion of active region magnetic fields as a random walk process due to supergranular motions. The slow breakup of magnetic field elements is difficult to explain in terms of any surface motion. However, this behavior and the sudden emergence of new flux in a supergranule appears more consistent with a model similar to the "flux-rope" model of Piddington (1975). It may well be true that strong subsurface magnetic fields

dominate convective motions to a far deeper level than previously thought. If surface magnetic flux strengths are as large as 2000G, subsurface fields may be concentrated to even larger strengths by convective motions. Thus, if the supergranule is roughly 10,000 km in depth (Mullan 1971, Simon and Weiss 1968), as predicted from theoretical considerations, the magnetic field might constrain the convective flow to a considerable degree as suggested by Wilson (1972b) for sunspot regions. The observation of infrequent motion of existing flux elements would support the idea that magnetic fields are intimately tied to a single convective cell. Clearly, detailed convective analysis including the effects of strong magnetic fields is necessary.

Chapman (1974) and Frazier (1974) have suggested that the observed downflow at supergranule vertices may be due to line profile changes in the magnetic field regions caused by heating in the low chromosphere. Since the lines used in part of this study were chosen to represent heights where this effect shows a range of importance, this hypothesis can be checked. The three non-magnetic lines were studied using a LTE computer program developed by R. W. Milkey for the KPNO CDC 6400 computer. The line profiles for these lines are provided in the KPNO Preliminary Solar Atlas (Brault and Testerman 1973). The profiles were matched using the HSRA model atmosphere (Gingerich et al. 1971) in the computer program described above. These

profiles were then compared to line profiles calculated for the magnetic field region using a model atmosphere for these regions supplied by Chapman (1970, 1974). The resulting line profiles are shown in Figure 12. As expected, the deeply formed wings are little effected by this change. However, the cores of $\lambda 5123$ and $\lambda 5434$ are formed in high enough levels so that the facular temperature change is significant. In each case the flat bottom of the profile signifies formation above the temperature minimum. At the least non-LTE conditions hold, the LTE conditions fail, and a greatly flattened core profile is expected for these two lines; also the possibility of a central reversal in the line is present. Since calibrations were obtained in non-magnetic regions the net effect of this profile change and possible central reversal would be to record substantially smaller velocities than are actually present. Since the velocities listed in Table 5 actually appear to become more negative for the $\lambda 5123$ and $\lambda 5434$ lines with increased field strength, it is probable that this effect is present. As the $\lambda 4065$ line shows no significant profile changes in the magnetic region it is reasonable to claim it is producing real data concerning velocities present in magnetic field regions. This leads to the conclusion that the downflows of 200 m/sec observed in these regions are real.

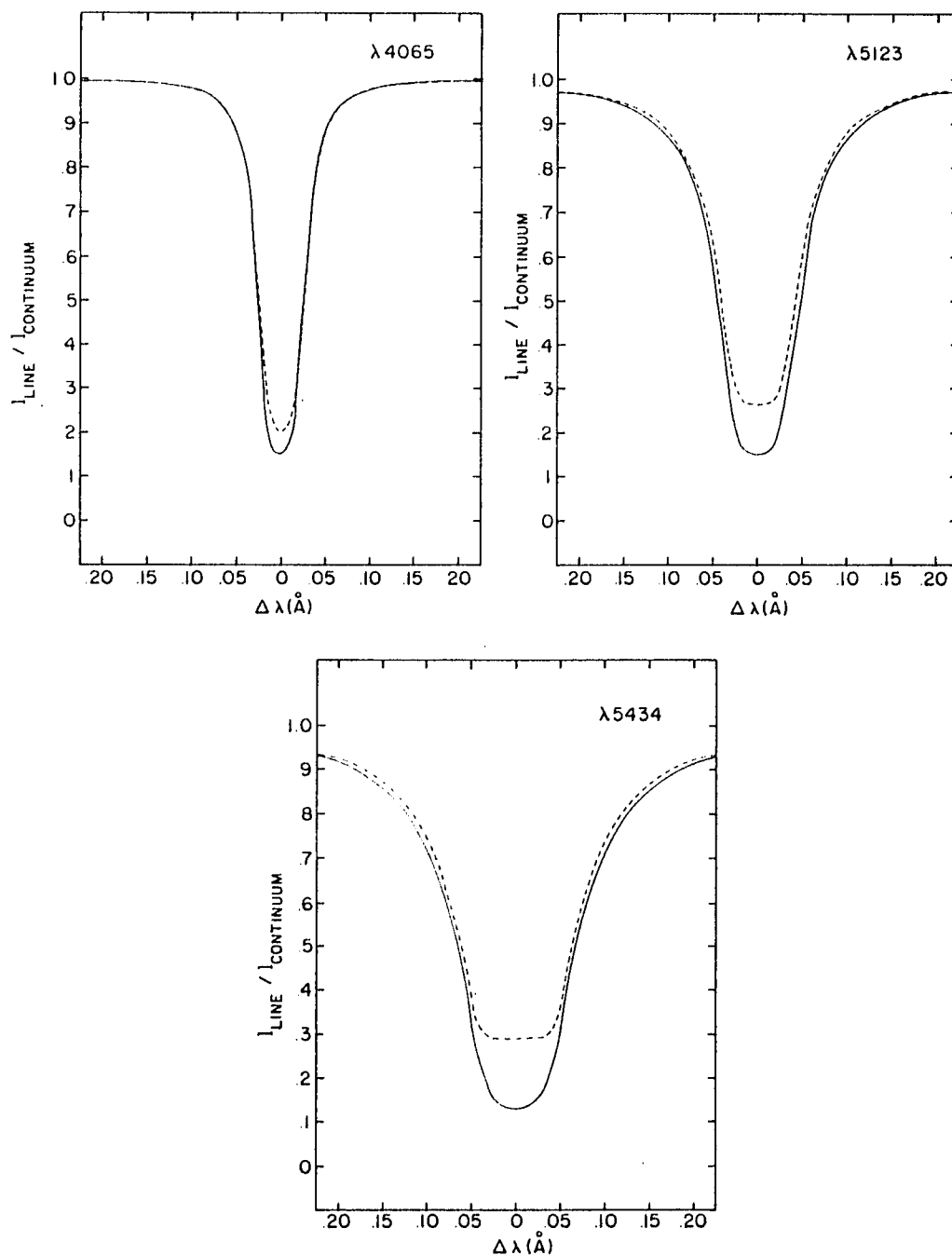


Figure 12. Line profile calculations for the non-magnetic lines with facular and non-facular atmospheres.

CHAPTER 4

STELLAR CONVECTION: THE dMe STARS

Broad-band photometry of red dwarf emission line stars (dMe stars) by Krzeminski (1969) and others has revealed quasi-periodic variations in many of these stars. These variations have periods of several days, the amplitudes generally do not exceed .3 magnitudes, and both the amplitude and phase of this behavior vary in an irregular manner over time spans of weeks (Krzeminski 1969). Spectroscopically, the dMe stars show relatively normal M type spectra, with the exception of strong lines such as the CaII H and K lines and often the Balmer lines which appear in emission. Many and possibly all of the dMe stars are flare stars (Kunkel 1973). The radio and optical energies in these flares are approximately 10^3 to 10^4 times larger than solar flare energies (Lovell 1971). Compared to the class of dwarf M stars as a whole, the dMe stars exhibit several interesting properties. While many dMe stars are very young objects, some very old and Population II stars also exhibit dMe characteristics (Veeder 1974, Greenstein and Arp 1969). Additionally some dMe stars, for example, YY Gem and BY Dra are close binaries, and all dM stars later than M5 are dMe stars (Joy and Abt 1974). A recent important result is that

the dMe stars appear to rotate faster than non-emission line M stars, with rotational velocities consistent with the observed several day photometric period (Anderson 1974).

Several models have been proposed to explain the dMe behavior. Evans (1971) suggested that the stars were close binaries and attributed the variations to clouds of material temporarily located at the Lagrangian points. Kron (1952), Chugainov (1966), Krzeminski (1969), and Evans (1971) have suggested that the variations were due to non-uniformities on the stellar surface or "starspots" which are brought into and out of view as the star rotates with a period of several days. This model adequately explains the changes in phase and amplitude, attributing them to the formation and destruction of starspots over time scales of several weeks on different parts of the star. The quantitative models constructed by Bopp and Evans (1973) and Torres and Mello (1973) require dark spots several hundred degrees cooler than the surrounding photosphere covering approximately 10% of the stellar surface. As with the sun, flares on the dMe stars seem to be associated with these spots (Bopp 1974). This model is particularly appealing since it is in many respects qualitatively similar to solar activity. However, the spots and associated variations are greater in extent and scale than those on the sun.

If the analogy to solar behavior is adopted it becomes clear that the spot model is somewhat of an

over-simplification. Solar spots, while appearing as dark, cooler regions in the photosphere, are associated with substantially larger chromospheric emission regions (see Zirin 1966). These emission regions are easily visible as bright patches in narrow-band photographs of the sun taken in bandpasses which show conditions high in the solar atmosphere.

It is thus of great interest to determine if dMe stars exhibit phenomena similar to the sun's active regions. If the dMe star activity is caused by solar-type active regions rotating into and out of view, it might be expected that photometric observations in a deep photospheric band would show a decrease in intensity as an active region rotated into view. The decrease in light caused by the dark cool spots should be accompanied by an intensity increase in a photometric band representing the stellar chromosphere; this increase originating in the chromospheric emission regions surrounding the spot. However, if the dMe light variations are the result of optically thick material at the Lagrangian points obscuring the stellar surface, as proposed in Evans' "grey veil" model, light variations in a given photometric band would be expected to correlate with all other bands regardless of the level in the stellar atmosphere which is represented.

The Narrow Band Observational Scheme

Broad-band photometry is not useful in attempting to differentiate between chromospheric and photospheric effects in dMe stars since the opacity in these late-type stars' atmospheres varies substantially over the filters' bandwidths. The light from the deep photospheric layers, possibly exhibiting the effects of a dark cool spot, may mask the effects of the higher chromospheric emission. This emission would only be noticeable in the spectral regions of high opacity. Thus, it is necessary to observe the star in narrow spectral bands which should represent specific levels in the stellar atmosphere. In this program, four narrow-band interference filters were used to isolate the desired spectral regions. These regions (wavelengths) were chosen to represent levels high, intermediate, and low within the stellar atmosphere in much the same manner as the band-passes in Chapter 2 represent different levels in the solar atmosphere. Table 6 lists the filters, their bandpasses, and approximate continuum optical depths corresponding to each bandpass. The filter bandpasses were chosen with the aid of the atmospheric opacity source calculations performed by Tsuji (1969), which include the effects of molecular absorption. These data reveal that a fairly low opacity region exists around 4800\AA . Since the opacity here was close to that at 8000\AA , the region of maximum energy output in dM stars, it was chosen to represent the photospheric

Table 6. Parameters of Bandpasses Used in the dMe Star Observations

Filter Wavelength	Full Width at Half Maximum	τ at 8000 Å that Corresponds to $\tau=1$ for This Filter	Filter Bandpass Description
$\lambda 5132$	38\AA	$\sim .1$	Continuum
$\lambda 4981$	24\AA	$.1 > \tau > .05^a$	TiO first overtone
$\lambda 4861$	15\AA	$< 10^{-2}$	H β
$\lambda 4839$	20\AA	1	Continuum

^aHighly temperature dependent.

level. The TiO (titanium oxide) bands become prominent around spectral type M0. They are interesting not only from the standpoint of the higher opacity they produce, but also due to the extreme temperature sensitivity of this opacity. Small increases in temperature would not only increase the source function but would also cause a weakening of the TiO band opacity. This would cause one to look deeper within the active emission regions, and see a much stronger source function than in the non-active chromosphere, providing that the region involved lies below the temperature minimum in the star's atmosphere. To take advantage of this temperature sensitivity, a filter was chosen with a bandpass near the first overtone TiO bandhead at 4955\AA . A continuum

filter at 5132\AA was used for comparison purposes. The calculations of Tsuji (1969) reveal that this represents a level in the atmosphere intermediate in depth between the high level in the atmosphere where the TiO bands are formed and the deep 4800\AA continuum level. The opacity at 5132\AA is roughly a factor of ten larger than that at 4839\AA ; thus this wavelength represents a level where $\tau_{8000\text{\AA}} \approx .1$. Bopp (1974) reported that emission lines in dMe stars were at maximum strength at times of enhanced flare activity. The emission lines may come from high chromospheric emission regions associated with the starspots. Consequently the fourth filter used was selected so that its bandpass included the H β emission line at 4861\AA . These four bandpasses thus represent a range of levels within the dMe atmosphere. Since the 1P21 and S20 photocathodes that were used have nearly flat response curves in the 4800\AA to 5200\AA region, it is to be expected that the magnitude differences found between different filters should accurately reflect the actual ratios of the monochromatic flux values F_{ν} at the different wavelengths observed.

In order to empirically establish the strength of the TiO band feature in this photometric system as a function of spectral type in these late-type stars, a number of late K and M dwarfs known not to be emission-line stars were observed with the Steward Observatory 229 cm telescope in October, 1973. These "spectral type standards"

and their spectral types are listed in Table 7. To show the actual TiO band strength, the relative intensity observed with the two filters has been corrected for spectral type energy distribution by assuming that the continuum energy distribution of these stars resembles that of a black body at an effective temperature corresponding to the specific spectral type (Johnson 1966). This corrected relative intensity, in magnitudes, is also displayed in Table 7 and plotted in Figure 13. It appears, as expected, that the TiO band begins to become significant around spectral type M0, increasing in strength with later spectral type. Again using the model of Tsuji (1969) it appears that the 4981Å filter represents a level with temperatures some 300°K cooler than the level represented by the 5132Å level in stars of spectral type M5.

Table 7. Dwarf M Star Spectral Type Standards

Star	Spectral Type	Rel. Strength of TiO Feature, Magnitudes
BD+5°2966	K2V	-.01
61 Cyg A	K5V	-.03
61 Cyg B	K7V	-.06
BD+43°44A	M1V	+.03
BD+36°2147	M2V	+.03
BD+20°2465	M4,5V	+.05
BD+43°44B	M6V	+.09

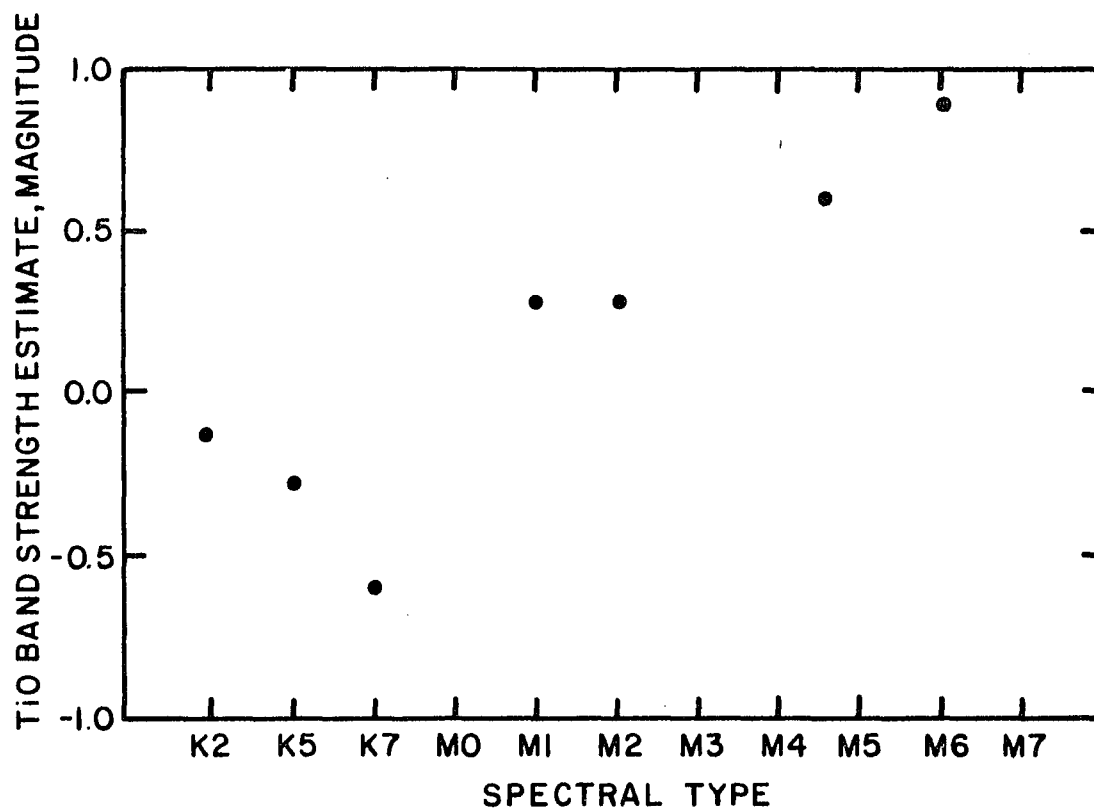


Figure 13. TiO band strength as a function of spectral type in the dwarf M stars.

A check on these calculations was obtained in the course of the observations during which the non-dMe star BD+5°1668, of spectral type M5, was extensively observed. It was possible to compare the relative flux at 4839Å and 5132Å for this star to determine if they indeed represent levels of different temperatures. It was found that if the 4839Å level was at a brightness temperature of 3300 K as indicated in Tsuji's (1969) 3000 K star model, the 5132Å level would have a temperature of 2950 ± 100 K. This is in good agreement with the value of 2800 K for the 5100Å level derived from the model.

Observations of Selected dMe Stars

The stars observed in this program are listed in Table 8 along with information on their properties. Two of them, YY Gem and FF And, were taken from the list of Torres and Mello (1973). They were chosen because of their known variability and periods. YY Gem is especially interesting since it is a close binary and offers a test of the influence of binary star processes on the dMe phenomenon. Ross 614 was chosen from a list of nearby stars given by Van de Kamp (1971). It was chosen because of the lack of evidence for a close companion, because of its late spectral type, and because its known space motion appears to exclude the possibility that it is a member of a known group or association, thus suggesting that it is not

Table 8. dMe Stars Observed

Star	Spectrum	V	Period (days)	Reference ^a
Ross 614	M5e	11.3	Unknown	(1)
FF And	MOe	10.4	2.17	(2)
YY Gem	M0.5e	9.1	0.814	(2)
BD+5°1668	M4	9.8	--	(1)
Ross 128	M5	11.1	--	(1)

^a(1) Van de Kamp (1971), (2) Torres and Mello (1973).

a young object. With a spectral type of dM5, it is the star of latest spectral type in this program and thus has the strongest TiO bands. Two additional stars, BD+5°1668 and Ross 128, were chosen from Van de Kamp's list to be used as check stars, since they are believed to display neither emission-line nor flare phenomena.

The data were obtained during nights in the period from 20 October 1973 to 15 March 1974 using the filter set described with photoelectric photometers on the Steward Observatory 91 cm and 229 cm reflectors and on the Kitt Peak National Observatory Number 2 91 cm reflector. Each observation consisted of an integration of the sky and a nearby comparison star of a magnitude similar to the program star before and after integrations in each color of

the program star. The data for each color were obtained sequentially in time and thirty to fifty minutes were required for a complete sequence in all four colors. Occasional observations of a third star were made to check for non-variability of the comparison star. Sufficient integration times were used to obtain internal accuracies of .01-.02 magnitudes. The star YY Gem presented an especially difficult problem since it is approximately 1' from the 1st magnitude star α Gem (Castor). Consequently the sky brightness was measured at positions on either side of YY Gem and the comparison star at the same distance from α Gem as the star under observation,

The resulting data are discussed below. They are also listed in Table 9. Magnitudes in each case are relative to the comparison star.

Ross 614

The comparison star for Ross 614 is an eleventh magnitude star 7' to the west northwest of Ross 614. From the data in Table 9 it is clear that Ross 614 was varying in all colors with amplitudes up to .1 magnitudes. While it was impossible to obtain a period of these variations from the limited data available, the star did vary substantially on time scales of a day, thus it is reasonable to assume a period of several days might exist,

Table 9. Table of dMe Star Observations

Star	Heliocentric	$\Delta m,$ $\lambda 4839$	$\Delta m,$ $\lambda 4861$	$\Delta m,$ $\lambda 4981$	$\Delta m,$ $\lambda 5132$
	J. D. (+2440000)				
Ross 614	2050.82	.36	.03	.22	.04
	2050.92	.40	.21	.27	.07
	2051.69	.37	.05	.24	.05
	2076.75	.29	.02	.20	.08
	2082.73	.38	.06	.24	.04
	2110.62	.34	.09	.21	.03
	2110.73	.37	.00	.21	.04
	2111.64	.32	.09	.28	.06
	2111.74	.34	.08	.26	.05
	2112.63	.35	.04	.25	.04
	2114.63	.30	.12	.27	.07
FF And	1995.73	--	--	1.34	1.22
	1995.96	--	--	1.15	1.15
	1997.75	--	--	1.17	1.17
	1997.86	--	--	1.20	1.17
	1998.69	--	--	1.28	1.24
	1998.83	--	--	1.25	1.21
	2051.66	1.28	1.06	1.21	1.19
	2076.63	1.32	1.00	1.26	1.12
	2081.65	1.25	1.07	1.33	1.19
	2082.63	--	--	1.18	1.22
	2083.62	1.28	0.96	1.19	1.18
	2086.62	1.32	1.00	1.23	1.19
YY Gem	1995.91	--	--	-.67	-.56
	1995.97	--	--	-.70	-.58
	1996.00	--	--	-.60	-.55
	1997.91	--	--	-.68	-.59
	1998.87	--	--	-.69	-.53
	1998.93	--	--	-.60	-.58
	2050.88	-.58	-.80	-.66	-.54
	2050.98	-.52	-.77	-.58	-.50
	2051.75	-.57	-.81	-.64	-.52
	2076.91	-.52	-.81	-.68	-.53
	2082.85	-.66	-.85	-.64	-.59
	2083.80	-.58	-.84	-.45	-.71
	2085.92	-.61	-.84	-.72	-.45
	2086.80	-.62	-.88	-.66	-.61
	2110.67	-.55	-.82	-.58	-.52
	2110.86	-.66	-.85	-.67	-.35
	2111.78	--	--	-.65	-.53
	2112.73	-.62	-.87	-.66	-.53

Table 9.--Continued

Star	Heliocentric J. D. (+2440000)	$\Delta m,$ $\lambda 4839$	$\Delta m,$ $\lambda 4861$	$\Delta m,$ $\lambda 4981$	$\Delta m,$ $\lambda 5132$
	2112.85	-.58	-.83	-.61	-.51
	2114.90	--	--	-.62	-.49
BD+5°1668	2051.73	1.55	1.45	1.35	1.14
	2076.84	1.52	1.36	1.41	1.16
	2082.79	1.56	1.35	1.37	1.15
	2083.76	--	--	1.37	1.15
	2110.65	1.51	1.37	--	--
	2110.79	1.34	1.35	1.27	1.14
	2111.68	1.38	1.39	1.38	1.16
	2112.68	1.50	1.37	1.39	1.16
	2114.72	1.51	1.40	1.38	1.16
Ross 128	2050.96	.98	.97	.86	.60
	2051.01	.98	1.00	.85	.57

Figure 14 shows the magnitude difference for each wavelength, Δm_λ , versus Δm_λ for the other colors. Systematic relationships between the variations in each color may be present. In most of the cases where points fall outside these correlations, the points are low weight points obtained with the Steward Observatory 91 cm telescope. Among these correlations it is noted that as the light level within the Ti0 band increased, the increases appear to be associated with a corresponding increase in the 5132\AA continuum, and an increase in H β emission. The variability in the low atmosphere appears to be anti-correlated with the variability in the high atmosphere, which is what may be expected if the variability itself is due to the presence of surface features analogous to the sun's active regions,

To test whether these changes are due to an overall change in some background source, we have shown in Figure 18 (p. 113) a plot of the Ti0 band strength, $C(\text{Ti0}) = \Delta m(4981) - \Delta m(5132)$ vs, $C(\text{H}\beta) = \Delta m(4861) - \Delta m(4839)$, the H β emission strength. It appears that a small decrease in Ti0 band strength is correlated with a large increase in H β emission line intensity. Also, small increases in the 5132\AA continuum correspond to larger increases in Ti0 intensity, or decreases in the Ti0 band strength, and even greater increases in H β intensity. A small decrease in light coming from the deepest layers of the atmosphere (through the 4839\AA continuum filter) seems to correspond to increases in light

ROSS 614

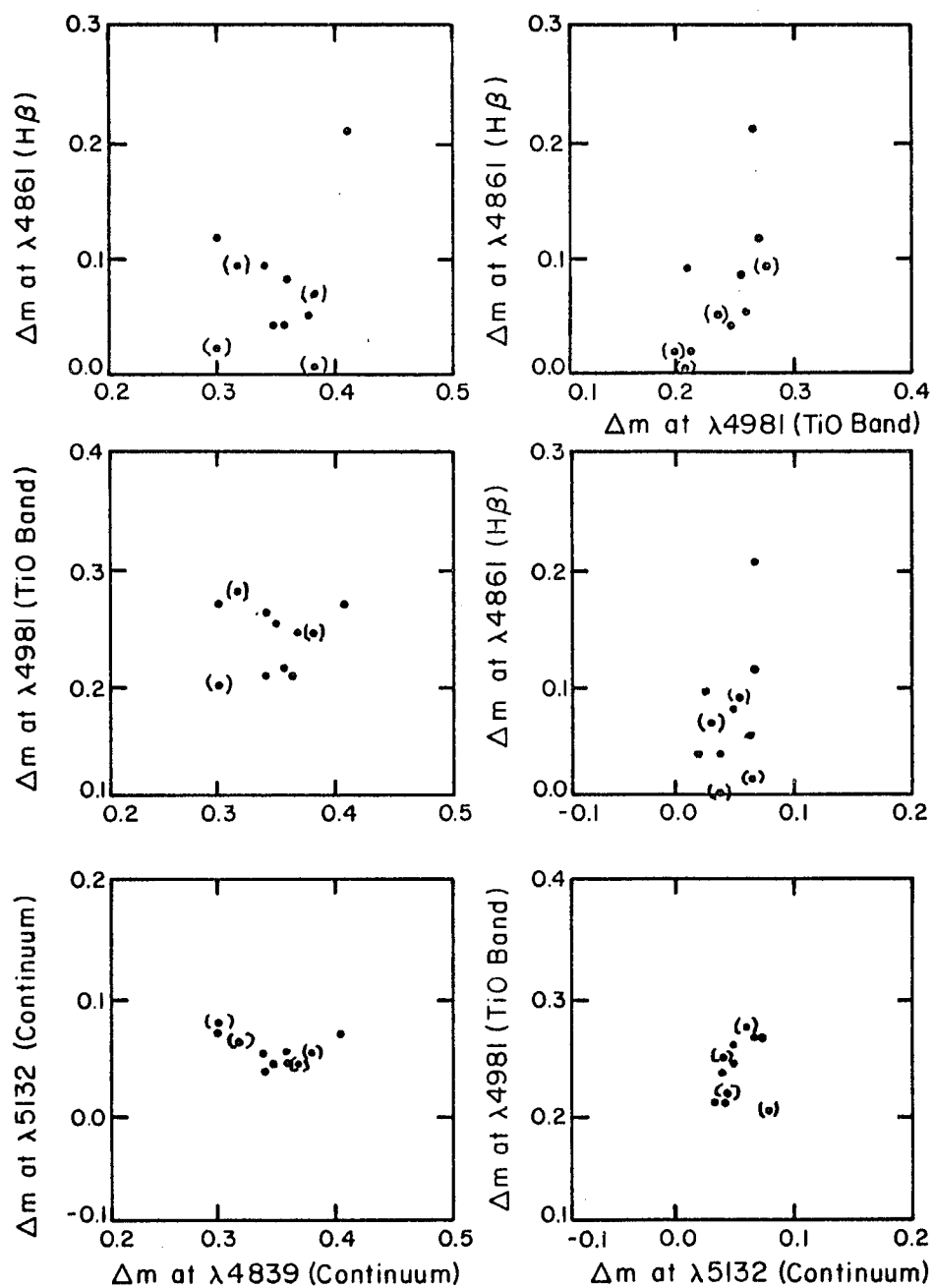


Figure 14. Magnitude-magnitude plots for the dMe star Ross 614 -- Low weight points denoted by ().

from the higher levels (through the 5132\AA filter and the 4981\AA filter), and to a large increase in chromospheric emission (through the $H\beta$ filter).

FF And (BD+34°106)

The comparison star for FF And is a tenth magnitude star $12'$ to the north northwest of FF And. While the Ti0 band is far less strong in this MOe star than in Ross 614, FF And seems to display a qualitatively similar behavior. Figure 15 shows these data, plotted wavelength against wavelength as with Ross 614. The only wavelengths for which a substantial amount of data were obtained for FF And were the $\lambda 4981$ Ti0 band and the $\lambda 5132$ continuum. As with Ross 614, a small increase in the 5132\AA continuum seems to correspond to a slightly larger increase in the light level within the Ti0 band. The four sets in which all four colors were obtained exhibited behavior consistent with that in Ross 614, although with such a small number of points this is not as significant a conclusion.

YY Gem

The comparison star is a tenth magnitude star $3'$ to the south of YY Gem. Figure 16 shows the magnitudes relative to the comparison star in each band plotted against one another as in Figures 14 and 15. The variations seem to be different from those in Ross 614 and FF And. While there are variations of .1 magnitudes in each band they

FF AND

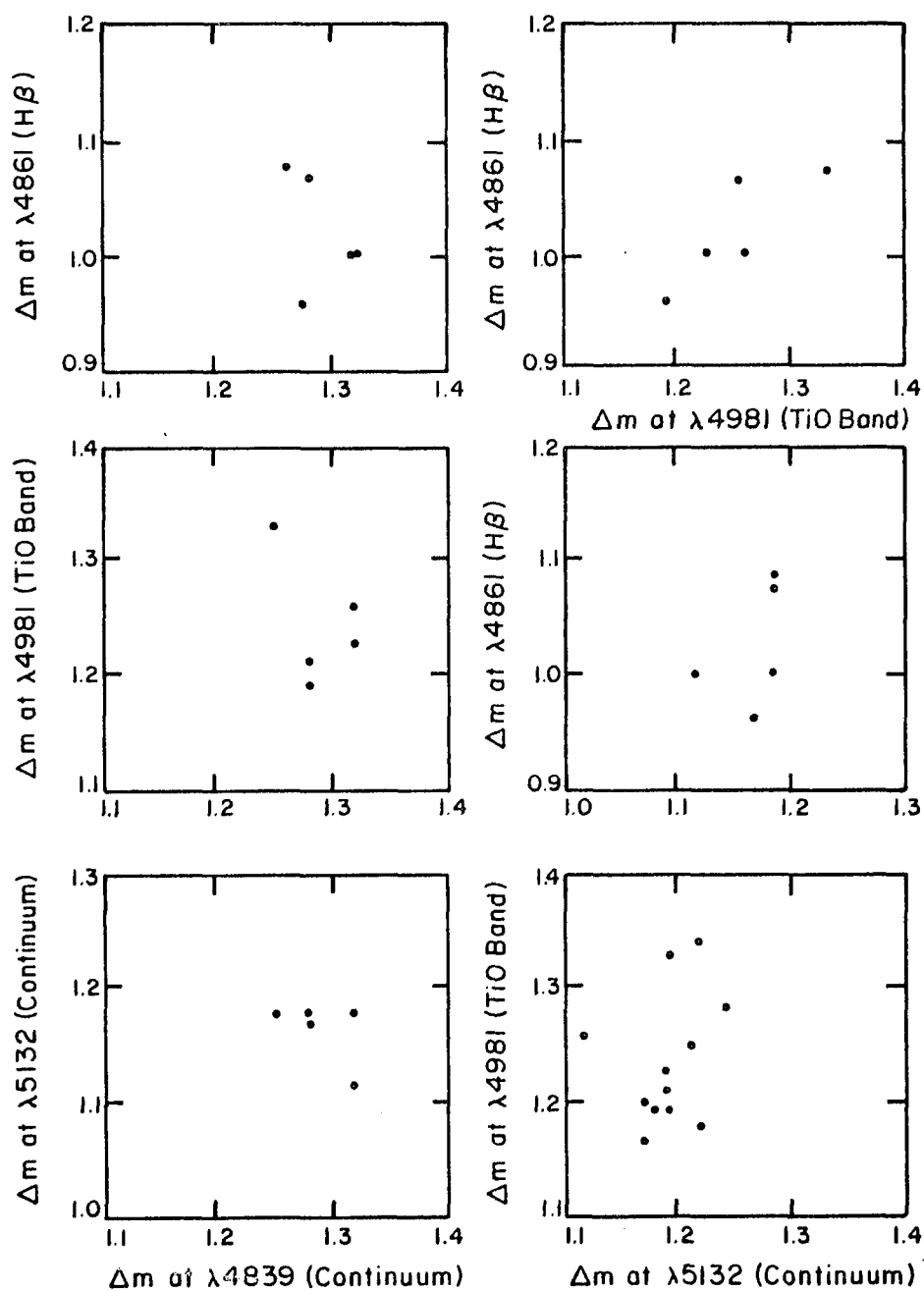


Figure 15. Magnitude-magnitude plots for the dMe star FF And,

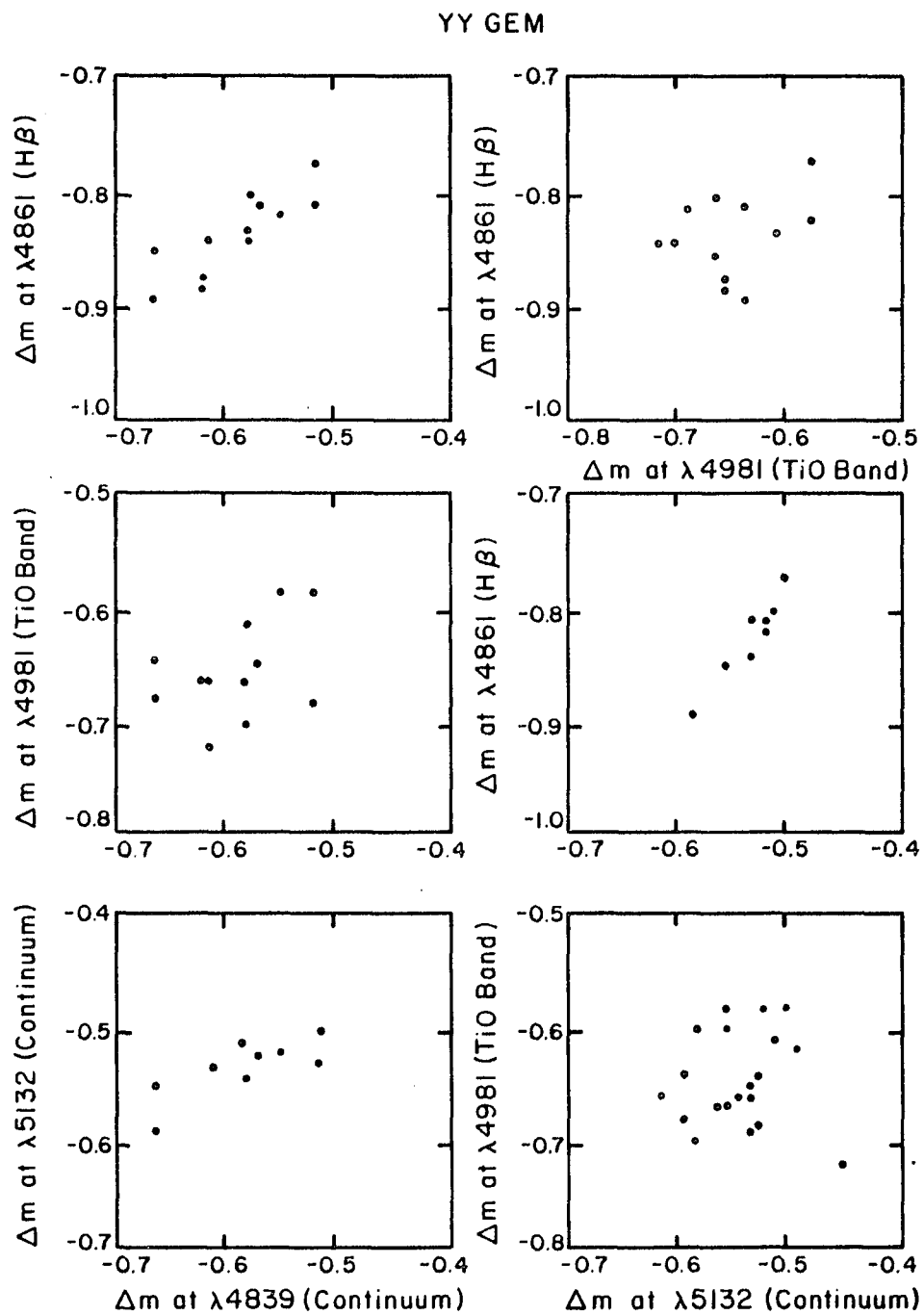


Figure 16, Magnitude-magnitude plots for the dMe star YY Gem.

appear to be largely independent of wavelength. The light in each band increases or decreases along with the others from the deepest level to the highest. The 4981\AA TiO versus the 5132\AA continuum plot shows behavior similar to the other stars, where a small increase in the 5132\AA light level corresponds to a larger increase in the TiO band light level. Figure 18 (p. 113), a plot of $C(\text{TiO})$ versus $C(\text{H}\beta)$ for YY Gem, shows that the $\text{H}\beta$ strength appears to be constant, independent of changes in the TiO band strength. In addition, the 4839\AA continuum magnitude appears positively correlated with the other magnitudes rather than negatively as with the other dMe stars.

Since the orbital period of YY Gem is known (Kron 1952), it may be possible to study the location on the star from which maximum light is produced. However, an uncertainty is present since the observations extended over several months and changes in phase of the variations may be present due to changes in the locations of possible emitting or absorbing regions on the stellar surface. Figure 19 (p. 114) shows a plot of the relative magnitudes in each color as a function of phase. There appears to be some correlation with maximum light appearing near $\phi = 1$.

It may well be true that YY Gem exhibits behavior different from the other stars due to its binary nature. Even though it was the first dMe star in which variations were attributed to surface spottedness (Kron 1952), here

the grey veil model of Evans (1971) attributing the variations to binary processes may be more appropriate. At least the $H\beta$ emission, which remains more or less constant, may arise from an extra-stellar location.

BD+5°1668

The comparison star is a ninth magnitude star 10' to the south. This non-dMe star showed no evidence of $H\beta$ emission. Figure 17 shows the data plotted as for the other stars. There are two points which fall well outside the apparent scatter of the rest of the points. The validity of these points is questionable as they were taken on nights on which sky conditions were somewhat variable. Other than these points, no variations were seen and no correlations between data in different bandpasses exist. However, on the basis of these data alone, no clear statement can be made concerning the variability of this star.

Ross 128

Two observations were made of this star. No significant variation was present between these.

The Origin of dMe Star Magnetic Fields

On the basis of the data discussed above, several conclusions can be drawn. The observations of Ross 614 are the most extensive and appear to best illustrate the solar-type active region premise. It is difficult to understand

BD +5° 1668

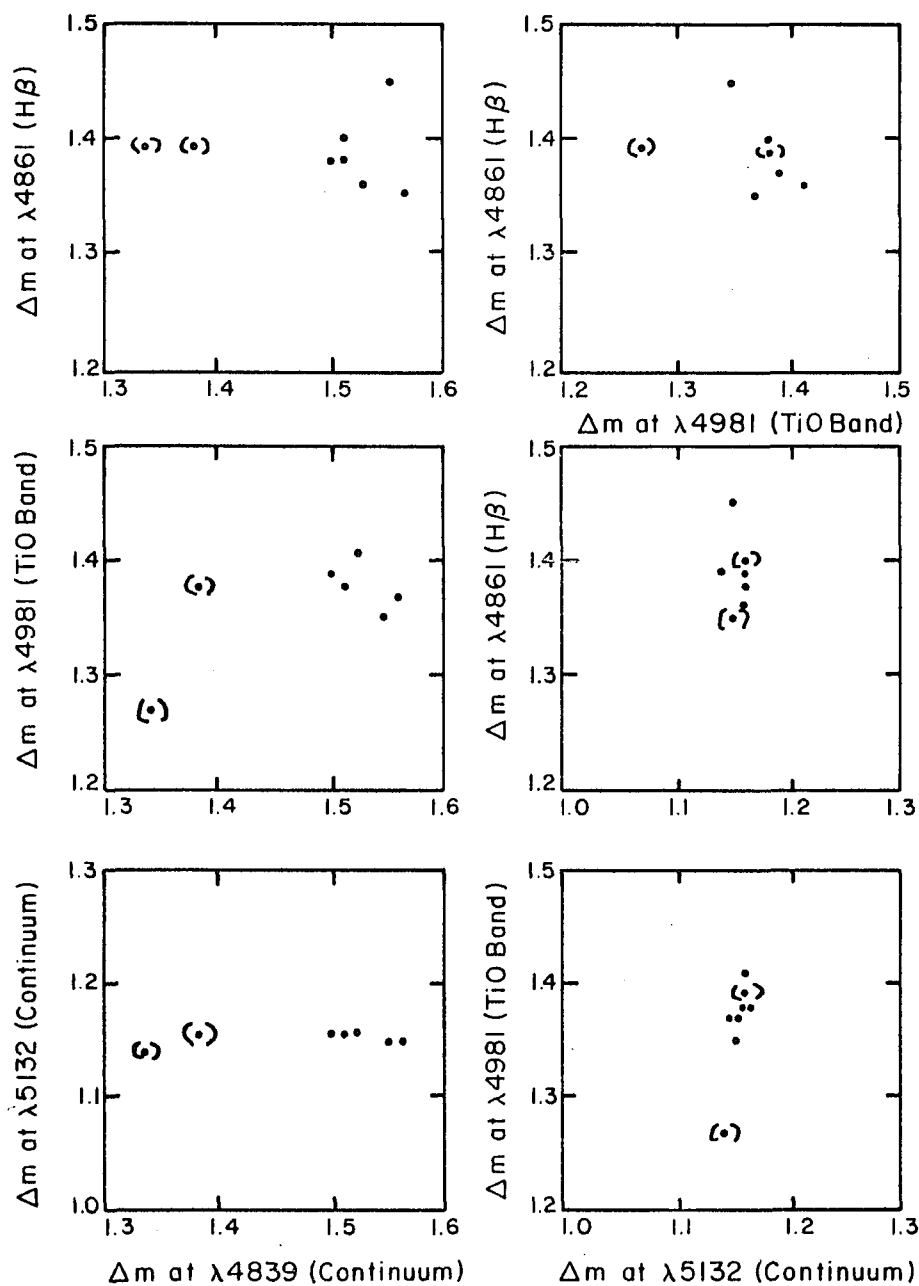


Figure 17. Magnitude-magnitude plots for the dM star BD+5°1668 -- Low weight points denoted by ().

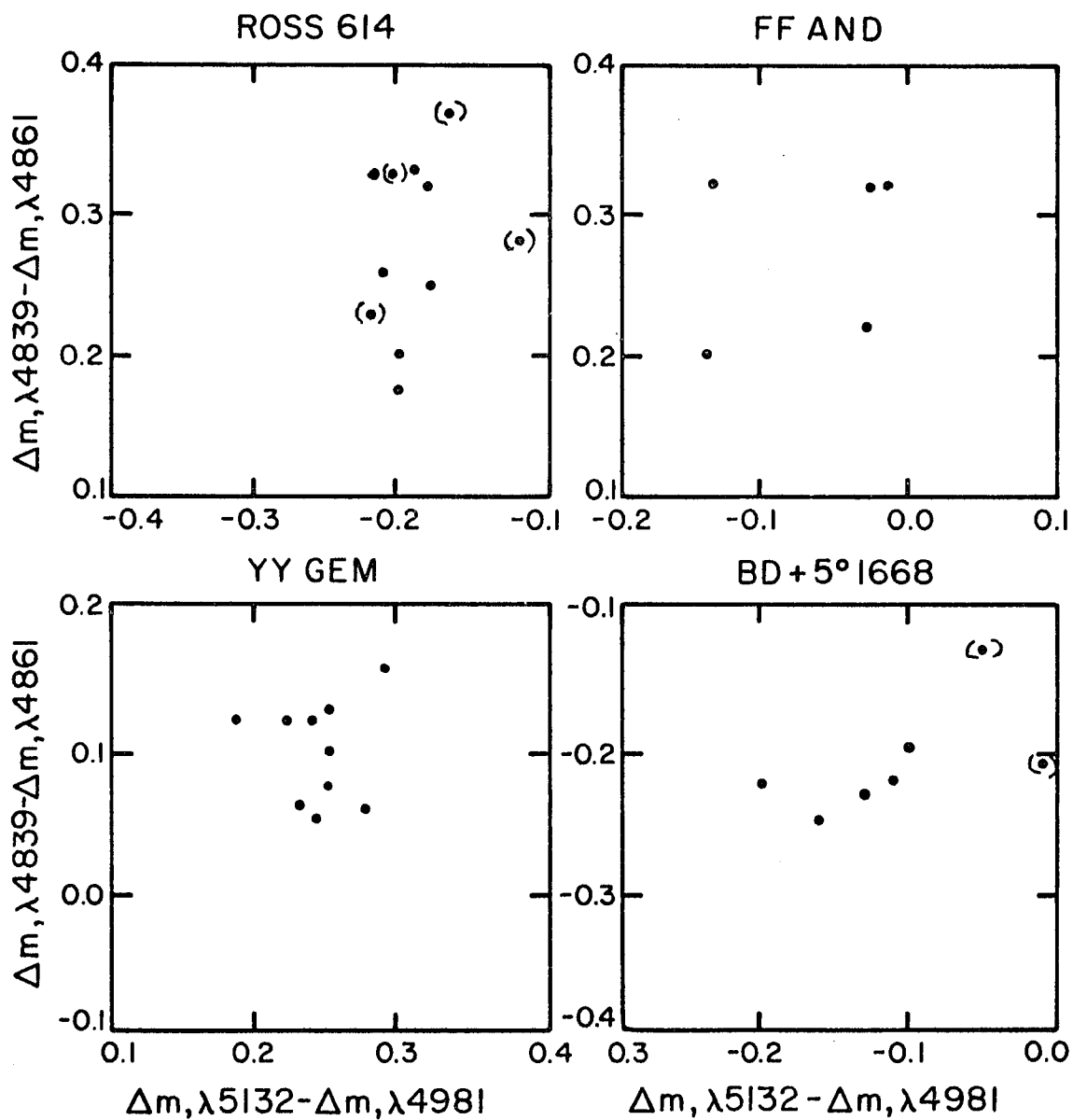


Figure 18. Color-color plots for all dMe stars observed
 -- Low weight points denoted by ().

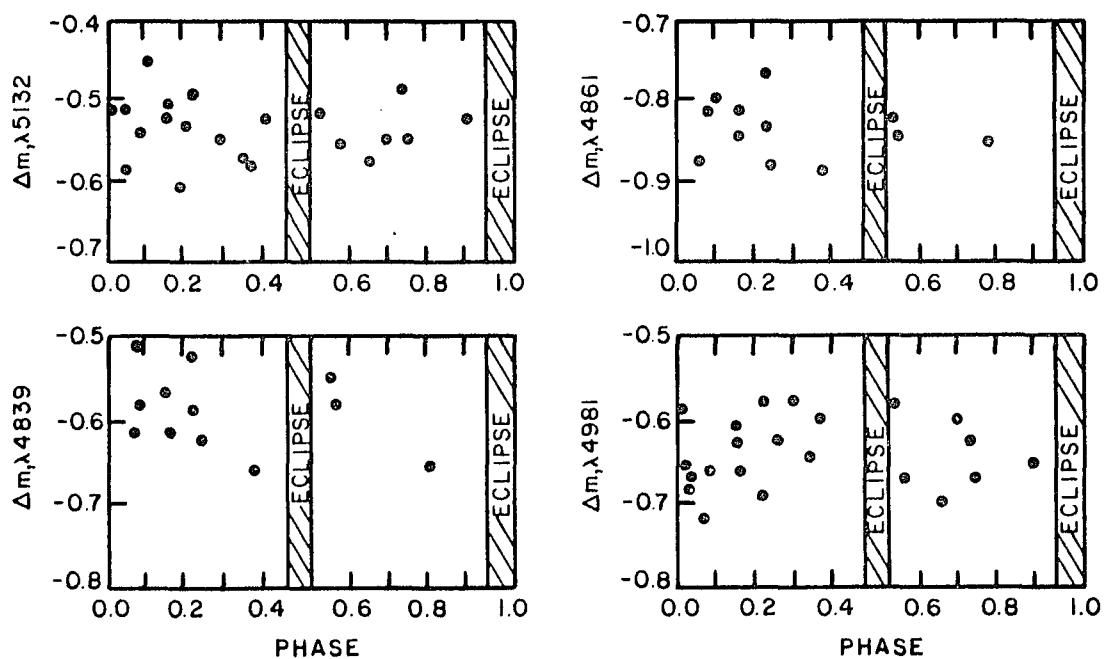


Figure 19. Magnitudes as a function of phase for the dMe star YY Gem.

how a mechanism exterior to the stellar atmosphere could produce apparent decreases in the flux from the deeper levels of the atmosphere while simultaneously producing increases in the flux from the higher levels. Thus the "grey veil" model as proposed by Evans (1971) and discussed by Torres and Mello (1973) can be ruled out as the cause of the variations in Ross 614.

The observations of Ross 614 seem consistent with a model in which large dark starspots exist in the stellar photosphere. Surrounding these spots are regions which are in emission in the higher chromospheric layers. The dark photospheric spots are responsible for intensity decreases observed at the 4839\AA continuum level while the much more extensive chromospheric emission regions produce the simultaneous intensity increases at the higher levels.

Additional results that appear to support this picture have been presented by Bopp (1974). Bopp observed maxima in the emission line strengths of several dMe stars on spectra uncontaminated with observed flares but which were taken during periods of high flare activity. He suggested that the fact that these emission line maxima correlated with periods of flare activity were indications of chromospheric activity associated with the flares. The observations presented here are consistent with this interpretation.

It is shown that, at least in two of the three dMe stars observed, these observations support the hypothesis that the variability of dMe stars is due to the rotation through the observer's field of view of active regions analogous to the sun's. It would appear from these observations that one can draw a more extended analogy between the spottedness of the dMe stars and surface activity on the sun than has been previously assumed. This offers larger opportunities for investigation into the nature of stellar surface activity, while at the same time making simple arguments based on less complete analogies with solar activity difficult to defend. For example, the close relationship suggested by Bopp and Evans (1973) between the energy dammed back in spots and that released in stellar flares seems dubious since it appears that no similar relation exists for the sun, as solar flares occur in regions without sunspots from time to time.

In the case of the sun, surface activity of the type which apparently exists on the dMe stars may result from an interaction between convective motions, rotation, and sub-surface magnetic fields (Parker 1955). It is reasonable to postulate a similar mechanism for the dMe star activity (Poveda 1964).

The existence of old dMe stars such as Ross 614 and others (Veeder 1974) precludes a primordial origin for the magnetic fields, since the diffusion time for magnetic

fields is short compared to the ages of the older dMe stars. Thus a mechanism for the production of magnetic fields is needed.

A mechanism has been suggested by Biermann (1950) and discussed by Mestel and Roxburgh (1962) which gives a magnetic field of the correct order of magnitude for the sun. The derivation of the "Biermann Battery" mechanism following that work is given here. From this result we will derive an estimate of the efficiency of the battery mechanism for generating dMe star magnetic fields. By considering the forces acting on the electron and ion components in a stellar plasma Biermann derived an equivalent form of Ohm's law for the current density \vec{j} , in esu units:

$$\vec{E} + \frac{\vec{v} \times \vec{H}}{c} + \frac{\nabla P_e}{n_e e} - \frac{\vec{j} \times \vec{H}}{c} = \frac{\vec{j}}{\sigma}, \quad (4.1)$$

The electric field \vec{E} results from charge separation essentially due to the differing masses of the proton and electron, \vec{v} is the velocity of material motions, H the magnetic field, ∇P_e the gradient of the electron pressure and σ the electrical conductivity. The rate of generation of magnetic field is then given by Maxwell's equation:

$$\frac{1}{c} \frac{\partial \mathbf{H}}{\partial t} = \text{curl } \vec{\mathbf{E}}$$

$$= \text{curl } \frac{\vec{\mathbf{v}} \times \vec{\mathbf{H}}}{c} - \text{curl } \frac{\vec{\mathbf{j}}}{\sigma} + \text{curl } \frac{\nabla P_e}{n_e} - \text{curl } \frac{\vec{\mathbf{j}} \times \vec{\mathbf{H}}}{e} \quad (4.2)$$

field motions	ohmic diffu- sion	battery term	Hall term
------------------	-------------------------	-----------------	--------------

Neglecting fluid motions and noting that the Hall term is only important for very large fields, an equilibrium between the battery generation of fields and ohmic diffusion will be reached after a time scale t given by Mestel and Roxburgh (1962) as:

$$t \sim \frac{4\pi\sigma}{c^2} R^2 \quad (4.3)$$

Using R as the size scale of the star, it is found that $t \sim 10^8$ years for the M dwarf stars; thus primordial fields would dissipate in the lifetime of the star. A complete solution to this equation is difficult; however, an estimate for the battery term can be obtained by noting that:

$$\frac{\nabla P_e}{n_e} = \frac{\nabla P}{\rho} \frac{A m_H}{e(1+z)} \quad (4.4)$$

where A is the atomic weight and z the atomic number. The term $\nabla P/\rho$ can be replaced using the hydrostatic equilibrium equation for a rotating star, so that:

$$\frac{\nabla P_e}{n_e} = \frac{m_H}{2e} (\vec{g} + \Omega^2 \vec{\omega}), \quad (4.5)$$

where \vec{g} is the gravitational acceleration, Ω is the angular velocity, $\vec{\omega}$ is the distance from the rotation axis in cylindrical coordinates, and where for simplicity we consider the case of pure hydrogen only. Unless $\Omega^2 \vec{\omega}$ is non-potential derivable the curl of this expression vanishes. However, stellar structure arguments (Mestel and Roxburgh 1962) would require differential rotation with a non-potential derivable centrifugal force, or the rotation would produce meridional circulation which in turn would rapidly induce such differential rotation. If it is assumed that the differential rotation is of the order of the rotation itself ($d\Omega/dr \sim \Omega/R$), then it follows that to order of magnitude:

$$\text{curl } \frac{\nabla P_e}{n_e} \sim \frac{m_H}{2e} \Omega^2. \quad (4.6)$$

Similarly, the ohmic diffusion term reduces to:

$$\text{curl } \frac{\vec{j}}{\sigma} = \text{curl } \left(\frac{c}{4\pi\sigma} \text{curl } \vec{H} \right) \sim \frac{c}{4\pi\sigma} \frac{H}{R^2} \quad (4.7)$$

The equilibrium magnetic field produced after a time t given by Equation (4.1) is thus of the order:

$$H \sim \frac{4\pi\sigma}{c} \frac{m_H}{2e} \Omega^2 R^2 \quad (4.8)$$

and toroidal in nature. Figure 20 shows derived field strength using stellar parameter data from Allen (1973) with stellar rotation periods ranging from a day to a year.

The observable magnetic fields normal to the stellar surface are presumably generated through a dynamo mechanism similar to that suggested by Parker (1955) in which convective motions in the rotating star interact with the sub-surface toroidal field. The process described above is thus undoubtedly an oversimplification since the interaction between the convective dynamo and differential rotation will produce complex magnetic behavior such as the oscillatory poloidal and toroidal field structures described by Leighton (1969) in his study of the 22-year solar cycle. One problem in generating dMe fields with the battery mechanism is that the dMe stars are convective to very deep levels. Indeed, at spectral types later than M5 the radiative core is calculated to disappear (Mullan 1975); however, a small radiative core may persist to later spectral types. And the battery mechanism described here, which only operates in the radiative stellar core, may well provide the basic "seed" field required by the dynamo mechanism.

Mestel and Roxburgh (1962) have shown that a small poloidal field would inhibit the generation of toroidal magnetic field by the battery mechanism. However, it is unlikely that such large scale poloidal fields exist in the dMe stars. If initially present, any large scale poloidal

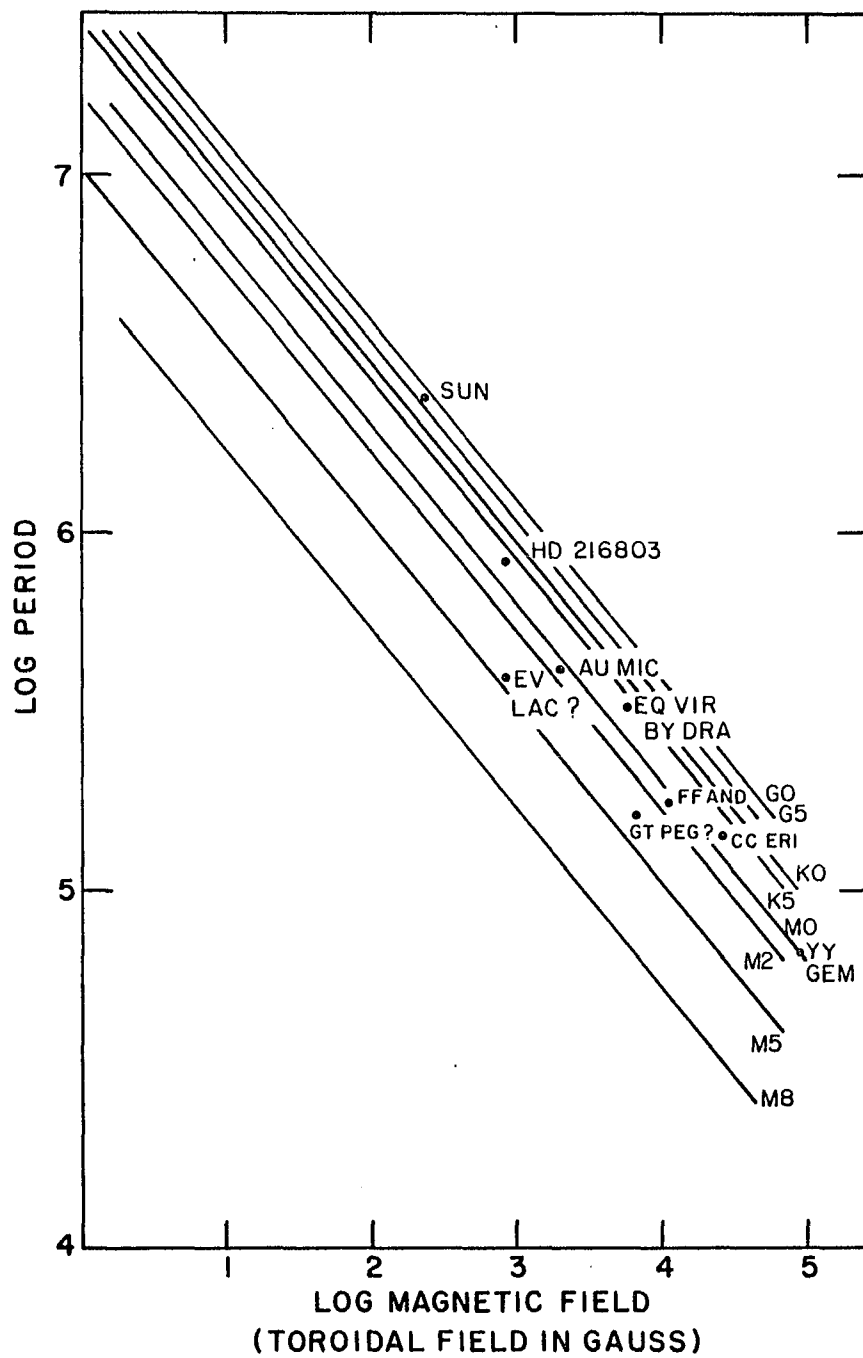


Figure 20. Calculated toroidal magnetic field as a function of rotational period compared with stars of known periods.

field of primordial origin would be dissipated by ohmic diffusion on the same time scale as the equilibrium time for generation of toroidal field (10^8 years for the M dwarf stars). The poloidal components produced by the convective dynamo are small scale surface fields and consequently would have no effect on the generation of a generalized toroidal field. Since the sun shows no evidence for a persistent poloidal field and the Biermann battery mechanism produces fields with strengths similar to those observed in the sun, it is reasonable to assume that this mechanism may be responsible for the generation of fields of significant strength in late type stars and can account for the existence of old dMe stars. While it is difficult to directly observe the operation of the battery mechanism since it stops at the top of the stellar core, the recent "flux rope" model of Piddington for the origin of solar surface field requires just such a deeply generated magnetic field produced by this process or a similar process.

The most notable feature of Figure 20 is the large toroidal magnetic field strength derived for the dMe stars with known periods (Torres and Mello 1973) which have been marked on the figure. These are approximately 10-100 times larger than the corresponding solar fields. To test this strong field prediction we turn to stellar flare observations. Since solar flares are a local phenomenon covering a fraction of the solar surface and appear to be rapid

releases of magnetic energy it is reasonable to assume that flare energies will be proportional to local magnetic energy densities, or since magnetic energy density is proportional to the square of the magnetic field strength:

$$E_{\text{FLARE}} \propto H^2, \quad (4.9)$$

Consequently it is possible to understand the stellar flare energies of 10^3 - 10^4 times solar flare energies as a manifestation of magnetic fields 10-100 the strength of solar fields in the dMe stars. However, this increased energy can also manifest itself as an increase in flare frequency. It is probably reasonable that both increases in flare rates and mean flare energies may be present.

Since the magnetic field derived in Equation (4.8) is proportional to the square of the stellar radius if the angular velocity is a constant, Equation (4.9) can be rewritten replacing the magnetic field:

$$E_{\text{FLARE}} \propto R^4. \quad (4.10)$$

If the assumption of constant gravity on the lower main sequence is adopted then the radius R and mass M of the dwarf M stars will follow a relation $R^2 \propto M$. If the further assumption of a mass-luminosity law taking the form $L \propto M^5$ is made, the flare energy relation becomes;

$$E_{\text{FLARE}} \propto L_{\text{STAR}}^{.4} \quad (4.11)$$

replacing energies with absolute magnitudes M_{FLARE} for the flare energy and M_{STAR} for the star luminosity,

$$M_{\text{FLARE}} \propto .4M_{\text{STAR}}. \quad (4.12)$$

This would imply that the dMe stars at constant angular velocities or constant periods should show reduced flare energies at later spectral type. Observational evidence for this exists from Kunkel (1973) who found maximum flare energy rates in each spectral type dMe star correlated with absolute magnitudes of the star, taking the form:

$$M_{\text{FLARE, Max}} = 10.8 + .408M_{\text{STAR, V}}. \quad (4.13)$$

If it is postulated that stars of each spectral type with maximum flare energies in that spectral type represent stars with similar angular velocities the proportionally constant of .408 between the flare energy magnitudes and visual star magnitudes may be understood as the result of decreasing stellar radius with spectral type at constant rotational period. Since Kunkel's relationship concerns energy rates, this analysis is valid whether the mean flare energy, flare rate, or both processes increase in the dMe stars.

CHAPTER 5

DISCUSSION OF RESULTS AND MODELS

In the preceding twenty years a substantial amount of study has been aimed at obtaining a unified theoretical understanding of the solar convection zone. This work has been reviewed in the first chapter. Many of the problems center around two key points, the apparent existence of highly ordered convective flows, and the interaction between these motions and the magnetic fields. In this chapter the observations reported earlier will be discussed in the light of a general model.

A review of the previously derived observational results is given in the first chapter; however, a summary is reproduced here.

1. A large scale horizontal motion with a 30,000 km scale exists on the sun. The cellular appearance of this phenomenon has led to this flow being attributed to a deep convective process originating perhaps 10,000 km below the surface.
2. Magnetic fields, with strengths on the order of 2000 G are observed to lie at the vertices of several supergranular cells. Chromospheric emission

and material downflows appear to be exactly co-spatial with these magnetic field elements.

3. A class of late type stars (dMe stars) with outer convective envelopes often exhibits surface activity, such as flares, which is qualitatively similar to solar magnetic activity.

The preceding chapters of this dissertation cover a number of subjects related to the above observations. These results are summarized below:

1. To a limit of 10K the only temperature structure associated with supergranulation exactly coincides with the magnetic field elements at supergranule boundaries. The temperature structure is in the sense of hotter temperatures in the chromosphere relative to non-magnetic regions and cooler temperatures in the deep photosphere. This behavior is consistent with the Chapman (1970, 1974) models of solar magnetic field regions.
2. Supergranule velocity cells have lifetimes near 35 hours in length. This value was derived from cross-correlation studies in time of the velocity cells themselves, and it is significantly longer than that derived from cross-correlation studies of the chromospheric emission network.

3. Two observations were obtained which strengthen the strong field observations of Harvey and Hall (1974). In order to consider these two results together they will be discussed below, rather than in the chapters from which they are taken.

As discussed in Chapter 3, the $\lambda 8468$ line cannot reliably be used to obtain velocity observations within regions where the magnetic field exceeds 1000G. With fields this strong the $\lambda 8468$ line becomes too highly Zeeman split to be used with the Sacramento Peak Diode Array system for velocity observations. We observed essentially zero velocities within magnetic field regions in this investigation. Indeed, at the locations with the larger apparent field strengths, the velocities obtained were increasingly negative. Since other investigators have reported positive downflows at these locations, and downflows were observed in our non-magnetic line $\lambda 4065$, this effect may be attributed to Zeeman splitting under strong fields ($B > 1000\text{G}$) as calculated in Chapter 3. However, it was also shown in Chapter 3 that lines formed fairly high in the atmosphere are strongly affected by the large temperature increases present in magnetic field regions relative to non-field regions. Flattening of line cores and possibly central line reversals resulting from this temperature change can also produce the negative velocities in magnetic field regions

which we observed with the non-magnetic lines $\lambda 5123$ and $\lambda 5434$. Consequently, both magnetic fields and their associated temperature effects can account for the lack of observable velocities in the $\lambda 8468$ observations. So while the $\lambda 8468$ results are consistent with fields exceeding 1000G, they do not in of themselves prove that fields this strong are present,

The temperature structure of magnetic field regions relative to non-magnetic field regions also can provide a means to estimate the magnetic field strength. Pressure balance exists between regions of magnetic field and surrounding non-field regions. Since magnetic fields contribute to the pressure in regions of thermal equilibrium we have:

$$P_z(Z) + P_m(Z) = P_e(Z) \quad (5.1)$$

or

$$P_z(Z) + \frac{B^2(Z)}{8\pi} = P_e(Z) \quad (5.2)$$

where $P_z(Z)$ is the gas pressure in magnetic field regions, $P_e(Z)$ is the gas pressure in non-field regions, and $P_m(Z) = \frac{B^2(Z)}{8\pi}$ the magnetic pressure in the field regions. The thermal gas pressure is obtained from the perfect gas law:

$$P_G(Z) = \frac{k}{m} \rho T \quad (5.3)$$

where k is the Boltzmann constant, m the mean particle mass, ρ the density, and T the temperature in degrees Kelvin. For a totally vertical field, horizontal pressure balance is maintained by either or both a decrease in temperature or density within the magnetic field region. These decreases most likely result from an inhibition of convection within the magnetic field region as described by Weiss (1964), Chitre (1963), and Deinzer (1965) for sunspots. As pointed out by Weiss, an upper limit to the temperature difference for a given field strength can be derived. This is an upper limit for several reasons. First, as mentioned above, a density decrease will have the same effect in reducing the gas pressure within the field region. Secondly, there is some radiative energy transfer into the cooler magnetic region from the hotter surrounding horizontal material. This would be expected to be especially significant in the small facular flux tubes under question. Since an observed temperature decrease is available, a lower limit to the magnetic field can be derived by solving Equation (5.3) for the field as a function of temperature difference assuming constant density and no radiative energy exchange:

$$\frac{k}{m} \rho T_z + \frac{B^2(Z)}{8\pi} = \frac{k}{m} \rho T_e \quad (5.4)$$

becomes

$$B^2 = \frac{8\pi k}{m} \rho (T_e - T_z) \quad (5.5)$$

From Chapter 2 a lower limit on $T_e - T_z$ was 50°K ; corrected for seeing and finite aperture this temperature change may be as large as 500°K . For these two values we get lower limits for B of 275G and 875G respectively for the $\tau_{5000} \approx 2$ levels at which the temperature differences were observed. As discussed above, a density change in the magnetic field regions could also provide for the reduced gas pressure, so these field strengths are absolute lower limits. Since a temperature change of 2500K would be required to account for 2000G fields from this simple analysis, a more extensive study such as those of Chitre (1963) and Deinzer (1965) for sunspots is necessary. However this observation and the velocity observation both indicate the magnetic fields are probably at least 1000G in strength. And both results are entirely consistent with the 2000G field observed by Harvey and Hall (1974).

4. Several forms of magnetic flux motion were observed and compared with supergranular velocity fields. Occasional appearances of new flux are associated with changes in the supergranular velocity field. It is reasonable to conjecture that these velocity changes denote the emergence of new supergranules. A second form of magnetic field motion consisted of a slow splitting and diffusion of existing flux concentrated at velocity cell boundaries. This diffusion proceeded in a more or less continuous

manner in all of our observations. While the data available covered less than one-third of a velocity cell lifetime, these observations would tend to support a model in which magnetic field elements remain with a single velocity supergranule throughout its lifetime on a one-to-one basis. That is, magnetic field elements emerge with the formation of new velocity cells, stay with those cells, and slowly dissipate during the approximately 40 hour velocity cell lifetime.

- 5, The case for attributing dMe star activity to solar type surface activity is strengthened by the observation that this activity behaves in a manner qualitatively similar to solar surface activity. That is, bright chromospheric emission regions appear to be associated with dark cool photospheric spots. The magnetic fields responsible for this activity may be produced through an interaction between rapid rotation and convective motions. In this manner it is possible to predict fields as strong as 10^5 G on some dMe stars,

The remainder of this chapter will be devoted to a discussion of these points and a qualitative model for solar and dMe star magnetic and convection zone interactions similar to those of Piddington (1975), Parker (1970), Dicke

(1970), and references therein. Briefly, this model consists of a rotating star with an outer convection zone. Strong magnetic fields exist in the convection zone which may be generated within the radiative core. These fields diffuse outwards and interact with ordered convective motions, producing the observed surface activity on the sun and dMe stars. Some of the key parameters and constraints in this model will be touched upon below.

Implications of the New Results for Models for
Convection Zone and Magnetic Field
Interactions

Two important points will now be considered; first does the surface magnetic and velocity activity represent physical processes close to the surface or at some deeper level, and secondly, what process is ultimately responsible for the magnetic fields themselves? Leighton (1964, 1969), in his model of the solar cycle, makes use of surface material motions to concentrate and distribute magnetic fields over the solar surface. However, if the fields are significantly stronger than he assumed, this process becomes difficult to accomplish. From a different standpoint, Mullan (1974) and Parker (1970) provide for the surface fields by a dynamo process in which very weak subsurface fields interact with convective motions, thereby becoming greatly enhanced. However, as discussed by

Piddington (1975), if the fields are initially as strong as 2000G, this process too may be substantially altered.

For magnetic field motions to become dominated by material motions, as in Leighton's (1969) model, the magnetic field energy density must exceed the kinetic energy density. For this to be true:

$$\frac{B^2}{8\pi} \geq \frac{3}{2} n k T \quad (5.6)$$

where B is the magnetic field strength, n the number density of particles, k the Boltzmann constant, and T the temperature in degrees Kelvin. A solution of this equation for B yields the critical value of the magnetic field strength at which the fields dominate material motions at a given level in the stellar envelope. Table 10 lists these field strengths for various levels within a solar type star (G2V) and a dMe type star (M0V) with stellar envelope parameters taken from Allen (1973). In the sun for field strengths of 2000G, the presumed surface value, material motions are dominated to about 500-1000 km below the visible surface, or to the bottom of the granular convection zone. However, for derived dMe field strengths of 50,000 G the material motions are magnetically dominated to depths of 10-20,000 km, well into the deep convection zones in these stars. It thus seems that small scale surface motions in both the sun and dMe stars are not responsible for any distribution of the surface magnetic fields, and if

Table 10. Magnetic Fields Needed to Dominate Fluid Motions as a Function of Depth in a G2V Star and an M0V Star

Type Star	Depth (km)	Magnetic Field (Gauss)
G2V	0	840
	1,000	2,010
	3,500	44,000
	7,000	90,500
	35,000	435,000
M0V	0	1,030
	8,000	35,000
	21,000	227,000
	42,000	1,160,000

anything, reflect the magnetic field structure rather than the converse. So it seems the observed magnetic field structure substantially reflects deep material motions.

Piddington (1975) has discussed at length the problems which the strong fields pose. Specifically the difficulties lie with the dynamo process in which a uniform weak magnetic field permeates a convection cell. Subsequent material motions are presumed to concentrate and expel these fields from the convective cell, accounting for the observed fields residing at the boundaries of convection cells. This process has been shown to proceed in a few cell rotations by Weiss (1964). Piddington (1975) has pointed out that the observed supergranular flow consists of at best only slightly more than a single convective cell

rotation. Not only is this insufficient to account for the observed expulsion of flux, it also predicts that the field concentration process itself should be observed in progress for most of the cells, rather than the 10-20% of the cells which seem to show flux concentration in this study. From the observations described in Chapter 3 the magnetic fields seem to move very rapidly to cell boundaries upon formation of the cell and remain essentially stationary for some 30-40 hours. However, the flux expulsion may occur in some deep level much more rapidly than the surface motions suggest. Additionally, as pointed out by Piddington, if field strengths as large as 2000 G are widespread, they may tend to stop the surface convection, rather than be concentrated by the convective motions.

The strong fields and long cell lifetimes have additional implications with regard to the Leighton (1969) flux dispersal mechanism. Smithson's (1973) study of magnetic field points indicated that the mean distance which a magnetic field element moved in 24 hours was approximately 7600 km. Smithson noted that this was far smaller than required to account for the observed flux dispersal. With 36-hour supergranule lifetimes, the random walk of surface flux by supergranules cannot account for the observed magnetic flux dispersal rates. Indeed, no random walk type of flux motions were observed in this investigation; however,

our total observing period was short (10 hours) compared with the random walk timescale (30-40 hours).

From these considerations, it becomes clear that the observable surface motions on the sun are insufficient to dominate magnetic field placement. The fact that supergranule velocity motions may be connected to a single set of flux elements as indicated in Chapter 3 and that no convective temperature structure associated with supergranulation is observable in the photosphere (Chapter 2) suggests that the surface flow is only a reflection of a much deeper phenomenon.

In order to investigate the origin and nature of the presumably deep processes which govern the observed surface activity, it is necessary to first consider the depth of the convection zone. The model of Simon and Weiss (1968) asserts that the deep convection zone consists of the supergranular convection zone extending to 10-20,000 km in depth, beneath which a "giant cell" convective region extends to over 100,000 km in depth. Mixing length calculations (Schwarzschild et al. 1957) result in a similar depth. However, the calculations of Mullan (1971) indicate that a far shallower convection zone, extending only to the bottom of the supergranular region at 10-20,000 km is present, Dicke (1970) discussed a means by which light element abundances can be used to obtain the convection zone depth,

Recent abundance work by Hall (1974) makes it possible to use this method.

As Dicke (1970, and references therein) has pointed out, the light elements lithium, beryllium, and boron are destroyed in nuclear reactions at temperatures appreciably lower than those encountered in the deep solar energy generation regions. If convective mixing in the outer solar envelope is present, an analysis of the light elements which may have been destroyed by nuclear reactions will place constraints upon how deep such mixing extends. While there are other possible forms of mixing besides convection, as discussed by Dicke, it remains the most efficient means of mixing. So in the outer sun it is reasonable to assume convection is the process responsible for all mixing.

The boron abundance has recently been analyzed by Hall (1974) and Hall and Engvold (1974). In that work, the elemental and isotope abundances relevant to this question were discussed. It was concluded that most of the primeval lithium, some of the beryllium, and none of the boron have been destroyed by solar mixing. Calculations of the percentage of these elements relative to their initial abundances expected for various levels in an unmixed sun have been made by Bochsler and Geiss (1973). A summary of these calculations is listed in Table 11 for the depths at which each element under consideration would be totally destroyed. Lithium appears to be totally depleted at a

Table 11. Light Element Depletion Information

Element	Abundance Relative to Hydrogen	Primordial Abundance	Depletion Depth from Bochsler and Geiss (1973)	Reference
Li ₇	$.63 \times 10^{-12}$	1.8×10^{-9}	200,000 km	Müller (1968)
Be ₉	$1.2 \pm .1 \times 10^{-11}$	3×10^{-11}	300,000 km	Ross and Aller (1974)
B ₁₀ ⁺ B ₁₁	$<1.2 \pm 0.6 \times 10^{-10}$	same (?)	450,000 km	Hall and Engvold (1974)

depth of around 200,000 km, beryllium at 300,000 km and boron at 450,000 km. The heavy depletion of lithium, if due to convective mixing, would suggest mixing extending to a level close to 200,000 km deep. The small depletion of beryllium is probably due to a slower non-convective mixing process, for example, meridional circulation. This fact and the non-depletion of boron indicates that the convection zone does not extend to depths as large as 300,000 km. An additional fact in favor of convective mixing and destruction of lithium is provided in the observations of Zappala (1972). He observed that lithium depletion occurs steadily with age for main sequence stars and that this depletion proceeds at a more rapid rate for later type main sequence stars. This would indicate that a process which occurs continuously with age, like convection, is responsible for the depletion of lithium, rather than a rapid mixing early in the stellar lifetime. The more rapid depletion in later type stars further points to convection as the mixing process, since the convection zone extends to the deeper and hotter levels, where more rapid destruction of lithium would be expected in later type main sequence stars (Mullan 1971).

The 200,000 km depth is consistent with the Simon and Weiss (1968) model of the convection zone with the giant cell motions originating at depths of 100,000-200,000 km serving as the primary mode of convection in the deep

convective layers. This is somewhat deeper than the depth calculated by Weymann and Sears (1965) who concluded that the lithium could not be convectively depleted. However, the inherent uncertainty in the convective depth calculations is probably great enough to allow the convection to extend to the depth indicated by the lithium depletion.

The observations and considerations discussed to this point appear to fit into a general set of models. A qualitative description of these models is given below.

In Chapter 4 it was demonstrated that strong toroidal fields can be generated in stellar interiors over the stellar lifetime. The components of this field which lie in the convection zone will be swept to the surface and presumably diffused away as solar surface fields are observed to do. This would suggest a continuous supply of field, presumably from the toroidal fields generated deep within the star. However, the detailed physical process by which the fields are brought to the surface and diffused away remains an open question. Several possibilities have been discussed by Leighton (1969) and others.

The key question relevant to this dissertation is the degree to which the magnetic fields interact with the convective motions before they are observed at the surface. The two possibilities to be discussed are that the fields diffuse into the convection zone as weak field sheets, which are then concentrated and amplified by convective

dynamo processes as described by Parker (1970, and references therein) and Mullan (1974), and the alternative hypothesis put forward by Piddington (1975) that magnetic fields in the sun exist in the form of strong twisted "ropes," with convection acting more to distribute these fields than to enhance them. The observations reported in the previous chapters appear to support the Piddington flux rope model, which attributes the observed distribution of fields to a breakup or unraveling of a larger deep flux rope. The fact that strong fields are not observed in the process of being enhanced, which argues that they exist in discrete forms prior to their interaction with the convective motions, and the additional fact that the time diffusion of the fields is too rapid to be due to convective random walking both support this hypothesis.

An important problem for the Piddington model involves the question of the origin of the flux ropes. It is not clear whether enough ready-made flux can diffuse from the zone underlying the convection to provide for the observed surface field. It is possible to calculate the rate of diffusion and field dispersal required by this model from the magnetohydrodynamic diffusion equation given in Mestel and Roxburgh (1962):

$$\frac{\partial \vec{B}}{\partial t} = \vec{v} \times (\vec{v} \times \vec{B}) + \eta \nabla^2 \vec{B} \quad (5.7)$$

where \vec{B} the magnetic field, η the magnetic diffusivity, and

\vec{v} any velocities which may be present within the material.

If it is assumed that the material motions interact with the fields, as the Piddington theory would suggest, the first term, or dynamo term, can be ignored. For an order of magnitude estimate the v^2 can be replaced by $\frac{1}{R^2}$ where R is the size scale of the region in which the diffusion is occurring; thus we obtain:

$$\frac{\Delta B}{\Delta t} \sim \eta \frac{B}{R^2} \quad (5.8)$$

a timescale for diffusion within the convection zone can be obtained by setting $\Delta B \sim B$ so that:

$$t_{\text{diff}} = \frac{R^2}{\eta} \quad (5.9)$$

The time to be considered for the diffusion is the time over which the fields change. This is observed to be the 11-year solar cycle. Leighton (1969), using a size scale of the supergranule scale ($\sim 10^4$ km) and a diffusivity of 10^{13} , (substantially larger than the $\eta \sim 10^7$ for ordinary resistive diffusivity) including such mechanisms as turbulent diffusion, was able to match the observed timescale. It is consequently a timescale of ~ 10 years which we wish to consider. In the deep convection zone ordinary resistive diffusivity is probably the sole diffusion mechanism with $\eta \sim 10^7$. Solving for the amount of flux diffused into the convection zone $\Delta \vec{B}$

$$\Delta \vec{B} = \eta \frac{\vec{B} \Delta t}{R^2} \quad (5.10)$$

with \vec{B} the value of toroidal field generated in the stellar core from Chapter 4 of $\sim 1000\text{G}$ for the sun, $\Delta t = 10^8$ sec, and R the total size of the convection zone of 10^{10} cm, a $\Delta\vec{B}$ of about 10^{-2}g is derived. This would imply that substantial convective dynamo action occurs since a uniform value of $\Delta B \sim 1\text{ G}$ (Weiss 1964) is needed to provide the observed surface field. However, the value for R of the total convection zone size is probably much too large, as flux would only need to diffuse a short distance into the convection zone before it would be rapidly carried to the surface by convective motions. If this distance is on the order of 10,000 km, an adequate amount of flux can be diffused out of the deep levels, without the necessity of convective dynamo action.

The Current State of Research on Convection and Further Work Which is Needed

The existing results and new observations added by this work are summarized below:

1. Strong magnetic fields can be created as the consequence of differential rotation in deep stellar interiors of the sun and other late type main sequence stars.
2. Ordered convective motions apparently exist to substantial depths within the sun.
3. Strong magnetic fields exist on the surface of the sun and probably on other late type stars. These

fields are strong enough and extensive enough to cause large scale variations in surface parameters such as temperature. On the sun the magnetic fields appear to outline a material motion called supergranulation. All processes which seem to be associated with the supergranulation such as chromospheric emission and photospheric temperature structure are directly connected to the magnetic fields.

4. Observations appear to be consistent with a generalized lower main sequence model in which strong fields are generated deeply within the star (Biermann 1950, Mestel and Roxburgh 1962, Dicke 1970, Mullan 1974). Subsequent interaction with an extensive convective envelope bring these fields to the surface, perhaps enhanced by dynamo action, where they may modify the surface structure and dissipate.

A quantitative description for the magnetic field convection zone interaction remains obscure. Indeed, a complete mathematical description of the convection itself is lacking. Leighton's (1969) model and the models discussed by Dicke (1970) are the best attempts to date on this problem. The observations discussed in this dissertation in general strengthen and constrain these models. From

these results a number of further problems appear which would additionally constrain the eventual model. These are summarized below:

1. The existence of strong fields correlated with rotation for late type stars is a very tentative result. Accurate stellar rotation rates for a large number of dM and dMe stars are needed. This information can be obtained from high resolution spectrograms. Such observations can now be accomplished for the intrinsically faint dM stars with the new echelle spectrographs and Fourier transform spectrographs under construction at several observatories. Just as important is the direct observation of the magnetic fields themselves. If the fields approach 10^5 Gauss in strength, as predicted, their observation can directly be made from the Zeeman splitting of magnetically sensitive lines. The conventional Zeeman polarization observational scheme of Babcock (1962) is probably of little use for several reasons. Not only does the circular polarization of the Zeeman absorption line components used by the Babcock technique disappear when the magnetic fields are 90° to the line of sight, the polarization occurs in opposite senses for opposite polarity fields. So for a solar type magnetic field, components of the field at opposite polarities, as may be

expected to lie close together on the stellar surface, would provide cancelling polarization effects and may be unobservable. An acceptable alternative is to attempt to observe the Zeeman split absorption line components themselves, as Harvey and Hall (1974) did for the sun and Preston (1969) did for the Ap stars, rather than attempting to observe the polarization effects of the Zeeman splitting. This could be accomplished using a pair of absorption lines, one highly Zeeman sensitive, the other non-magnetically sensitive. A high resolution study of these lines would reveal, if fields as strong as 10^4 - 10^5 Gauss cover 10-30% of the stellar surface as predicted, the Zeeman sigma components several angstroms to either side of the magnetically sensitive line. The magnitude of the separation is not a function of magnetic field geometry, only the field strength. If the fields are all more or less the same strength, as on the sun, these Zeeman line components may be visible on the same spectra used for the rotational study. These splittings are not apparent on existing medium dispersion spectra for the dMe stars, however existing spectra are of low accuracy. Since the magnetic fields may cover a very small area of the stellar surface, the highest possible photometric precision is desirable.

Additionally, since temperature changes associated with magnetic field regions may be present, relatively weak deeply formed lines should be used to minimize temperature effects; as with the lines used for the vertical velocity study in Chapter 3.

2. If it is assumed that the surface distribution of magnetic fields matches the distribution of deep convective motions, the conclusion that there are only two sizes of convection cell deep in the convection zone is reached. The supergranular cell, with a scale of $\sim 10^4$ km, and the giant cell with a scale of $\sim 10^5$ km seem to be the only convective size scale present in addition to the surface granular convection with a scale of 10^3 km. However, convective theory would predict an entire spectrum of sizes throughout the convection zone due to the extremely turbulent nature of the convection. It may well turn out that the fluid mechanics of highly turbulent plasmas behave in a far more organized manner than predicted by current theory, as suggested by Spiegel (1972). Schwarzschild (1975) following an analysis similar to that of Simon and Weiss (1968) for the sun, has predicted large ordered convection cells for the M supergiant stars. The less than 10 convective cells which would be present seems consistent with the light and radial velocity

variations discussed by Weymann (1963) and Brooke, Lambert, and Barnes (1974). Direct stellar surface observation of this phenomenon which is now possible using speckle interferometry (Lynds, Worden, and Harvey 1974) should provide an additional check on the ordered convective cell hypothesis.

3. Extensions of the solar observations made here are needed. A long-term study of supergranular magnetic and velocity fields covering many cell lifetimes would allow exact magnetic diffusion rates to be determined. Additionally an infrared study at more wavelengths with higher spatial resolution would make it possible to determine in detail the deep photospheric temperature structure of magnetic field regions. If observed, the small velocity flows ($v < .1$ km/sec) which presumably accompany giant cell motions, would strengthen the case for attributing them to deep convective motions.
4. The dissipation of solar surface fields in a time as short as 11 years is difficult to accomplish without a fast diffusion mechanism (Leighton 1969). Several suggestions have been made concerning the nature of this diffusion, involving for example turbulent motions to cause field line reconnection as observed in the chromosphere by Sheeley et al. (1975). However, none of the suggestions are wholly

satisfactory. Observationally, there exist several possibilities for studying this problem. If the Leighton (1969) model for solar activity is applied to the rapidly rotating dMe stars they would be expected to show greatly accelerated magnetic diffusion and stellar cycle processes (Leighton 1974). Since convective cell lifetime and size parameters can be estimated for these stars (Mullan 1971, 1974), a careful observation of the magnetic field and surface activity evolution can be used to check Leighton's diffusion mechanism and convective stellar cycle calculations.

5. Piddington's (1975) suggestions of a "flux rope" model present several difficulties. While the observations seem to support the qualitative model, the small bundles of strong flux near the surface present a theoretical problem. While deep within the convection zone the confinement of the fields to a small area presents no problem, near the surface confinement by the relatively weak material motions is difficult. Furthermore, while the large bundles of flux probably diffuse into the convection zone to be carried to the surface by convective motions as described earlier, the exact quantitative process is unclear. If a detailed set of physical conditions within the flux points can be obtained by

extending the observations in Chapter 2, a more extensive analysis such as that done by Chitre (1963) and Deinzer (1965) for sunspots is possible. Such an analysis of conditions within the flux rope may provide an understanding of the physical mechanisms involved.

REFERENCES

- Allen, C. W. 1973, Astrophysical Quantities (London: Athlone Press).
- Anderson, C. M. 1974, unpublished manuscript, Department of Astronomy, University of Wisconsin.
- Babcock, H. W. 1953, Ap. J., 118, 387.
- Babcock, H. W. 1961, Ap. J., 133, 572.
- Babcock, H. W. 1962, in Stars and Stellar Systems, Vol. 1, ed. W. A. Hiltner (Chicago: University of Chicago Press), p. 107.
- Bahng, J., and Schwarzschild, M. 1961, Ap. J., 134, 312.
- Beckers, J. M. 1968, Solar Phys., 5, 108.
- Beckers, J. M., and Parnell, R. L. 1969, Solar Phys., 9, 39.
- Biermann, L. 1950, Zs. F. Naturforsch., 5a, 65.
- Bochsler, P., and Geiss, J. 1973, Solar Phys., 32, 3.
- Bohm-Vitense, E. 1958, Zs. f. Ap., 46, 108.
- Bopp, B. W. 1974, M.N.R.A.S., 166, 79.
- Bopp, B. W., and Evans, D. S. 1973, M.N.R.A.S., 164, 343.
- Bracewell, R. M. 1965, The Fourier Transform and Its Applications (New York: McGraw-Hill).
- Brault, J. W., and Testerman, L. 1973, Preliminary Edition of the Kitt Peak Solar Atlas.
- Brault, J. W., and White, O. R. 1971, Astr. and Ap., 13, 169.
- Brooke, A. L., Lambert, D. L., and Barnes, T. G. 1974, Pub. A.S.P., 86, 419.
- Bumba, V. 1967, in Plasma Astrophysics, ed. P. A. Sturrock (London: Academic Press), p. 182.

- Bumba, V., and Howard, R. F. 1965, Ap. J., 141, 1492.
- Chandrasekhar, S. 1961, Hydrodynamic and Hydromagnetic Stability (Oxford: Clarendon Press).
- Chapman, G. A. 1970, Solar Phys., 14, 315.
- Chapman, G. A. 1974, unpublished manuscript, Aerospace Corporation Observatory, California.
- Chitre, S. M. 1963, M.N.R.A.S., 126, 431.
- Chugainov, P. F. 1966, Inf. Bull. Var. Stars, No. 122.
- Clark, A., Jr., and Johnson, H. K. 1967, Solar Phys., 2, 433.
- Deinzer, W. 1965, Ap. J., 141, 548.
- Deubner, F. L. 1967, Solar Phys., 2, 133.
- Deubner, F. L. 1972a, Solar Phys., 17, 6.
- Deubner, F. L. 1972b, Solar Phys., 22, 263.
- Dicke, R. H. 1970, Ann. Rev. Astr. and Ap., 8, 297.
- Dunn, R. B., Rust, D. M., and Spence, G. E. 1974, Proc. SPIE, 44, 109.
- Dunn, R. B., and Zirker, J. B. 1973, Solar Phys., 33, 281.
- Evans, D. S. 1971, M.N.R.A.S., 154, 329.
- Evans, J., and Michard, R. 1962, Ap. J., 136, 493.
- Evershed, E., and Royds, T. 1913, M.N.R.A.S., 73, 554.
- Frazier, E. N. 1970, Solar Phys., 14, 89.
- Frazier, E. N. 1974, Solar Phys., 38, 69.
- Frenkiel, F. W., and Schwarzschild, M. 1952, Ap. J., 118, 422.
- Gingerich, O., Noyes, R. W., Kalkofen, W., and Cuny, Y. 1971, Solar Phys., 18, 347.
- Greenstein, J. L., and Arp, H. 1969, Ap. J. (Letters), 149, 3.

- Hall, D. N. B. 1974, unpublished manuscript, Kitt Peak National Observatory, Arizona.
- Hall, D. N. B., and Engvold, O. 1974, unpublished manuscript, Kitt Peak National Observatory, Arizona,
- Hart, A. B. 1954, M.N.R.A.S., 114, 2.
- Hart, A. B. 1956, M.N.R.A.S., 116, 38.
- Harvey, J. W., and Hall, D. N. B. 1974, private communication, Kitt Peak National Observatory, Arizona,
- Iroshnikov, R. S. 1969, Soviet Astr. A. J., 13, 73.
- Johnson, H. L. 1966, Ann. Rev. Astr. and Ap., 4, 193.
- Joy, A. H., and Abt, H. A. 1974, Ap. J. Suppl., No. 252,
- Kron, G. E. 1952, Ap. J., 115, 301.
- Krzeminski, W. 1969, in Low Luminosity Stars, ed. S. Kumar (London: Gordon and Breach), p. 57.
- Kunkel, W. E. 1973, Ap. J. Suppl., 25, 1.
- Labonte, B., and Simon, G. W. 1975, private communication, Sacramento Peak Observatory, New Mexico.
- Leighton, R. B. 1964, Ap. J., 140, 1559.
- Leighton, R. B. 1969, Ap. J., 156, 1.
- Leighton, R. B. 1974, private communication, California Institute of Technology, California.
- Leighton, R. B., Noyes, R. W., and Simon, G. W. 1962, Ap. J., 135, 474.
- Liu, Sou-Yang, 1974, Solar Phys., 30, 3.
- Livingston, W. C. 1974, unpublished manuscript, Kitt Peak National Observatory, Arizona.
- Livingston, W. C., and Orrall, F. Q. 1974, Solar Phys., 39, 301.
- Lovell, B. 1971, Quart. J.R.A.S., 12, 98.

- Lynds, C. R., Worden, S. P., and Harvey, J. W. 1974, Bull. AAS, 6, 459.
- Mestel, L., and Roxburgh, I. W. 1962, Ap. J., 136, 615.
- Milkey, R. W. 1972, unpublished data, Kitt Peak National Observatory, Arizona.
- Mullan, D. J. 1971, M.N.R.A.S., 154, 467.
- Mullan, D. J. 1974, Ap. J., 192, 149.
- Mullan, D. J. 1975, unpublished manuscript, Bartol Research Foundation, Pennsylvania.
- Müller, F. A. 1968, in The Origin and Distribution of the Elements, ed. L. H. Ahrens (Oxford, N. Y.: Pergamon Press), p. 155.
- Musman, S. 1971, in IAU Symp. 43, Solar Magnetic Fields, ed. R. Howard (Dordrecht: Reidel), p. 86.
- Musman, S., and Rust, D. M. 1970, Solar Phys., 13, 261.
- November, L., Altrock, R., Simon, G., Milkey, R., and Worden, S. P. 1975, submitted for publication, Solar Phys.
- Öpik, E. J. 1950, M.N.R.A.S., 110, 559.
- Osterbrock, D. 1961, Ap. J., 134, 347.
- Parker, E. N. 1955, Ap. J., 121, 49.
- Parker, E. N. 1963, Ap. J., 138, 552.
- Parker, E. N. 1970, Ap. J., 160, 383.
- Parker, E. N. 1974, Comments presented in November, 1974 at the KPNO Solar Physics Conference.
- Pellew, A., and Southwell, R. V. 1940, Proc. Roy. Soc. of London, 176A, 312.
- Piddington, J. H. 1975, unpublished manuscript, CSIRO, Australia.
- Plaskett, H. H. 1916, Ap. J., 43, 145.

- Plaskett, J. S. 1915, Ap. J., 42, 373.
- Poveda, A. 1964, Nature, 292, 1319.
- Preston, G. W. 1969, Ap. J., 157, 247.
- Rogers, E. H. 1970, Solar Phys., 13, 57.
- Ross, J. E., and Aller, L. H. 1974, Solar Phys., 36, 21.
- Schlesinger, F. 1916, Pub. of the Allegheny Obs., II, 56.
- Schwarzschild, M. 1958, Structure and Evolution of the Stars (Princeton: Princeton University Press).
- Schwarzschild, M. 1975, Ap. J., 195, 137.
- Schwarzschild, M., Howard, R., and Härm, R. 1957, Ap. J., 125, 233.
- Sheeley, N. R., Jr., Bohlin, J. D., Brueckner, G. E.,
Purcell, J. D., Scherrer, V. E., and Tousey, R.
1975, Naval Research Laboratory Preprint.
- Simon, G. W. 1966, Ap. J., 145, 411.
- Simon, G. W., and Leighton, R. B. 1964, Ap. J., 140, 1120.
- Simon, G. W., and Weiss, N. O. 1968, Zs. f. Ap., 69, 435.
- Sistla, G., and Harvey, J. W. 1970, Solar Phys., 12, 16.
- Smithson, R. C. 1973, Solar Phys., 29, 365.
- Spiegel, E. A. 1963, Ap. J., 138, 216.
- Spiegel, E. A. 1964, Ap. J., 139, 959.
- Spiegel, E. A. 1965, Ap. J., 141, 1068.
- Spiegel, E. A. 1966, Trans. IAU, 12B, 539.
- Spiegel, E. A. 1971, Ann. Rev. Astr. and Ap., 9, 323.
- Spiegel, E. A. 1972, Ann. Rev. Astr. and Ap., 10, 261.
- Stuart, F. E., and Rush, J. H. 1954, Ap. J., 120, 245.
- Sykora, J. 1970, Solar Phys., 13, 292.

- Tannenbaum, A. S., Wilcox, J. M., Frazier, E. N., and Howard, R. 1969, Solar Phys., 9, 328.
- Torres, C. A. O., and Mello, F. S. 1973, Astro. and Ap., 27, 231.
- Tsuji, T. 1969, in Low Luminosity Stars, ed. S. Kumar (London: Gordon and Breach), p. 457.
- Turon, P. J., and Lena, P. 1973, Solar Phys., 30, 3.
- Van de Kamp, P. 1971, Ann. Rev. Astr. and Ap., 9, 103.
- Vassiljeva, G. Y. 1967, Solar Phys., 1, 16.
- Vaughn, A. H., and Zirin, H. R. 1968, Ap. J., 152, 123.
- Veeder, G. I. 1974, A. J., 79, 702.
- Vickers, G. T. 1971, Ap. J., 163, 363.
- Vitense, E. 1953, Zs. f. Ap., 32, 135.
- Weiss, N. O. 1964, M.N.R.A.S., 128, 225.
- Weiss, N. O. 1966, Proc. Roy. Soc. of London, 293A, 310.
- Weiss, N. O. 1968, in IAU Symp. 35: Structure and Development of Solar Active Regions (Holland: Reidel), p. 111.
- Weymann, R. J. 1963, Ann. Rev. Astr. and Ap., 1, 97.
- Weymann, R. J., and Sears, R. L. 1965, Publ. A.S.P., 77, 141.
- Wilson, P. R. 1972a, Solar Phys., 27, 354.
- Wilson, P. R. 1972b, Solar Phys., 27, 363.
- Wolff, C. L. 1972, Ap. J. (Letters), 176, L87.
- Zappala, R. R. 1972, Ap. J., 172, 57.
- Zirin, H. 1966, The Solar Atmosphere (Waltham: Blaisdell).